
TENSOR GENERALIZED CANONICAL CORRELATION ANALYSIS

Fabien Girka^{1,2}Arnaud Gloaguen³Laurent Le Brusquet¹Violetta Zujovic²Arthur Tenenhaus^{1,2}**ABSTRACT**

Regularized Generalized Canonical Correlation Analysis (RGCCA) is a general statistical framework for multi-block data analysis. RGCCA enables deciphering relationships between several sets of variables and subsumes many well-known multivariate analysis methods as special cases. However, RGCCA only deals with vector-valued blocks, disregarding their possible higher-order structures. This paper presents Tensor GCCA (TGCCA), a new method for analyzing higher-order tensors with canonical vectors admitting an orthogonal rank- R CP decomposition. Moreover, two algorithms for TGCCA, based on whether a separable covariance structure is imposed or not, are presented along with convergence guarantees. The efficiency and usefulness of TGCCA are evaluated on simulated and real data and compared favorably to state-of-the-art approaches.

1 Introduction

The study of a given phenomenon under multiple views can hopefully reveal a more significant part of the mechanisms at stake rather than considering each view separately. In order to design a study under such a paradigm, measurements are usually acquired through different modalities resulting in multimodal/multi-view/multiblock/multi-source data. One statistical framework suited explicitly for the joint analysis of such multi-source data is Regularized Generalized Canonical Correlation Analysis (RGCCA) (Tenenhaus and Tenenhaus, 2011; Tenenhaus et al., 2017). RGCCA is designed with a flexible yet simple algorithmic framework that encompasses a large number of well-known multi-block component methods. This includes Canonical Correlation Analysis (Hotelling, 1936), Partial Least Squares Regression (Wold et al., 1983), many variants of correlation/covariance-based multiblock component methods (e.g., Carroll's GCCA (Carroll, 1968), MAXVAR (Kettenring, 1971), MAXBET (Van de Geer, 1984), Multiple Co-Inertia Analysis (Chessel and Hanafi, 1996), to cite a few). See Tenenhaus et al. (2017) for a detailed overview.

However, RGCCA can only treat vector-valued data (a.k.a first-order tensors) at the population level, whereas sometimes their natural structure is of higher order. This is the case, for example, in electroencephalography (EEG) (time \times channels and sometimes \times frequencies), social network (users \times channels \times servers), process analysis (monitored variables \times time \times batches), or text-mining (concepts \times documents \times languages) data. Taking into account such underlying tensor structure is not only a way to properly analyze the data but it can also improve the interpretation of the results, provide more robust estimators, associated with faster algorithms.

Tensor versions of vector-valued methods have been developed for a wide variety of problems (Acar et al., 2011; Zhou et al., 2013; Papalexakis et al., 2017). These methods usually perform tensor analysis by imposing a tensor factorization model on the estimated vectors associated with each variable. Among the most known models are the CANDECOMP/PARAFAC (CP) decomposition (Harshman, 1970; Carroll and Chang, 1970) and the Tucker decomposition (Tucker, 1963, 1964). Kim and Cipolla (2009); Lu (2013); Gloaguen et al. (2020); Chen et al. (2021)

¹ Université Paris-Saclay, CNRS, CentraleSupélec, Laboratoire des signaux et systèmes, 91190, Gif-sur-Yvette, France.

² Sorbonne Université, Institut du Cerveau - Paris Brain Institute - ICM, Inserm, CNRS, APHP, Hôpital Pitié Salpêtrière Univ. Hosp., DMU Neurosciences 6, Paris, France.

³ Centre National de Recherche en Génomique Humaine, Institut François Jacob, CEA, Université Paris-Saclay, 91057, Évry, France.

have proposed extensions of CCA where the canonical vectors are constrained to follow a CP decomposition model of rank-1. In Min et al. (2019), the imposed CP decomposition is of rank-R.

Moreover, since the variables are supposed to bear a natural tensor structure, a central question for Tensor-based CCA methods is the resulting structure of the covariance matrices associated with each block. Min et al. (2019) addressed this question by proposing a separable structure to the block covariance matrices.

A first attempt to propose a tensor version of RGCCA was made in Gloaguen et al. (2020) with Multiway GCCA (MGCCA), but limited to matrix-valued data (a.k.a second-order tensor) at the population level, and where canonical vectors are modeled with a rank-1 CP decomposition, together with a separable structure for covariance matrices. In the line of Gloaguen et al. (2020), we propose Tensor Generalized Canonical Correlation Analysis (TGCCA), a new tensor version of RGCCA, by enforcing an orthogonal rank-R CP decomposition to the canonical vectors and relaxing the separable assumption. TGCCA can (i) handle an arbitrary number of blocks, (ii) handle tensor-valued data of any order, (iii) extract, from each block, canonical vectors modeled with an orthogonal rank-R CP decomposition, (iv) handle separable and non-separable covariance structure. To the extent of our knowledge, no tensor CCA method that gathers all these four properties has yet been proposed. Finally, algorithms designed to solve the TGCCA optimization problem are provided with theoretical convergence guarantees and experimental validation.

The remainder of the paper is organized as follows. In Section 2, we describe the RGCCA problem. Section 3 presents the TGCCA optimization problem with and without the separable assumptions. The two strategies rely on the same master algorithm but with different core updates presented in Section 4. In Section 5, we conduct numerical experiments to illustrate the benefits of the proposed methods compared to existing ones. We further evaluate our method on real data in Section 6. Finally, we discuss the limitations of our approach and perspectives in Section 7.

Our code is freely available on [github](#)¹.

2 RGCCA at the population level

We consider L random vectors $\mathbf{x}_1, \dots, \mathbf{x}_l, \dots, \mathbf{x}_L$. We assume that each random vector $\mathbf{x}_l \in \mathbb{R}^{p_l}$ has a zero mean and a covariance matrix Σ_{ll} . Let $\Sigma_{lk} = \mathbb{E}[\mathbf{x}_l \mathbf{x}_k^\top]$ be the cross-covariance matrix between \mathbf{x}_l and \mathbf{x}_k . Let $\mathbf{w}_l \in \mathbb{R}^{p_l}$ be the non-random canonical vector associated with the block \mathbf{x}_l . The objective of RGCCA is to find composite random variables $y_l = \mathbf{w}_l^\top \mathbf{x}_l$ associated with each block that summarizes the relevant information between and within the blocks. RGCCA at the population level is defined as the following optimization problem:

$$\begin{aligned} & \underset{\mathbf{w}_1, \dots, \mathbf{w}_L}{\text{maximize}} \sum_{l,k=1}^L c_{lk} g(\mathbf{w}_l^\top \Sigma_{lk} \mathbf{w}_k) \\ & \text{s.t. } \mathbf{w}_l^\top \mathbf{M}_l \mathbf{w}_l = 1, l = 1, \dots, L. \end{aligned} \quad (1)$$

- The function g is any continuously differentiable convex function. Its derivative is noted g' . If $c_{ll} \neq 0$ for some l the constraint $g'(x) \geq 0$ for $x \geq 0$ must be added in order to guarantee the objective function to be multi-convex (i.e., convex with respect to each \mathbf{w}_l while holding all others fixed).
- The design matrix $\mathbf{C} = \{c_{lk}\}$ is a symmetric $L \times L$ matrix of non-negative elements describing the network of connections between blocks that the user wants to consider. Usually, $c_{lk} = 1$ between two connected blocks and 0 otherwise.
- Each block regularization matrix $\mathbf{M}_l \in \mathbb{R}^{p_l \times p_l}$ is symmetric positive-definite.

Many correlation and covariance-based component methods, including CCA, fall under this general formulation. See Tenenhaus et al. (2017) for a detailed overview.

For higher-order blocks, the RGCCA notations introduced above need to be extended. The following subsection reviews the notations and basic tensor operations needed for presenting TGCCA. We follow the terminology and notation introduced in Kolda and Bader (2009).

¹<https://github.com/GFabien/TGCCA-supplementary-material>

3 Population TGCCA

3.1 Notations

Scalars, vectors, matrices and higher order tensors are represented by x , \mathbf{x} , \mathbf{X} and \mathcal{X} , respectively. The shorthand $[n]$ will be used to denote the index set $\{1, \dots, n\}$. Let \mathcal{X} be a tensor of order d , it means there exists $\{p_1, \dots, p_d\} \in \mathbb{N}^d$ such that $\mathcal{X} \in \mathbb{R}^{p_1 \times \dots \times p_d}$ i.e. \mathcal{X} has d modes, where the m^{th} mode is of dimension p_m . Tensor elements can be described by $x_{i_1 \dots i_d}$ with $i_m \in [p_m]$ for $m \in [d]$.

Tensor fibers are the extension of matrix rows and columns: mode- m fibers are vectors of p_m elements obtained by fixing all indices except the m^{th} , leading to $\mathbf{x}_{i_1 \dots i_{m-1} i_{m+1} \dots i_d}$. Tensors can be matricized or unfolded along a given mode. The mode- m matricization of tensor $\mathcal{X} \in \mathbb{R}^{p_1 \times \dots \times p_d}$ is denoted $\mathbf{X}_{(m)}$ and is of dimension $p_m \times \prod_{j \neq m} p_j$. This operation arranges the mode- m fibers of \mathcal{X} in a matrix. As matrices, tensors can be vectorized. For a matrix, $\mathbf{A} = [\mathbf{a}_1 \ \dots \ \mathbf{a}_p]$, the vectorized version of \mathbf{A} is $\mathbf{a} = \text{Vec}(\mathbf{A}) = [\mathbf{a}_1^\top \ \dots \ \mathbf{a}_p^\top]^\top$ where \top denotes the transpose operator. Therefore we can define the mode- m vectorization of \mathcal{X} by the vectorization of its mode- m matricization.

We use the symbols \circ for the outer product and \otimes for the Kronecker product.

Finally, a tensor $\mathcal{X} \in \mathbb{R}^{p_1 \times \dots \times p_d}$ is said to be of rank one if there exists d vectors $\mathbf{w}_1, \dots, \mathbf{w}_d \in \mathbb{R}^{p_1 \times \dots \times p_d}$ of unit norm and a scalar λ such that $\mathcal{X} = \lambda \mathbf{w}_1 \circ \dots \circ \mathbf{w}_d$. As for matrices, we can talk about rank- R tensors if they cannot be expressed as the sums of less than R rank-one tensors: $\mathcal{X} = \sum_{r=1}^R \lambda^{(r)} \mathbf{w}_1^{(r)} \circ \dots \circ \mathbf{w}_d^{(r)}$. This decomposition, called CANDECOMP/PARAFAC (CP) (Carroll and Chang, 1970; Harshman, 1970) will be denoted $\mathbf{x} = \llbracket \boldsymbol{\lambda}; \mathbf{W}_1, \dots, \mathbf{W}_d \rrbracket$. It implicitly defines the quantities $\mathbf{w}^{(r)} = \mathbf{w}_d^{(r)} \otimes \dots \otimes \mathbf{w}_1^{(r)}$, $\mathbf{W} = [\mathbf{w}^{(1)} \ \dots \ \mathbf{w}^{(R)}]$, and $\boldsymbol{\lambda} = [\lambda^{(1)} \ \dots \ \lambda^{(R)}]^\top$, such that

$$\mathbf{x} = \sum_{r=1}^R \lambda^{(r)} \mathbf{w}_d^{(r)} \otimes \dots \otimes \mathbf{w}_1^{(r)} = \sum_{r=1}^R \lambda^{(r)} \mathbf{w}^{(r)} = \mathbf{W} \boldsymbol{\lambda}.$$

We talk about orthogonal rank when the factors $\mathbf{w}^{(r)}$ are orthogonal. If the factors $\mathbf{w}_m^{(r)}$ are orthogonal for every $m \in [d]$, we then talk about completely orthogonal rank (Kolda, 2001).

In the following sections, we consider L random tensors $\mathcal{X}_1, \dots, \mathcal{X}_L$. Each random tensor $\mathcal{X}_l \in \mathbb{R}^{p_{l,1} \times \dots \times p_{l,d_l}}$ is of order d_l and the dimension of the m^{th} mode of \mathcal{X}_l is equal to $p_{l,m}$. We denote the mode-1 vectorization of \mathcal{X}_l by \mathbf{x}_l . We assume that the random vector \mathbf{x}_l has a zero mean and a covariance matrix $\boldsymbol{\Sigma}_{ll}$. Let $\boldsymbol{\Sigma}_{lk} = \mathbb{E}[\mathbf{x}_l \mathbf{x}_k^\top]$ be the cross-covariance matrix between \mathbf{x}_l and \mathbf{x}_k . We note \mathbf{w}_l an unknown non-random canonical vector of dimension $p_l = \prod_{m=1}^{d_l} p_{l,m}$.

3.2 MGCCA optimization problem

As the proposed work extends MGCCA, we first introduce its optimization problem. In the case of MGCCA, $\forall l \in [L], d_l = 2$. Hence, the following optimization problem given in Equation (2.2) of Gloaguen et al. (2020):

$$\begin{aligned} & \underset{\mathbf{w}_1, \dots, \mathbf{w}_L}{\text{maximize}} \sum_{l,k=1}^L c_{lk} \mathfrak{g}(\mathbf{w}_l^\top \boldsymbol{\Sigma}_{lk} \mathbf{w}_k) \\ & \text{s.t. } \mathbf{w}_l^\top \mathbf{M}_l \mathbf{w}_l = 1, \text{ and } \mathbf{w}_l = \mathbf{w}_{l,2} \otimes \mathbf{w}_{l,1}, l \in [L]. \end{aligned} \quad (2)$$

Gloaguen et al. (2020) make the additional assumption that the matrices $\mathbf{M}_l \in \mathbb{R}^{p_l \times p_l}$ can be written as the Kronecker product of two matrices $\mathbf{M}_{l,1} \in \mathbb{R}^{p_{l,1} \times p_{l,1}}$ and $\mathbf{M}_{l,2} \in \mathbb{R}^{p_{l,2} \times p_{l,2}}$: $\mathbf{M}_l = \mathbf{M}_{l,2} \otimes \mathbf{M}_{l,1}$. We qualify matrices with such a structure as separable matrices. Therefore, the change of variables $\mathbf{v}_l = \mathbf{M}_l^{\frac{1}{2}} \mathbf{w}_l$ leads to this new set of constraints for (2) (Equation (2.6) in Gloaguen et al. (2020)):

$$\mathbf{v}_l^\top \mathbf{v}_l = 1 \text{ and } \mathbf{v}_l = \mathbf{v}_{l,2} \otimes \mathbf{v}_{l,1}, l \in [L]. \quad (3)$$

Thus, MGCCA aims to maximize the criterion of RGCCA under the assumption that the canonical vectors admit a CP decomposition of rank 1 and that the regularization matrices \mathbf{M}_l are separable.

3.3 TCCA optimization problem

Another close related work is TCCA from Min et al. (2019). They maximize the CCA criterion: $\mathbf{w}_1^\top \Sigma_{12} \mathbf{w}_2$ under the constraints that $\mathbf{w}_l^\top \Sigma_{ll} \mathbf{w}_l = 1$ and that the canonical vectors admit rank- R_l CP decompositions:

$$\mathbf{w}_l = [\boldsymbol{\lambda}; \mathbf{W}_{l,1}, \dots, \mathbf{W}_{l,d}], \mathbf{W}_{l,m} \in \mathbb{R}^{p_{l,m} \times R_l}, l \in [2]. \quad (4)$$

With such structures, canonical vectors can describe more complex interactions than those extracted with MGCCA while keeping a low degree of freedom compared to RGCCA.

3.4 TGCCA optimization problem

We now introduce the TGCCA optimization problem. Like MGCCA, we want to maximize the flexible criterion of RGCCA. Like TCCA, we want to consider rank- R_l CP decompositions of d_l^{th} -order tensors. Hence, a natural optimization problem that generalizes both MGCCA and TCCA consists in maximizing the criterion of (1) under the following constraints:

$$\begin{aligned} \mathbf{w}_l^\top \mathbf{M}_l \mathbf{w}_l &= 1, \text{ and } \mathbf{w}_l = [\boldsymbol{\lambda}_l; \mathbf{W}_{l,1}, \dots, \mathbf{W}_{l,d}], \\ \mathbf{W}_{l,m} &\in \mathbb{R}^{p_{l,m} \times R_l}, l \in [L]. \end{aligned} \quad (5)$$

To ensure that the solution of (5) does not degenerate in practice, we add orthogonality constraints between the rank-1 factors $\mathbf{w}_l^{(r)}$ of the CP decomposition. This additional constraint aims to prevent collinearity between factors. We can consider orthogonality constraints of the type $\mathbf{w}_l^{(r)\top} \mathbf{K}_l \mathbf{w}_l^{(s)} = \delta_{rs}$ where δ is the Kronecker delta, and $\mathbf{K}_l \in \mathbb{R}^{p_l \times p_l}$ is any symmetric positive-definite matrix.

Separable TGCCA. Under the assumption that matrices \mathbf{M}_l are separable: $\mathbf{M}_l = \mathbf{M}_{ld} \otimes \dots \otimes \mathbf{M}_{l1}$ with $\mathbf{M}_{lm} \in \mathbb{R}^{p_{lm} \times p_{lm}}$ for $m \in [d]$, we choose $\forall l \in [L]$, $\mathbf{K}_l = \mathbf{M}_l$. Therefore, applying the change of variables $\mathbf{v}_l = \mathbf{M}_l^{\frac{1}{2}} \mathbf{w}_l$ and $\mathbf{Q}_{lk} = \mathbf{M}_l^{-\frac{1}{2}} \Sigma_{lk} \mathbf{M}_k^{-\frac{1}{2}}$ leads to the separable TGCCA optimization problem:

$$\begin{aligned} \text{maximize}_{\mathbf{v}_1, \dots, \mathbf{v}_L} \quad & \sum_{l,k=1}^L c_{lk} \mathbf{g}(\mathbf{v}_l^\top \mathbf{Q}_{lk} \mathbf{v}_k) \quad \text{s.t.} \quad \mathbf{v}_l^\top \mathbf{v}_l = 1, \\ \mathbf{v}_l &= [\boldsymbol{\lambda}_l; \mathbf{V}_{l,1}, \dots, \mathbf{V}_{l,d}], \mathbf{V}_{l,m} \in \mathbb{R}^{p_{l,m} \times R_l}, \\ \text{and } \mathbf{V}_l^\top \mathbf{V}_l &= \mathbf{I}_{R_l} \quad l \in [L]. \end{aligned} \quad (6)$$

As $\mathbf{v}_l = \mathbf{V}_l \boldsymbol{\lambda}_l$, the constraints of (6) imply that $\boldsymbol{\lambda}_l^\top \boldsymbol{\lambda}_l = 1$. Setting $R_l = 1$ and $d_l = 2$, we see that we get the MGCCA problem with the constraints described in (3).

Non-separable TGCCA. In the general case (i.e., no separability assumption on \mathbf{M}_l), the problem is hard to solve (see Appendix A for a detailed discussion), so we propose to study a relaxed version of (5) with orthogonality constraints. Indeed, we authorize $\mathbf{w}_l^\top \mathbf{M}_l \mathbf{w}_l \leq 1$ and impose $\mathbf{W}_l^\top \mathbf{W}_l = \mathbf{I}_{R_l}$. The constraints on $\boldsymbol{\lambda}_l$ and \mathbf{W}_l are entangled since $\mathbf{w}_l^\top \mathbf{M}_l \mathbf{w}_l = \boldsymbol{\lambda}_l^\top \mathbf{W}_l^\top \mathbf{M}_l \mathbf{W}_l \boldsymbol{\lambda}_l$ and $\mathbf{W}_l^\top \mathbf{M}_l \mathbf{W}_l$ does not simplify for an arbitrary orthonormal matrix \mathbf{W}_l . To disentangle them, we can observe the following fact:

$$\begin{aligned} \mathbf{w}_l^\top \mathbf{M}_l \mathbf{w}_l &\leq \|\mathbf{w}_l\|_2 \|\mathbf{M}_l \mathbf{w}_l\|_2, \\ &\leq \|\mathbf{M}_l\|_2 \|\mathbf{w}_l\|_2^2, \\ &\leq \|\mathbf{M}_l\|_2 \mathbf{w}_l^\top \mathbf{w}_l \\ &= \|\mathbf{M}_l\|_2 \boldsymbol{\lambda}_l^\top \mathbf{W}_l^\top \mathbf{W}_l \boldsymbol{\lambda}_l = \|\mathbf{M}_l\|_2 \|\boldsymbol{\lambda}_l\|_2^2. \end{aligned}$$

The Cauchy-Schwarz inequality was used to get the second line and $\|\cdot\|_2$ is the matrix norm such that $\|\mathbf{A}\|_2 = \sup_{\mathbf{u}, \|\mathbf{u}\|_2=1} \|\mathbf{A}\mathbf{u}\|_2$. Finally, imposing $\|\boldsymbol{\lambda}_l\|_2 \leq \|\mathbf{M}_l\|_2^{-\frac{1}{2}}$ makes sure that the relaxed constraint is satisfied, whatever the choice of \mathbf{W}_l . Consequently, we define the non-separable TGCCA optimization problem as:

$$\begin{aligned} \text{maximize}_{\mathbf{w}_1, \dots, \mathbf{w}_L} \quad & \sum_{l,k=1}^L c_{lk} \mathbf{g}(\mathbf{w}_l^\top \Sigma_{lk} \mathbf{w}_k) \\ \text{s.t. } \mathbf{w}_l &= [\boldsymbol{\lambda}_l; \mathbf{W}_{l,1}, \dots, \mathbf{W}_{l,d_l}], \mathbf{W}_{l,m} \in \mathbb{R}^{p_{l,m} \times R_l}, \\ \mathbf{W}_l^\top \mathbf{W}_l &= \mathbf{I}_{R_l}, \text{ and } \|\boldsymbol{\lambda}_l\|_2 \leq \|\mathbf{M}_l\|_2^{-\frac{1}{2}} \quad l \in [L]. \end{aligned} \quad (7)$$

This last formulation hides the impact of the structure of \mathbf{M}_l as it appears only through its matrix norm, which is its highest singular value. Therefore, we will take into account \mathbf{M}_l in the optimization scheme instead (see calculations in Appendix A).

In a nutshell, both the separable and non-separable TGCCA optimization problems boil down to maximizing the criterion of RGCCA on compact sets $\Omega = \Omega_1 \times \dots \times \Omega_L$, where Ω_l is the constraint space of \mathbf{w}_l or \mathbf{v}_l (the proof that Ω is compact can be found in Appendix B). Both problems look for solutions that admit CP decompositions of orthogonal ranks R_l .

3.5 An algorithm for maximizing a multi-convex continuously differentiable function

Given a multi-convex continuously differentiable function $f(\mathbf{w}_1, \dots, \mathbf{w}_L) : \mathbb{R}^{p_1} \times \dots \times \mathbb{R}^{p_L} \rightarrow \mathbb{R}$ and compact sets $\Omega_l \subset \mathbb{R}^{p_l}, l \in [L]$, we are interested in the following general optimization problem:

$$\underset{\mathbf{w}_1, \dots, \mathbf{w}_L}{\text{maximize}} f(\mathbf{w}_1, \dots, \mathbf{w}_L) \quad \text{s.t.} \quad \mathbf{w}_l \in \Omega_l, l \in [L]. \quad (8)$$

In Tenenhaus et al. (2017), a master algorithm for maximizing a continuously differentiable multi-convex function, under the constraint that each \mathbf{w}_l belongs to a compact set Ω_l , is proposed. As problems (6) and (7) fall under this configuration, this master algorithm can be used for TGCCA. This algorithm is based on a Block Coordinate Ascent (BCA) strategy (de Leeuw, 1994), which consists in updating sequentially only one canonical vector $\mathbf{w}_l \in \mathbb{R}^{p_l}$ (while keeping all the others fixed) in a way that increases the objective function. This is where the multi-convexity of the function f comes in hand: as a convex function lies above its linear approximation at \mathbf{w}_l , for any $\tilde{\mathbf{w}}_l \in \Omega_l$, the following inequality holds:

$$f(\mathbf{w}_1, \dots, \mathbf{w}_{l-1}, \tilde{\mathbf{w}}_l, \mathbf{w}_{l+1}, \dots, \mathbf{w}_L) \geq f(\mathbf{w}) + \nabla_l f(\mathbf{w})^\top (\tilde{\mathbf{w}}_l - \mathbf{w}_l) = l_l(\tilde{\mathbf{w}}_l, \mathbf{w}), \quad (9)$$

where $\mathbf{w} = (\mathbf{w}_1, \dots, \mathbf{w}_L)$ and $\nabla_l f(\mathbf{w})$ is the partial gradient of f with respect to \mathbf{w}_l :

$$\nabla_l f(\mathbf{w}) = 2 \sum_{k=1}^L c_{lk} \mathbf{g}'(\mathbf{w}_l^\top \Sigma_{lk} \mathbf{w}_k) \Sigma_{lk} \mathbf{w}_k.$$

Maximizing $l_l(\tilde{\mathbf{w}}_l, \mathbf{w})$ defined in (9) over $\tilde{\mathbf{w}}_l$ is then equivalent to find

$$\underset{\tilde{\mathbf{w}}_l \in \Omega_l}{\text{argmax}} \nabla_l f(\mathbf{w})^\top \tilde{\mathbf{w}}_l = r_l(\mathbf{w}). \quad (10)$$

On the one hand, from the definitions of $r_l(\mathbf{w})$ and $l_l(\mathbf{w}_l, \mathbf{w})$ in respectively (10) and (9), $l_l(r_l(\mathbf{w}), \mathbf{w}) \geq l_l(\mathbf{w}_l, \mathbf{w}) = f(\mathbf{w})$. On the other hand, according to (9), $f(\mathbf{w}_1, \dots, \mathbf{w}_{l-1}, r_l(\mathbf{w}), \mathbf{w}_{l+1}, \dots, \mathbf{w}_L) \geq l_l(r_l(\mathbf{w}), \mathbf{w})$. Thus, the proposed update (10) increases the value of the objective function. This fact remains true even if $r_l(\mathbf{w})$ is no longer the maximizer of $\nabla_l f(\mathbf{w})^\top \tilde{\mathbf{w}}_l$, as long as $\nabla_l f(\mathbf{w})^\top r_l(\mathbf{w}) \geq \nabla_l f(\mathbf{w})^\top \mathbf{w}_l$.

Algorithm 1: Master algorithm for optimization problem (8).

Result: $\mathbf{w}_1^s, \dots, \mathbf{w}_L^s$ (approximate solution of (8))

Initialization: $\mathbf{w}_l^0 \in \Omega_l, l = 1, \dots, L, \varepsilon;$

$s = 0;$

repeat

for $l = 1$ **to** L **do**

$\mathbf{w}_l^{s+1} = r_l(\mathbf{w}_1^{s+1}, \dots, \mathbf{w}_{l-1}^{s+1}, \mathbf{w}_l^s, \dots, \mathbf{w}_L^s)$

end

$s = s + 1;$

until $f(\mathbf{w}_1^{s+1}, \dots, \mathbf{w}_L^{s+1}) - f(\mathbf{w}_1^s, \dots, \mathbf{w}_L^s) < \varepsilon;$

The master algorithm, without details on how to compute update (10), can be found in Algorithm 1. For studying the convergence properties of Algorithm 1, it is useful to introduce some additional notations. Let $c_l : \Omega \mapsto \Omega$ be an operator defined as $c_l(\mathbf{w}) = (\mathbf{w}_1, \dots, \mathbf{w}_{l-1}, r_l(\mathbf{w}), \mathbf{w}_{l+1}, \dots, \mathbf{w}_L)$ and $c : \Omega \mapsto \Omega$ be defined as $c = c_L \circ \dots \circ c_1$, where \circ stands for the function composition.

We consider the sequence $\{\mathbf{w}^s = (\mathbf{w}_1^s, \dots, \mathbf{w}_L^s)\}_{s=0}^\infty$ generated by Algorithm 1. Using the operator c , the "for loop" inside Algorithm 1 can be replaced by the following recurrence relation:

$$\mathbf{w}^{s+1} = c(\mathbf{w}^s). \quad (11)$$

To study the convergence properties of Algorithm 1, we will consider the infinite sequence $\{\mathbf{w}^s\}_{s=0}^\infty$ generated by (11). The convergence properties of Algorithm 1 are summarized in the next proposition.

Proposition 1. *Let $\{\mathbf{w}^s\}_{s=0}^\infty$ be any sequence generated by the recurrence relation $\mathbf{w}^{s+1} = c(\mathbf{w}^s)$ with $\mathbf{w}^0 \in \Omega$. Then, the following properties hold:*

- *The sequence $\{f(\mathbf{w}^s)\}_{s=0}^\infty$ is monotonically increasing and therefore convergent as f is bounded on Ω . This result implies the monotonic convergence of Algorithm 1.*
- *If the infinite sequence $\{f(\mathbf{w}^s)\}_{s=0}^\infty$ involves a finite number of distinct terms, then the last distinct point satisfies $c(\mathbf{w}^s) = \mathbf{w}^s$ and therefore is a stationary point of problem (8).*
- *The limit of any convergent subsequence of $\{\mathbf{w}^s\}_{s=0}^\infty$ is a fixed point of c .*
- *$\lim_{s \rightarrow \infty} f(\mathbf{w}^s) = f(\mathbf{w}^*)$, where \mathbf{w}^* is a fixed point of c .*
- *The sequence $\{\mathbf{w}^s\}_{s=0}^\infty$ is asymptotically regular: $\lim_{s \rightarrow \infty} \sum_{l=1}^L \|\mathbf{w}_l^{s+1} - \mathbf{w}_l^s\| = 0$. This result implies that if the threshold ϵ in Algorithm 1 is made sufficiently small, the output of Algorithm 1 will be as close as wanted to a stationary point of (8).*
- *If the equation $\mathbf{w} = c(\mathbf{w})$ has a finite number of solutions, then the sequence $\{\mathbf{w}^s\}_{s=0}^\infty$ converges to one of them.*

The TGCCA algorithm inherits from the convergence properties of the algorithm from Tenenhaus et al. (2017) as long as the solution found for (10) exists and is unique.

4 Updates for TGCCA

Let assume that we have n observations of the L tensor blocks: $(\mathcal{X}_{1,i}, \dots, \mathcal{X}_{L,i})_{i \in [n]}$. Our goal is to estimate $\mathbf{w}_1, \dots, \mathbf{w}_L$ solution of (6) and (7) where Σ_{lk} and \mathbf{M}_l are replaced with their estimates, respectively $\hat{\Sigma}_{lk}$ and $\hat{\mathbf{M}}_l$. In subsection 4.1, we focus on the separable case and the special case of matrix blocks is detailed in subsection 4.2. The non-separable case is presented in Appendix A. The main difference with the separable case lies in the update of λ_l .

4.1 Update for sample separable TGCCA

In case regularization matrices have a separable structure, our goal is to find a solution of (10) where \mathbf{Q}_{lk} is replaced with its estimated counterpart. In practice, $\hat{\mathbf{M}}_l$ and $\hat{\Sigma}_{lk}$ are estimated and $\hat{\mathbf{Q}}_{lk} = \hat{\mathbf{M}}_l^{-\frac{1}{2}} \hat{\Sigma}_{lk} \hat{\mathbf{M}}_k^{-\frac{1}{2}}$.

We can note that $\mathbf{v}_l^{(r)}$ is a linear function of $\mathbf{v}_{l,m}^{(r)}$. Indeed, $\mathbf{v}_l^{(r)} = \mathbf{V}_{l,(-m)}^{(r)} \mathbf{v}_{l,m}^{(r)}$, where $\mathbf{V}_{l,(-m)}^{(r)} = (\mathbf{v}_{l,d_l}^{(r)} \otimes \dots \otimes \mathbf{v}_{l,m+1}^{(r)} \otimes \mathbf{I}_{p_{l,m}} \otimes \mathbf{v}_{l,m-1}^{(r)} \otimes \dots \otimes \mathbf{v}_{l,1}^{(r)}) \in \mathbb{R}^{p_l \times p_{l,m}}$. We can also observe that

$$\begin{aligned} \nabla_l f(\mathbf{v})^\top \mathbf{v}_l &= \sum_{r=1}^R \lambda_l^{(r)} \nabla_l f(\mathbf{v})^\top \mathbf{V}_{l,(-m)}^{(r)} \mathbf{v}_{l,m}^{(r)} \\ &= \text{Tr}(\mathbf{F}^\top \mathbf{V}_{l,m}), \end{aligned} \quad (12)$$

$$\text{with } \mathbf{F} = [\mathbf{f}^{(1)} \dots \mathbf{f}^{(R)}]$$

$$\text{and } \mathbf{f}^{(r)} = \lambda_l^{(r)} \mathbf{V}_{l,(-m)}^{(r)\top} \nabla_l f(\mathbf{v}) \in \mathbb{R}^{p_{l,m}}.$$

The interest in formulation (12) is the separation of an entire mode, embodied by $\mathbf{V}_{l,m}$, from all the others. As a consequence, we propose to use BCA here to alternate between λ_l and $\mathbf{V}_{l,m}$ for $m \in [d_l]$. Hence we define $\Omega_{l,m}^v = \{\mathbf{V}_{l,m} \in \mathbb{R}^{p_{l,m} \times R_l}; \mathbf{V}_{l,m}^\top \mathbf{V}_{l,m} = \mathbf{I}_{R_l}\}$ the feasible set for $\mathbf{V}_{l,m}$ and the intermediate update

$$\mathbf{r}_{l,m}(\mathbf{v}) = \underset{\mathbf{V}_{l,m} \in \Omega_{l,m}^v}{\text{argmax}} \text{Tr}(\mathbf{F}^\top \mathbf{V}_{l,m}) = \mathbf{S} \mathbf{T}^\top, \quad (13)$$

where \mathbf{S} and \mathbf{T} are respectively the left and right singular vectors of the rank- R_l Singular Value Decomposition (SVD) of \mathbf{F} (orthogonal Procrustes problem, (Everson, 1997)). It is worth noting here that the update for mode m is unique if $\mathbf{F} \in \mathbb{R}^{p_{l,m} \times R_l}$ has full rank.

By choosing this update for every mode m , we implicitly imposed a completely orthogonal rank to the vector \mathbf{v}_l . In fact, imposing orthogonality constraints on one mode is enough. In this case, this update should be chosen for a given mode m , and the update for every other mode q would directly be $\mathbf{r}_{l,q}(\mathbf{v}) = \left[\frac{\mathbf{f}^{(1)}}{\|\mathbf{f}^{(1)}\|_2} \cdots \frac{\mathbf{f}^{(R_l)}}{\|\mathbf{f}^{(R_l)}\|_2} \right]$.

From a tensor point of view, $\mathbf{f}^{(r)}/\lambda_l^{(r)}$ can be seen as the result of the mode products between the folded version of $\nabla_l f(\mathbf{v})$: $\mathcal{F} \in \mathbb{R}^{p_{l,1} \times \cdots \times p_{l,d_l}}$ and all the $\mathbf{v}_{l,q}^{(r)}$ for $q \in [d_l] \setminus \{m\}$. Therefore, the matrices $\mathbf{V}_{l,(-m)}^{(r)}$ do not need to be computed in practice, limiting the algorithm's complexity.

From Cauchy-Schwartz, the update on λ_l is:

$$\mathbf{r}_{l,\lambda}(\mathbf{v}) = \underset{\lambda_l, \|\lambda_l\|_2=1}{\operatorname{argmax}} \nabla_l f(\mathbf{v})^\top \mathbf{V}_l \lambda_l = \frac{\mathbf{V}_l^\top \nabla_l f(\mathbf{v})}{\|\mathbf{V}_l^\top \nabla_l f(\mathbf{v})\|_2}. \quad (14)$$

Updating each $\mathbf{V}_{l,m}$ using (13) and then updating λ_l using (14) yields a unique update for (10) that increases the value of the objective function.

4.2 Special case of matrix blocks

When $d_l = 2$, i.e. block l has intrinsically a matrix structure, we can make an observation similar to (12). Indeed, let $\mathbf{F} \in \mathbb{R}^{p_{l,1} \times p_{l,2}}$ be a reshaped version of $\nabla_l f(\mathbf{v})$ and $\Lambda_l = \operatorname{diag}(\lambda_l)$,

$$\sum_{r=1}^{R_l} \lambda_l^{(r)} \nabla_l f(\mathbf{v})^\top (\mathbf{v}_{l,2}^{(r)} \otimes \mathbf{v}_{l,1}^{(r)}) = \operatorname{Tr}(\Lambda_l \mathbf{V}_{l,1}^\top \mathbf{F} \mathbf{V}_{l,2}).$$

A closed form solution of $\underset{\Lambda_l, \mathbf{V}_{l,1}, \mathbf{V}_{l,2}}{\operatorname{argmax}} \operatorname{Tr}(\Lambda_l \mathbf{V}_{l,1}^\top \mathbf{F} \mathbf{V}_{l,2})$ cannot be found but applying one iteration of the tandem algorithm from Everson (1997) increases the criterion and gives

$$\mathbf{r}_{l,1}(\mathbf{v}) = \mathbf{S}, \quad \mathbf{r}_{l,2}(\mathbf{v}) = \mathbf{T} \quad \text{and} \quad \mathbf{r}_{l,\lambda}(\mathbf{v}) = \frac{\boldsymbol{\delta}}{\|\boldsymbol{\delta}\|_2},$$

where $\mathbf{S} \operatorname{diag}(\boldsymbol{\delta}) \mathbf{T}^\top$ is the rank- R_l SVD of \mathbf{F} . If the R_l^{th} singular value of \mathbf{F} is not degenerated, then the proposed update is unique. This is equivalent to alternate between $(\mathbf{V}_{l,1}, \mathbf{V}_{l,2})$ and λ_l . If $R_l = 1$, we retrieve the update of MGCCA (Equation (2.10) in Gloaguen et al. (2020)).

5 Numerical experiments

5.1 Methods

To evaluate the quality of the estimates provided by TGCCA, we generate blocks using the data model presented in Appendix G, based on the probabilistic TCCA model of Min et al. (2019). Our simulations aim to assess the ability of TGCCA and state-of-the-art approaches to recover the canonical vectors used to generate the data. The cosine between the true canonical vectors and the estimated ones is used as an indicator of quality: $\alpha_l = \frac{|\mathbf{w}_l^\top \hat{\mathbf{w}}_l|}{\|\mathbf{w}_l\|_2 \|\hat{\mathbf{w}}_l\|_2}$. In our comparisons, we include MGCCA (Gloaguen et al., 2020), Tensor CCA (TCCA) (Min et al., 2019), and two-dimensional CCA (2DCCA) (Chen et al., 2021). Finally, RGCCA and the per block SVD are considered as baselines. If appropriate, the method's rank is added as a suffix and the separable assumption as a prefix with "sp". As shown in Section 4.2, spTGCCA1 is equivalent to MGCCA, so only MGCCA will be reported in the tables.

5.2 Results

Table 1 reports the results of the compared methods. The median and the quantiles (2.5% and 97.5%) on the different data folds of the cosines and computation times (in seconds) are reported. TCCA and TGCCA are run 5 times per fold, and the model with the best criterion is kept each time while 2DCCA is run only once using a so-called "effective" strategy for the choice of the starting point (Chen et al., 2021).

Table 1: Cosine between the true and the estimated canonical vectors as well as computation times. Median and quantiles (2.5% and 97.5%) are reported.

Model	Gas	Cross (small)	Computation time
2DCCA1	0.30 (0.01, 0.89)	0.43 (0.16, 0.85)	3.09 (2.76, 4.50)
TCCA1	0.89 (0.22, 0.90)	0.85 (0.32, 0.86)	7.72 (7.38, 9.17)
TGCCA1	0.89 (0.87, 0.90)	0.85 (0.83, 0.86)	8.70 (8.50, 10.26)
spTCCA1	0.89 (0.22, 0.90)	0.85 (0.32, 0.86)	7.43 (7.24, 8.04)
MGCCA	0.89 (0.87, 0.90)	0.86 (0.83, 0.86)	4.98 (4.66, 5.16)
2DCCA3	0.04 (0.01, 0.21)	0.13 (0.05, 0.31)	1.50 (1.41, 3.09)
TCCA3	0.89 (0.87, 0.90)	0.85 (0.83, 0.86)	7.93 (7.73, 8.92)
TGCCA3	0.91 (0.78, 0.94)	0.92 (0.79, 0.96)	10.87 (10.11, 13.93)
spTCCA3	0.89 (0.87, 0.90)	0.85 (0.83, 0.86)	7.32 (7.22, 7.51)
spTGCCA3	0.92 (0.82, 0.94)	0.93 (0.83, 0.96)	5.62 (5.44, 6.31)
RGCCA	0.17 (0.05, 0.26)	0.11 (0.06, 0.20)	13.12 (12.67, 14.07)
SVD	0.00 (0.00, 0.01)	0.01 (0.00, 0.03)	5.78 (5.44, 6.07)

Table 2: Cosine between the true and the estimated canonical vectors as well as computation times. Median and quantiles (2.5% and 97.5%) are reported (3D settings).

Model	Cross	Cross (small) 3D	Computation time
TCCA1	0.88 (0.87, 0.89)	0.88 (0.85, 0.88)	17.31 (16.74, 18.94)
TGCCA1	0.88 (0.87, 0.89)	0.88 (0.85, 0.88)	14.29 (13.24, 21.84)
spTCCA1	0.88 (0.87, 0.89)	0.88 (0.85, 0.88)	15.70 (15.32, 23.05)
spTGCCA1	0.88 (0.87, 0.89)	0.87 (0.87, 0.88)	15.90 (15.10, 24.15)
TCCA3	0.88 (0.87, 0.89)	0.88 (0.85, 0.88)	23.89 (19.64, 26.21)
TGCCA3	0.98 (0.96, 1.00)	0.88 (0.82, 0.88)	21.58 (20.46, 25.45)
spTCCA3	0.88 (0.87, 0.89)	0.88 (0.85, 0.88)	17.96 (15.65, 20.41)
spTGCCA3	0.98 (0.96, 0.99)	0.99 (0.95, 0.99)	49.52 (27.35, 113.45)
RGCCA	0.97 (0.92, 0.98)	0.98 (0.84, 0.98)	115.32 (113.21, 116.23)
SVD	0.01 (0.00, 0.03)	0.01 (0.00, 0.03)	1.62 (1.54, 1.73)

Firstly, it appears that all algorithms solving the rank-1 TCCA problem behave similarly. Only TGCCA takes advantage of the use of higher rank. Both TGCCA and TCCA seek canonical vectors with the same underlying rank- R CP structure. The main difference between the two models relies on the fact that TCCA does not impose orthogonal rank-1 factors. In our experiments, TCCA3 extracted canonical vectors $\{\hat{\mathbf{w}}_l^{(r)}\}_{r \in [3]}$ that are almost collinear. This degenerate solution of TCCA3 justifies the orthogonality constraints in TGCCA.

2DCCA aims to extract R rank-1 canonical vectors with orthogonal canonical components $\mathbf{X}_{l,(1)} \mathbf{w}_l$. A deflation strategy is used to ensure orthogonality between components. As 2DCCA3 is designed to find 3 distinct canonical components of rank 1 with the same weights, the reconstructed vectors $\hat{\mathbf{w}}_l = \sum_{r=1}^R \hat{\mathbf{w}}_{l,d_l}^{(r)} \otimes \cdots \otimes \hat{\mathbf{w}}_{l,1}^{(r)}$ do not correspond to the true canonical vectors.

Looking at the tables in Appendix G, it is worth noticing that RGCCA and SVD need a higher signal-to-noise ratio (SNR) to perform equally well as TGCCA3 and spTGCCA3.

We perform an additional experiment with 3D canonical vectors. The conclusions are similar, except for RGCCA, which performs much better due to changes in the noise generation process. (see Table 2 and Appendix G.5). 2DCCA was excluded because we did not implement a higher-order version algorithm.

Table 3: Cosine between the true and the estimated concentrations with computation times (mean and standard deviation). The cosine for the best model over the 100 runs is reported between parentheses.

Chemical	TGCCA	CMTF	ACMTF
Val-Tyr-Val	0.961 ± 0.006 (0.962)	0.625 ± 0.228 (0.999)	0.608 ± 0.204 (0.949)
Trp-Gly	0.907 ± 0.026 (0.920)	0.505 ± 0.260 (0.978)	0.538 ± 0.225 (0.947)
Phe	0.834 ± 0.096 (0.870)	0.556 ± 0.341 (0.981)	0.637 ± 0.300 (0.703)
Malto	0.998 ± 0.000 (0.998)	0.995 ± 0.002 (0.992)	0.995 ± 0.002 (0.991)
Propanol	0.998 ± 0.000 (0.998)	0.533 ± 0.319 (0.997)	0.518 ± 0.295 (0.991)
Computation time	3.926 ± 0.209	93.723 ± 43.599	111.782 ± 45.052

6 Evaluation on real data

6.1 Chemical mixtures dataset

In this section, we evaluate the ability of TGCCA to retrieve the signatures/patterns related to different chemicals in given mixtures from the dataset publicly available at <http://www.models.life.ku.dk/joda/prototype> (Acar et al., 2014b). In this dataset, a set of 28 mixtures with known chemical composition was measured using different analytical techniques, i.e., NMR (Nuclear Magnetic Resonance) spectroscopy and LC-MS (Liquid Chromatography-Mass Spectrometry), resulting in two blocks of data. The first one is a third-order tensor of dimensions $28 \times 13324 \times 8$, and the second one is a matrix of dimensions 28×168 . In this dataset, 4 of the chemicals can be identified in both blocks, while the last one does not appear in the matrix block (Acar et al., 2014b). We choose to extract 1 component of rank 2 and 3 components of rank 1 using the same deflation strategy for orthogonal components as in Gloaguen et al. (2020). We use $g : x \rightarrow x^2$ and choose to take identity matrices for \mathbf{M}_l , so we use spTGCCA in this Section.

We compare our approach with CMTF and Advanced CMTF (ACMTF) methods (Acar et al., 2011, 2014b). CMTF aims at solving the following optimization problem:

$$\underset{\mathbf{A}, \mathbf{B}, \mathbf{C}, \mathbf{V}, \boldsymbol{\lambda}, \boldsymbol{\sigma}}{\operatorname{argmin}} \quad \|\mathcal{X} - \llbracket \boldsymbol{\lambda}; \mathbf{A}, \mathbf{B}, \mathbf{C} \rrbracket\|_F^2 + \|\mathbf{Y} - \mathbf{A}\boldsymbol{\Sigma}\mathbf{V}^\top\|_F^2 \quad (15)$$

with $\boldsymbol{\Sigma} = \operatorname{diag}(\boldsymbol{\sigma})$, \mathbf{A} , \mathbf{B} , \mathbf{C} and \mathbf{V} being matrices with R columns. Hence, CMTF looks for the best rank- R decompositions of both the tensor and matrix blocks, with the \mathbf{A} matrix being shared between both blocks. ACMTF allows both shared and unshared components between blocks by adding penalties to enforce sparsity on the coefficients $\boldsymbol{\lambda}$ and $\boldsymbol{\sigma}$. Doing so, the model becomes able to select different columns of the matrix \mathbf{A} in each block. This is particularly interesting with this dataset since one of the chemicals does not appear in the matrix block. Implementations of CMTF and ACMTF were used from the MATLAB CMTF Toolbox v1.1, 2014.

As in Acar et al. (2014b), blocks are divided by their Frobenius norms. An additional centering step is performed before applying TGCCA. We run 100 times each model with random initial points and report the cosines (mean and standard deviation) between the true concentrations of the chemicals in the mixture and the estimated ones in Table 3. The computation times (in seconds) are also reported.

It is known that the (A)CMTF algorithm is sensitive to initialization. On the opposite, TGCCA seems really stable in this experiment while being much faster than CMTF. We can also observe that, for TGCCA, the cosines are very high and the standard deviations very low for the first two extracted chemicals (Malto and Propanol). In contrast, the cosines decrease, and the standard deviations increase for the next ones. This is expected because the deflation strategy imposes that the vectors of concentrations of the different chemicals are orthogonal, which is not the case for this dataset. Hence, the next components cannot be recovered perfectly. As this limitation does not apply to CMTF and ACMTF, it is not surprising that the best model over the 100 runs for CMTF (reported in parenthesis in Table 3) reaches higher cosines than the best model for TGCCA for 3 of the 5 chemicals.

6.2 The Multi-PIE Face dataset

To further evaluate our model, we perform an analysis similar to the one performed in Lu (2013) using faces from the Multi-PIE Face dataset (Gross et al., 2008). We select images (of dimensions 64×64) from 100 subjects in two different views and 15 different illumination conditions and organize them in two 4th-order tensor blocks of dimensions $100 \times 64 \times 64 \times 15$ corresponding to the two views. The goal is to learn a common latent subspace between the two blocks and then use this latent representation to match subjects across the two views. We use 100 new subjects to evaluate the matching performances. Each new subject comes with images in the two views, and we vary the number of

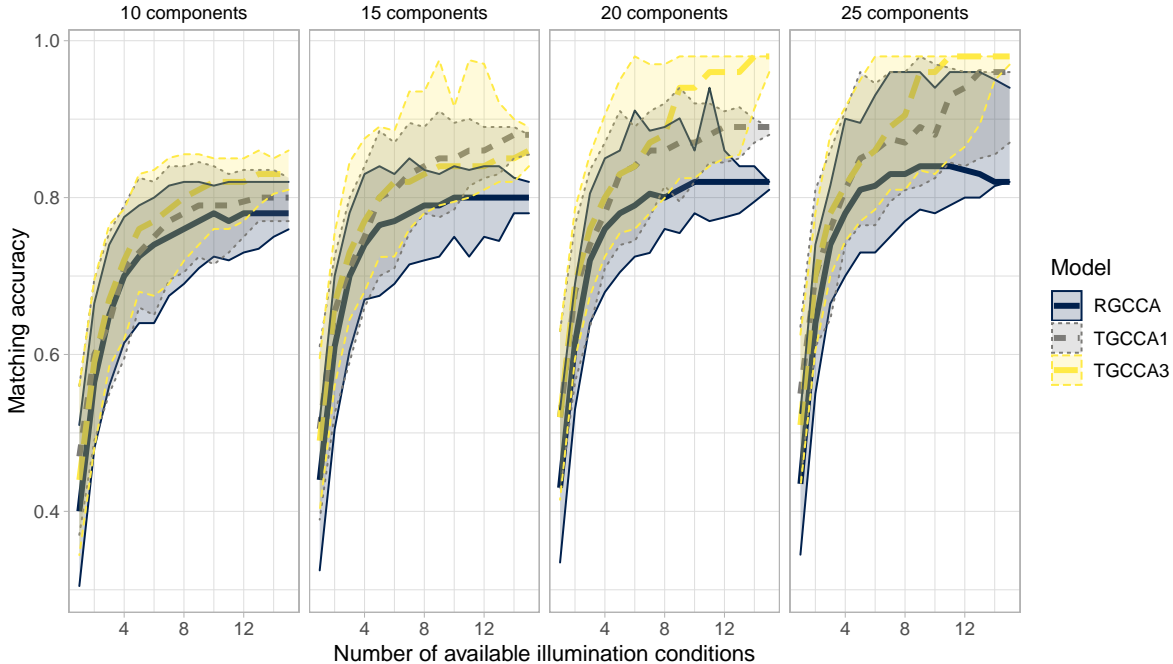


Figure 1: Matching accuracy on the test set for different models and different number of components. Experiments are repeated 100 times. Ribbons contain 95% of the points around the median for each model.

illumination conditions from 1 to 15. Therefore, we want to pair tensors of dimensions $64 \times 64 \times i$ where $i \in [15]$. Since the latent subspace is learned using all illumination conditions, if $i < 15$, there are missing slices in the tensors. This problem can be overcome by imputing the missing slices to the means of the training subjects (see Appendix F for a justification). The illumination conditions are randomly sampled, so they may differ across views for a given subject. We suppose that the illumination condition for each image is unknown. Therefore, we train a Linear Discriminant Analysis (LDA) classifier on the $100 \times 15 \times 2 = 3000$ available images of the training set to predict the illumination condition of each image. These images were downsampled and vectorized to the dimension $16 \times 16 = 256$ to reduce the number of variables while keeping enough information to perform the classification task.

Once the illumination conditions have been predicted and the tensors completed with missing slices, they are projected on the learned subspace. Subjects are then paired across the views by solving Integer Linear Programming to find the assignment that maximizes the sum of cosines between paired projections. Finally, the metric of interest is the accuracy of the matching.

We compare here RGCCA and TGCCA of ranks 1 and 3. As they are $64 \times 64 \times 15 = 61440$ variables for 100 subjects, we do not try to estimate the covariance matrices but instead, use the identity matrices as the regularization matrices M_l . Results based on the number of available illumination conditions per subject are shown in Figure 1. As illumination conditions are randomly sampled, we repeat the experiments 100 times. Rank-3 TGCCA seems to perform slightly better than rank-1 TGCCA, itself performing slightly better than RGCCA, and the matching accuracy increases with the number of available illumination conditions. Furthermore, it is important to note that RGCCA must estimate 61440 parameters while rank-1 TGCCA estimates $(64 + 64 + 15) \times 1 = 143$ parameters and rank-3 TGCCA estimates $(64 + 64 + 15) \times 3 = 429$ parameters per component and block. Figure 8 shows the obtained canonical vectors with the three methods. While rank-1 and rank-3 TGCCA focus on capturing what varies between subjects, RGCCA produces canonical vectors that are much closer to actual faces. Therefore, RGCCA is probably more prone to overfitting than the TGCCA models, which may explain their better results here. Figure 1 also shows that by increasing the number of components, the matching accuracy increases more for TGCCA models than RGCCA.

7 Conclusion and Discussion

We have proposed Tensor Generalized Canonical Correlation Analysis as a general framework for analyzing several higher-order tensors and matrices jointly. TGCCA relies on the RGCCA framework on which we imposed that an

orthogonal rank-R CP decomposition models the canonical vectors. Both separable and non-separable TGCCA give promising results, while separable TGCCA seems faster. Convergence of our algorithms is guaranteed, up to uniqueness conditions that can be monitored at run time.

If orthogonality constraints allow interesting results, they may not coincide with the true underlying structure of the data. A solution could be to impose angle constraints like in Acar et al. (2014a).

We now introduce some points for further investigations. Without noise, overestimating the rank would lead to have extra factors with zero weights. On real data, both the noise and the relevant information would be estimated by additional factors. Thus, a procedure to find the best rank is of great interest and under investigation.

TGCCA extracts the canonical vector for each block sequentially. Extracting the next canonical vectors can be done using a deflation strategy (see Gloaguen et al. (2020) for details). This approach imposes the canonical components to be orthogonal, which is not the case in the real dataset we studied. A procedure that extracts all sets of canonical vectors simultaneously is currently under investigation.

To fully benefit from the $L \geq 2$ setting, an interesting research line would be defining higher-order correlations (Luo et al., 2015; Merker and Schuldt, 2020; Wang and Zheng, 2020) and incorporating them in the criterion to optimize.

Acknowledgments

This work is supported by a public grant overseen by the French National Research Agency (ANR) through the program UDOPIA, project funded by the ANR-20-THIA-0013-01. We would also like to thank Eun Jeong Min and Hua Zhou for sharing their implementation of TCCA with us.

References

- Acar, E., Kolda, T. G., and Dunlavy, D. M. (2011). All-at-once optimization for coupled matrix and tensor factorizations.
- Acar, E., Nilsson, M., and Saunders, M. (2014a). A flexible modeling framework for coupled matrix and tensor factorizations. In *2014 22nd European Signal Processing Conference (EUSIPCO)*, pages 111–115.
- Acar, E., Papalexakis, E. E., Gürdeniz, G., Rasmussen, M. A., Lawaetz, A. J., Nilsson, M., and Bro, R. (2014b). Structure-revealing data fusion. *BMC Bioinformatics*, 15(1).
- Barthelmé, S. and Tschumperlé, D. (2019). imager: an r package for image processing based on cimg. *Journal of Open Source Software*, 4(38):1012.
- Carroll, J. (1968). A generalization of canonical correlation analysis to three or more sets of variables. In *Proceeding 76th Conv. Am. Psych. Assoc.*, pages 227–228.
- Carroll, J. D. and Chang, J.-J. (1970). Analysis of individual differences in multidimensional scaling via an n-way generalization of “eckart-young” decomposition. *Psychometrika*, 35(3):283–319.
- Chen, Y.-L., Kolar, M., and Tsay, R. S. (2021). Tensor canonical correlation analysis with convergence and statistical guarantees. *Journal of Computational and Graphical Statistics*, 0(0):1–17.
- Chessel, D. and Hanafi, M. (1996). Analyse de la co-inertie de K nuages de points. *Revue de Statistique Appliquée*, 44:35–60.
- de Leeuw, J. (1994). Block-relaxation algorithms in statistics. In *Studies in Classification, Data Analysis, and Knowledge Organization*, pages 308–324. Springer Berlin Heidelberg.
- Everson, R. (1997). Orthogonal, but not orthonormal, procrustes problems. In *Advances in Computational Mathematics* . (Submitted). Available from <http://www.ee.ic.ac.uk/research/neural/everson>.
- Gloaguen, A., Philippe, C., Frouin, V., Gennari, G., Dehaene-Lambertz, G., Brusquet, L. L., and Tenenhaus, A. (2020). Multiway generalized canonical correlation analysis. *Biostatistics*.
- Gross, R., Matthews, I., Cohn, J., Kanade, T., and Baker, S. (2008). Multi-pie. In *2008 8th IEEE International Conference on Automatic Face & Gesture Recognition*, pages 1–8.
- Hardoon, D. R., Szedmak, S., and Shawe-Taylor, J. (2004). Canonical Correlation Analysis: An Overview with Application to Learning Methods. *Neural Computation*, 16(12):2639–2664.
- Harshman, R. A. (1970). Foundations of the PARAFAC procedure: Models and conditions for an "explanatory" multi-modal factor analysis. *UCLA Working Papers in Phonetics*, 16:1–84.
- Hoff, P. D. (2011). Separable covariance arrays via the tucker product, with applications to multivariate relational data. *Bayesian Analysis*, 6(2).

- Hotelling, H. (1936). Relations between two sets of variables. *Biometrika*, 28(3-4):321–377.
- Kettenring, J. R. (1971). Canonical analysis of several sets of variables. *Biometrika*, 58:433–451.
- Kim, T.-K. and Cipolla, R. (2009). Canonical correlation analysis of video volume tensors for action categorization and detection. *IEEE Transactions on Pattern Analysis and Machine Intelligence*, 31(8):1415–1428.
- Kolda, T. G. (2001). Orthogonal tensor decompositions. *SIAM Journal on Matrix Analysis and Applications*, 23(1):243–255.
- Kolda, T. G. and Bader, B. W. (2009). Tensor decompositions and applications. *SIAM Review*, 51(3):455–500.
- Lu, H. (2013). Learning canonical correlations of paired tensor sets via tensor-to-vector projection. In *Proceedings of the Twenty-Third International Joint Conference on Artificial Intelligence, IJCAI '13*, page 1516–1522. AAAI Press.
- Luo, Y., Tao, D., Ramamohanarao, K., Xu, C., and Wen, Y. (2015). Tensor canonical correlation analysis for multi-view dimension reduction. *IEEE Transactions on Knowledge and Data Engineering*, 27(11):3111–3124.
- Merker, J. and Schuldt, G. (2020). On the construction of multivariate correlation coefficients. In *Proceedings of the 2020 3rd International Conference on Mathematics and Statistics, ICoMS 2020*, page 6–10, New York, NY, USA. Association for Computing Machinery.
- Min, E. J., Chi, E. C., and Zhou, H. (2019). Tensor canonical correlation analysis. *Stat*, 8(1):e253. e253 sta4.253.
- Papalexakis, E. E., Faloutsos, C., and Sidiropoulos, N. D. (2017). Tensors for data mining and data fusion. *ACM Transactions on Intelligent Systems and Technology*, 8(2):1–44.
- R Core Team (2020). *R: A Language and Environment for Statistical Computing*. R Foundation for Statistical Computing, Vienna, Austria.
- Tenenhaus, A. and Tenenhaus, M. (2011). Regularized generalized canonical correlation analysis. *Psychometrika*, 76(2):257–284.
- Tenenhaus, M., Tenenhaus, A., and Groenen, P. J. F. (2017). Regularized generalized canonical correlation analysis: A framework for sequential multiblock component methods. *Psychometrika*, 82(3):737–777.
- Tian, Y., Peng, X., Zhao, L., Zhang, S., and Metaxas, D. N. (2018). Cr-gan: Learning complete representations for multi-view generation.
- Tucker, L. R. (1963). Implications of factor analysis of three-way matrices for measurement of change. In Harris, C. W., editor, *Problems in measuring change.*, pages 122–137. University of Wisconsin Press, Madison WI.
- Tucker, L. R. (1964). The extension of factor analysis to three-dimensional matrices. In Gulliksen, H. and Frederiksen, N., editors, *Contributions to mathematical psychology.*, pages 110–127. Holt, Rinehart and Winston, New York.
- Van de Geer, J. (1984). Linear relations among k sets of variables. *Psychometrika*, 49:70–94.
- Wang, J. and Zheng, N. (2020). Measures of correlation for multiple variables.
- Wold, S., Martens, H., and Wold, H. (1983). The multivariate calibration problem in chemistry solved by the PLS method. In *In Proc. Conf. Matrix Pencils, Ruhe A. and Kastrom B. (Eds), March 1982, Lecture Notes in Mathematics, Springer Verlag, Heidelberg*, pages 286–293.
- Zhou, H., Li, L., and Zhu, H. (2013). Tensor regression with applications in neuroimaging data analysis. *Journal of the American Statistical Association*, 108(502):540–552.

A Non-separable TGCCA

We detail in this Section the choice of the formulation of the non-separable TGCCA optimization problem (7) and how we propose to tackle this problem.

A.1 Formulation of non-separable TGCCA

As stated in Section 3, we seek to solve

$$\underset{\mathbf{w}_1, \dots, \mathbf{w}_L}{\text{maximize}} \sum_{l,k=1}^L c_{lk} \mathbf{g}(\mathbf{w}_l^\top \boldsymbol{\Sigma}_{lk} \mathbf{w}_k) \quad (16)$$

$$\text{s.t. } \mathbf{w}_l^\top \mathbf{M}_l \mathbf{w}_l = 1, \mathbf{w}_l = \llbracket \boldsymbol{\lambda}; \mathbf{W}_{l,1}, \dots, \mathbf{W}_{l,d} \rrbracket, \mathbf{W}_{l,m} \in \mathbb{R}^{p_{l,m} \times R_l}, \text{ and } \mathbf{W}_l^\top \mathbf{K}_l \mathbf{W}_l = \mathbf{I}_{R_l} \quad l \in [L].$$

The two natural choices for \mathbf{K}_l are $\mathbf{K}_l = \mathbf{M}_l$ and $\mathbf{K}_l = \mathbf{I}_{p_l}$.

In the first case, $\mathbf{w}_l^\top \mathbf{M}_l \mathbf{w}_l = \boldsymbol{\lambda}_l^\top \mathbf{W}_l^\top \mathbf{M}_l \mathbf{W}_l \boldsymbol{\lambda}_l = \boldsymbol{\lambda}_l^\top \boldsymbol{\lambda}_l$. Therefore, the constraint $\mathbf{w}_l^\top \mathbf{M}_l \mathbf{w}_l = 1$ becomes $\|\boldsymbol{\lambda}_l\|_2 = 1$. According to (10), we have to find \mathbf{w}_l that allows to increase the value of the objective function. Using the same trick as in Section 4.1, we can observe that $\mathbf{w}_l^{(r)} = \mathbf{W}_{l,(-m)}^{(r)} \mathbf{w}_{l,m}^{(r)}$ with $\mathbf{W}_{l,(-m)}^{(r)} = (\mathbf{w}_{l,d_l}^{(r)} \otimes \dots \otimes \mathbf{w}_{l,m+1}^{(r)} \otimes \mathbf{I}_{p_{l,m}} \otimes \mathbf{w}_{l,m-1}^{(r)} \otimes \dots \otimes \mathbf{w}_{l,1}^{(r)}) \in \mathbb{R}^{p_l \times p_{l,m}}$ and that:

$$\nabla_l f(\mathbf{w})^\top \mathbf{w}_l = \sum_{r=1}^R \lambda_l^{(r)} \nabla_l f(\mathbf{w})^\top \mathbf{W}_{l,(-m)}^{(r)} \mathbf{w}_{l,m}^{(r)} = \text{Tr}(\mathbf{F}^\top \mathbf{W}_{l,m}), \quad (17)$$

$$\text{with } \mathbf{F} = [\mathbf{f}^{(1)} \quad \dots \quad \mathbf{f}^{(R)}] \quad \text{and} \quad \mathbf{f}^{(r)} = \lambda_l^{(r)} \mathbf{W}_{l,(-m)}^{(r)\top} \nabla_l f(\mathbf{w}) \in \mathbb{R}^{p_{l,m}}.$$

We can traduce the orthogonality constraint into the following constraints:

$$\begin{cases} \mathbf{w}_{l,m}^{(r)\top} \mathbf{W}_{l,(-m)}^{(r)\top} \mathbf{M}_l \mathbf{W}_{l,(-m)}^{(r)} \mathbf{w}_{l,m}^{(r)} = 1 \\ \mathbf{w}_{l,m}^{(r)\top} \mathbf{W}_{l,(-m)}^{(r)\top} \mathbf{M}_l \mathbf{w}_{l,m}^{(s)} = 0 \quad \text{for } r \neq s. \end{cases}$$

Unfortunately, it is not possible to find a matrix $\mathbf{M}_{l,m}$ such that $\mathbf{W}_{l,m}^\top \mathbf{M}_{l,m} \mathbf{W}_{l,m} = \mathbf{I}_{R_l}$. Therefore, we cannot end up with a problem of the following kind:

$$\underset{\mathbf{W}_{l,m}}{\text{argmax}} \text{Tr}(\mathbf{F}^\top \mathbf{W}_{l,m}) \quad \text{s.t.} \quad \mathbf{W}_{l,m}^\top \mathbf{M}_{l,m} \mathbf{W}_{l,m} = \mathbf{I}_{R_l}.$$

In this case, we did not find a better solution than to solve for each $\mathbf{w}_{l,m}^{(r)}$ in turn the optimization problems:

$$\underset{\mathbf{w}_{l,m}^{(r)}}{\text{argmax}} \mathbf{f}^{(r)\top} \mathbf{w}_{l,m}^{(r)} \quad \text{s.t.} \quad \begin{cases} \mathbf{w}_{l,m}^{(r)\top} \mathbf{W}_{l,(-m)}^{(r)\top} \mathbf{M}_l \mathbf{W}_{l,(-m)}^{(r)} \mathbf{w}_{l,m}^{(r)} = 1 \\ \mathbf{w}_{l,m}^{(r)\top} \mathbf{W}_{l,(-m)}^{(r)\top} \mathbf{M}_l \mathbf{w}_{l,m}^{(s)} = 0 \quad \text{for } r \neq s. \end{cases} \quad (18)$$

By writing the Lagrangian of (18), it is possible to find a closed form solution. The issue is that the constraints are no longer separated between the different $\mathbf{w}_{l,m}^{(r)}$, which leads the optimization scheme to get stuck in uninteresting points. See Figure 2 for an illustration of this phenomenon in a toy case. This is why we looked for another choice of the matrix \mathbf{K}_l and decided to try with $\mathbf{K}_l = \mathbf{I}_{R_l}$.

A.2 Update for non-separable TGCCA

Choosing $\mathbf{K}_l = \mathbf{I}_{R_l}$ leads to the optimization problem introduced in equation (7):

$$\underset{\mathbf{w}_1, \dots, \mathbf{w}_L}{\text{maximize}} \sum_{l,k=1}^L c_{lk} \mathbf{g}(\mathbf{w}_l^\top \boldsymbol{\Sigma}_{lk} \mathbf{w}_k)$$

$$\text{s.t. } \mathbf{w}_l = \llbracket \boldsymbol{\lambda}; \mathbf{W}_{l,1}, \dots, \mathbf{W}_{l,d_l} \rrbracket, \mathbf{W}_{l,m} \in \mathbb{R}^{p_{l,m} \times R_l}, \mathbf{W}_l^\top \mathbf{W}_l = \mathbf{I}_{R_l}, \|\boldsymbol{\lambda}_l\|_2 \leq \|\mathbf{M}_l\|_2^{-\frac{1}{2}} \quad l \in [L].$$

As shown in (17), for each $\mathbf{W}_{l,m}$, we have

$$\mathbf{r}_{l,m}(\mathbf{w}) = \underset{\mathbf{W}_{l,m}, \mathbf{W}_{l,m}^\top \mathbf{W}_{l,m} = \mathbf{I}_{R_l}}{\text{argmax}} \text{Tr}(\mathbf{F}^\top \mathbf{W}_{l,m}) = \mathbf{S} \mathbf{T}^\top, \quad (19)$$

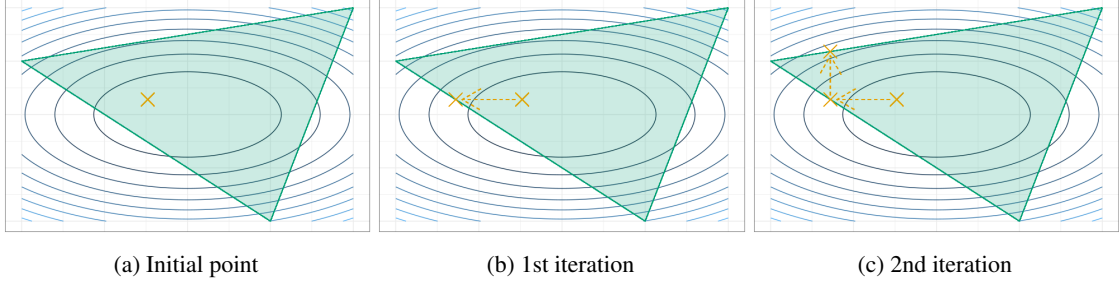


Figure 2: Illustration of the BCA strategy to maximize a convex function under entangled constraints. The concentric curves represent the levels of the function and the green triangle is the feasible set. After the second update, the BCA algorithm is stuck and cannot move anymore but the point is not a local maximum.

where \mathbf{S} and \mathbf{T} are respectively the left and right singular vectors of the rank- R_l SVD of \mathbf{F} . Hence we get the same kind of solution as 13.

What is specific to this non-separable case is the update of λ_l . To simplify the notations, we will note $\mathbf{u}_l = \mathbf{W}_l^\top \nabla_l f(\mathbf{w})$. We could try to do like before and search for

$$\lambda_l^{\text{opt}} = \underset{\lambda_l, \|\lambda_l\|_2 \leq \|\mathbf{M}_l\|_2^{-\frac{1}{2}}}{\text{argmax}} \quad \mathbf{u}_l^\top \lambda_l = \frac{\mathbf{u}_l}{\|\mathbf{M}_l\|_2^{-\frac{1}{2}} \|\mathbf{u}_l\|_2}.$$

However, this solution implies that we do not take into account the structure of \mathbf{M}_l in our optimization scheme. As our first goal was to solve (16), for a fixed \mathbf{W}_l , we consider:

$$\lambda_l^{\text{ref}} = \underset{\lambda_l, \lambda_l^\top \mathbf{W}_l^\top \mathbf{M}_l \mathbf{W}_l \lambda_l = 1}{\text{argmax}} \quad \mathbf{u}_l^\top \lambda_l = \frac{(\mathbf{W}_l^\top \mathbf{M}_l \mathbf{W}_l)^{-1} \mathbf{u}_l}{\sqrt{\mathbf{u}_l^\top (\mathbf{W}_l^\top \mathbf{M}_l \mathbf{W}_l)^{-1} \mathbf{u}_l}}.$$

To ensure that $\lambda_l^{\text{ref}\top} \mathbf{W}_l^\top \mathbf{M}_l \mathbf{W}_l \lambda_l^{\text{ref}}$ remains below 1 after the update of \mathbf{W}_l , we showed in Section 3 that we need to normalize λ_l^{ref} so that $\|\lambda_l^{\text{ref}}\|_2 \leq \|\mathbf{M}_l\|_2^{-\frac{1}{2}}$. Unfortunately, there is no guarantee that this new point would still allow to increase the value of the objective function.

Let λ_l^{prev} be the value of λ_l before the update. We define the following ball and hyperplane:

$$\begin{aligned} \mathcal{B}_\alpha &= \{\lambda_l \in \mathbb{R}^{R_l}; \lambda_l^\top \lambda_l \leq \alpha\} \\ \mathcal{H}_\epsilon &= \{\lambda_l \in \mathbb{R}^{R_l}; \mathbf{u}_l^\top \lambda_l \geq \epsilon\} \end{aligned}$$

We can aim for a compromise between λ_l^{ref} and λ_l^{opt} by projecting λ_l^{ref} on the intersection of the ball \mathcal{B}_α and \mathcal{H}_ϵ with $\alpha = \|\mathbf{M}_l\|_2^{-1}$ and $\epsilon \in [\mathbf{u}_l^\top \lambda_l^{\text{prev}}, \mathbf{u}_l^\top \lambda_l^{\text{opt}}]$. We arbitrarily choose $\epsilon = \frac{1}{2} (\mathbf{u}_l^\top \lambda_l^{\text{prev}} + \mathbf{u}_l^\top \lambda_l^{\text{opt}})$. From the definitions of λ_l^{prev} and λ_l^{opt} we are sure that $\epsilon \geq 0$.

Once we have computed λ_l^{ref} , two cases arise: either $\frac{\mathbf{u}_l^\top \lambda_l^{\text{ref}}}{\|\mathbf{M}_l\|_2^{-\frac{1}{2}} \|\lambda_l^{\text{ref}}\|_2} \geq \epsilon$ or $\frac{\mathbf{u}_l^\top \lambda_l^{\text{ref}}}{\|\mathbf{M}_l\|_2^{-\frac{1}{2}} \|\lambda_l^{\text{ref}}\|_2} < \epsilon$. In the first case, we can take

$$r_{l,\lambda}(\mathbf{w}) = \frac{\lambda_l^{\text{ref}}}{\|\mathbf{M}_l\|_2^{-\frac{1}{2}} \|\lambda_l^{\text{ref}}\|_2}. \quad (20)$$

In the second case, we have to find the projection λ_l^{ref} on the intersection of the frontiers of \mathcal{B}_α and \mathcal{H}_ϵ . This is equivalent to solve

$$\underset{\lambda_l}{\text{argmin}} \quad \frac{1}{2} \|\lambda_l - \lambda_l^{\text{ref}}\|_2^2 \quad \text{s.t.} \quad \lambda_l^\top \lambda_l = \alpha \text{ and } \mathbf{u}_l^\top \lambda_l = \epsilon \quad (21)$$

The Lagrangian associated with optimization problem (21) is

$$\mathcal{L}(\lambda_l, \mu, \nu) = \frac{1}{2} \|\lambda_l - \lambda_l^{\text{ref}}\|_2^2 + \frac{1}{2} \mu (\lambda_l^\top \lambda_l - \alpha) + \nu (\mathbf{u}_l^\top \lambda_l - \epsilon),$$

where $\mu, \nu \in \mathbb{R}$ are the Lagrange multipliers. Cancelling the derivative of the Lagrangian function with respect to λ_l yields the following stationary equation:

$$(1 + \hat{\mu}) \hat{\lambda}_l - \lambda_l^{\text{ref}} + \hat{\nu} \mathbf{u}_l = 0 \quad (22)$$

We can already notice that, if $(1 + \hat{\mu}) = 0$, λ_l^{ref} is collinear with \mathbf{u}_l , so $\frac{\lambda_l^{\text{ref}}}{\|\mathbf{M}_l\|_2^{-\frac{1}{2}} \|\lambda_l^{\text{ref}}\|_2} = \lambda_l^{\text{opt}}$. Thus, the optimal point we seek is $\hat{\lambda}_l = \lambda_l^{\text{opt}}$. We suppose now that $(1 + \hat{\mu}) \neq 0$.

Left multiplying (22) by \mathbf{u}_l^\top , it comes

$$\begin{aligned} \epsilon(1 + \hat{\mu}) - \mathbf{u}_l^\top \lambda_l^{\text{ref}} + \hat{\nu} \mathbf{u}_l^\top \mathbf{u}_l &= 0 \\ \Rightarrow \hat{\nu} &= \frac{\mathbf{u}_l^\top \lambda_l^{\text{ref}} - \epsilon(1 + \hat{\mu})}{\mathbf{u}_l^\top \mathbf{u}_l}. \end{aligned} \quad (23)$$

Left multiplying (22) by $\hat{\lambda}_l^\top$, we get

$$\begin{aligned} \alpha(1 + \hat{\mu}) - \hat{\lambda}_l^\top \lambda_l^{\text{ref}} + \hat{\nu} \epsilon &= 0 \\ \Rightarrow \alpha(1 + \hat{\mu})^2 + \hat{\nu} \epsilon(1 + \hat{\mu}) + (\hat{\nu} \mathbf{u}_l - \lambda_l^{\text{ref}})^\top \lambda_l^{\text{ref}} &= 0 \text{ multiplying by } (1 + \hat{\mu}) \text{ and reinjecting (22)} \\ \Rightarrow \left(\alpha - \frac{\epsilon^2}{\mathbf{u}_l^\top \mathbf{u}_l} \right) (1 + \hat{\mu})^2 - \lambda_l^{\text{ref}\top} \lambda_l^{\text{ref}} + \frac{(\mathbf{u}_l^\top \lambda_l^{\text{ref}})^2}{\mathbf{u}_l^\top \mathbf{u}_l} &= 0 \text{ reinjecting (23)} \end{aligned}$$

We observe that $(1 + \hat{\mu})$ satisfies a binomial equation and that

$$\begin{aligned} \lambda_l^{\text{ref}\top} \lambda_l^{\text{ref}} - \frac{(\mathbf{u}_l^\top \lambda_l^{\text{ref}})^2}{\mathbf{u}_l^\top \mathbf{u}_l} &= \lambda_l^{\text{ref}\top} (\mathbf{I}_{R_l} - \mathbf{u}_l (\mathbf{u}_l^\top \mathbf{u}_l)^{-1} \mathbf{u}_l^\top) \lambda_l^{\text{ref}} \\ &= \lambda_l^{\text{ref}\top} \mathbf{P}_{\mathbf{u}_l^\perp} \lambda_l^{\text{ref}} \\ &= \|\mathbf{P}_{\mathbf{u}_l^\perp} \lambda_l^{\text{ref}}\|_2^2, \end{aligned}$$

where $\mathbf{P}_{\mathbf{u}_l^\perp}$ is the projector on the hyperplane orthogonal to $\text{span}(\mathbf{u}_l)$. We can show that, for every $\epsilon \in [\mathbf{u}_l^\top \lambda_l^{\text{prev}}, \mathbf{u}_l^\top \lambda_l^{\text{opt}}]$, $\frac{\epsilon^2}{\mathbf{u}_l^\top \mathbf{u}_l} \leq \alpha$. Indeed, $\forall \epsilon \in [\mathbf{u}_l^\top \lambda_l^{\text{prev}}, \mathbf{u}_l^\top \lambda_l^{\text{opt}}]$, $\exists \gamma \in [0, 1]$, $\epsilon = ((1 - \gamma) \lambda_l^{\text{prev}} + \gamma \lambda_l^{\text{opt}})^\top \mathbf{u}_l$. Therefore,

$$\begin{aligned} \frac{\epsilon^2}{\mathbf{u}_l^\top \mathbf{u}_l} &= ((1 - \gamma) \lambda_l^{\text{prev}} + \gamma \lambda_l^{\text{opt}})^\top \mathbf{u}_l (\mathbf{u}_l^\top \mathbf{u}_l)^{-1} \mathbf{u}_l^\top ((1 - \gamma) \lambda_l^{\text{prev}} + \gamma \lambda_l^{\text{opt}}) \\ &= \|\mathbf{P}_{\mathbf{u}_l} ((1 - \gamma) \lambda_l^{\text{prev}} + \gamma \lambda_l^{\text{opt}})\|_2^2 \text{ where } \mathbf{P}_{\mathbf{u}_l} \text{ is the orthogonal projector on } \text{span}(\mathbf{u}_l) \\ &\leq \|((1 - \gamma) \lambda_l^{\text{prev}} + \gamma \lambda_l^{\text{opt}})\|_2^2 \text{ since } \|\mathbf{P}_{\mathbf{u}_l}\|_2 \leq 1 \\ &\leq (1 - \gamma) \|\lambda_l^{\text{prev}}\|_2^2 + \gamma \|\lambda_l^{\text{opt}}\|_2^2 \text{ using the norm convexity} \\ &= \alpha. \end{aligned}$$

If $\frac{\epsilon^2}{\mathbf{u}_l^\top \mathbf{u}_l} = \alpha$, we have that $\mathbf{P}_{\mathbf{u}_l^\perp} \lambda_l^{\text{ref}} = 0$ so we fall back to the case where λ_l^{ref} is collinear with \mathbf{u}_l . Otherwise we get

$$(1 + \hat{\mu}) = \pm \frac{\|\mathbf{P}_{\mathbf{u}_l^\perp} \lambda_l^{\text{ref}}\|_2}{\sqrt{\alpha - \frac{\epsilon^2}{\mathbf{u}_l^\top \mathbf{u}_l}}}. \quad (24)$$

Finally, if λ_l^{ref} is not collinear with \mathbf{u}_l , using equations (22), (23) and (24), we find

$$\hat{\lambda}_l = \frac{\epsilon}{\mathbf{u}_l^\top \mathbf{u}_l} \mathbf{u}_l + \sqrt{\alpha - \frac{\epsilon^2}{\mathbf{u}_l^\top \mathbf{u}_l}} \frac{\mathbf{P}_{\mathbf{u}_l^\perp} \lambda_l^{\text{ref}}}{\|\mathbf{P}_{\mathbf{u}_l^\perp} \lambda_l^{\text{ref}}\|_2}, \quad (25)$$

where the sign is determined by looking for the solution that minimizes (21). Thanks to this formulation, we managed to find an update for $\hat{\lambda}_l$ that takes into account the structure of \mathbf{M}_l through the contribution of λ_l^{ref} .

B Compactness of the feasible set

The proof of Proposition 1 directly follows the demonstration proposed in Tenenhaus et al. (2017). It relies on two key ingredients: (i) the compactness of the feasible set of the optimization problem and (ii) the uniqueness of the update. While the uniqueness of the update relies on rank conditions and cannot be a priori verified but can be monitored at runtime, the compactness of the feasible set can be proven as follows.

The feasible set Ω_l associated with both problems (6) and (7) can be defined as:

$$\Omega_l = \{\mathbf{w}_l \in \mathbb{R}^{p_l}; \mathbf{w}_l = \sum_{r=1}^{R_l} \lambda_l^{(r)} \mathbf{w}_l^{(r)}; \mathbf{w}_l^{(r)} = \mathbf{w}_{l,d_l}^{(r)} \otimes \dots \otimes \mathbf{w}_{l,1}^{(r)}; \mathbf{W}_l^\top \mathbf{W}_l = \mathbf{I}_{R_l}; \lambda_l^\top \lambda_l \leq \alpha\}. \quad (26)$$

In the case of (6), we have $\lambda_l^\top \lambda_l = 1$ but this does not change the proof.

To show the result, we introduce the following sets:

$$\begin{aligned} \Omega_{\text{norm}} &= \{\mathbf{w}_l \in \mathbb{R}^{p_l}; \mathbf{w}_l^\top \mathbf{w}_l = 1\}, \\ \Omega_{\text{kron}} &= \{\mathbf{w}_l \in \mathbb{R}^{p_l}; \mathbf{w}_l = \mathbf{w}_{l,d_l} \otimes \dots \otimes \mathbf{w}_{l,1}\}, \\ \Omega_{\text{mat}} &= \{\mathbf{W}_l \in \mathbb{R}^{p_l \times R_l}; \mathbf{W}_l = [\mathbf{w}_l^{(1)} \quad \dots \quad \mathbf{w}_l^{(R_l)}]; \mathbf{w}_l^{(r)} \in \Omega_{\text{norm}} \cap \Omega_{\text{kron}}\}, \\ \Omega_{\text{orth}} &= \{\mathbf{W}_l \in \mathbb{R}^{p_l \times R_l}; \mathbf{W}_l^\top \mathbf{W}_l = \mathbf{I}_{R_l}\}, \\ \Lambda_l &= \{\lambda_l \in \mathbb{R}^{R_l}; \lambda_l^\top \lambda_l \leq \alpha\}. \end{aligned}$$

Using these sets, a new way to express Ω_l is derived:

$$\Omega_l = \{\mathbf{w}_l \in \mathbb{R}^{p_l}; \mathbf{w}_l = \mathbf{W}_l \lambda_l; \mathbf{W}_l \in \Omega_{\text{mat}} \cap \Omega_{\text{orth}}; \lambda_l \in \Lambda_l\}$$

Therefore, Ω_l is the image of the set $\Lambda_l \times (\Omega_{\text{mat}} \cap \Omega_{\text{orth}})$ by the continuous application $f : (\lambda_l, \mathbf{W}_l) \mapsto \mathbf{W}_l \lambda_l$. The proof that Ω_l is compact then reduces to prove that Λ_l and $\Omega_{\text{mat}} \cap \Omega_{\text{orth}}$ are compact.

Λ_l is compact as the norm-2 ball of radius α in \mathbb{R}^{R_l} which is of finite dimension. In the case $\lambda_l^\top \lambda_l = \alpha$, Λ_l becomes the boundary of this ball which remains a compact.

We will now show that $\Omega_{\text{mat}} \cap \Omega_{\text{orth}}$ is compact as the intersection of a compact set with a closed set.

- Ω_{norm} is a compact set as the boundary of the norm-2 unit ball.
- Ω_{kron} is a closed set. It is a standard result in geometric algebra and a specificity of the set of rank-1 tensors.
- $\Omega_{\text{norm}} \cap \Omega_{\text{kron}}$ is compact as the intersection of a closed and a compact set.
- Ω_{mat} is the image of $\times_{R_l} (\Omega_{\text{norm}} \cap \Omega_{\text{kron}})$ (the Cartesian product R_l times) by the continuous operator that arranges vectors into a matrix. Hence, Ω_{mat} is compact.
- Ω_{orth} is the set of semi-orthogonal matrices. This set is closed (and even compact but we only need it to be closed).

Consequently, $\Omega_{\text{mat}} \cap \Omega_{\text{orth}}$ is compact and we have shown that Ω_l is a compact set.

In the case where only one mode m bears the orthogonality, similar arguments can be derived to show that Ω_l is indeed compact.

C Rank versus number of canonical components

Introducing CCA with canonical vectors admitting a rank- R CP decomposition may create a confusion between the rank of the decomposition and the number of extracted canonical components. This section describes the differences between the two concepts and between MGCCA with the deflation procedure imposing "orthogonality on the weight vectors" (see Section 2.4.2 of Gloaguen et al. (2020)) and TGCCA.

C.1 Extracting K canonical components

In the main text, the described optimization problems aim to find the first canonical component for each block given by $\mathbf{y}_l^{[1]} = \mathbf{X}_l \mathbf{w}_l^{[1]}$. This first canonical component summarizes the information between and within the blocks but as the first component of Principal Component Analysis (PCA) alone does not always wholly explain the dataset, this first canonical component will not always be enough. We want to find other canonical components by finding new sets of canonical vectors in this context. One of the possible ways is to impose that the new canonical components are not correlated with the previous ones. This can be written:

$$\begin{aligned} & \underset{\mathbf{w}_1^{[2]}, \dots, \mathbf{w}_L^{[2]}}{\text{maximize}} \sum_{l,k=1}^L c_{lk} \mathfrak{g} \left(\mathbf{w}_l^{[2]\top} \Sigma_{lk} \mathbf{w}_k^{[2]} \right) \\ & \text{s.t.} \quad \begin{cases} \mathbf{w}_l^{[2]\top} \mathbf{M}_l \mathbf{w}_l^{[2]} = 1, \quad l \in [L] \\ \mathbf{w}_l^{[2]\top} \Sigma_{lk} \mathbf{w}_k^{[1]} = 0, \quad (l, k) \in [L]^2. \end{cases} \end{aligned} \quad (27)$$

This is the usual way of searching for the next canonical components, see for example Haroon et al. (2004). This can be implemented in practice by applying a deflation strategy to each block \mathbf{X}_l : $\mathbf{X}_l^{[1]} = \mathbf{X}_l - \mathbf{y}_l^{[1]} \left(\mathbf{y}_l^{[1]\top} \mathbf{y}_l^{[1]} \right)^{-1} \mathbf{y}_l^{[1]\top} \mathbf{X}_l$, consider $\Sigma_{lk}^{[1]}$ the covariance between $\mathbf{X}_l^{[1]}$ and $\mathbf{X}_k^{[1]}$, and solve:

$$\underset{\mathbf{w}_1^{[2]}, \dots, \mathbf{w}_L^{[2]}}{\text{maximize}} \sum_{l,k=1}^L c_{lk} \mathfrak{g} \left(\mathbf{w}_l^{[2]\top} \Sigma_{lk}^{[1]} \mathbf{w}_k^{[2]} \right) \quad \text{s.t.} \quad \mathbf{w}_l^{[2]\top} \mathbf{M}_l \mathbf{w}_l^{[2]} = 1, \quad l \in [L]. \quad (28)$$

This is what is done for example in Section 2.4.1 of Gloaguen et al. (2020).

Another possibility is to impose different constraints on the new set of canonical vectors with respect to the first ones. In Section 2.4.2 of Gloaguen et al. (2020), the authors impose that $\mathbf{w}_l^{[2]\top} \mathbf{w}_l^{[1]} = 0$. Therefore the different canonical vectors, for a given block, are orthogonal. Using the rank-1 CP decompositions of the canonical vectors, it imposes that either $\mathbf{w}_{l,1}^{[2]\top} \mathbf{w}_{l,1}^{[1]} = 0$ or $\mathbf{w}_{l,2}^{[2]\top} \mathbf{w}_{l,2}^{[1]} = 0$. They show that this leads to the proposition of a new deflation procedure that guarantees to get a new canonical vector satisfying the constraint.

Whatever the choices of constraints on the different sets of canonical vectors, the procedures can be iterated to extract K sets of canonical vectors.

C.2 Rank- R TGCCA vs MGCCA with R components

Using the last presented approach and extracting R components, MGCCA generates $\mathbf{W}_l^{\text{MGCCA}} = \left[\mathbf{w}_l^{[1]}, \dots, \mathbf{w}_l^{[R]} \right]$ for each block. From this, we can construct $\mathbf{w}_l^{\text{MGCCA}} = \sum_{r=1}^R \mathbf{w}_l^{[r]}$ which results in a vector that admits an orthogonal rank- R CP decomposition for which each factor of the decomposition has the same contribution ($\forall r \in [R], \lambda_l^{[r]} = 1$). On the contrary, rank- R TGCCA generates $\mathbf{w}_l^{\text{TGCCA}} = \sum_{r=1}^R \lambda_l^{(r)} \mathbf{w}_l^{(r)}$ so TGCCA has the flexibility to weight differently the different factors and can reduce the importance of the factors that are just modelling noise. Furthermore, the criteria they optimize are different:

$$\text{crit}^{\text{MGCCA}} = \sum_{l,k=1}^L c_{lk} \sum_{r=1}^R \mathfrak{g} \left(\mathbf{w}_l^{[r]\top} \Sigma_{lk}^{[r]} \mathbf{w}_k^{[r]} \right), \quad (29)$$

$$\text{crit}^{\text{TGCCA}} = \sum_{l,k=1}^L c_{lk} \mathfrak{g} \left(\sum_{r,s=1}^R \lambda_l^{(r)} \lambda_l^{(s)} \mathbf{w}_l^{(r)\top} \Sigma_{lk} \mathbf{w}_k^{(s)} \right). \quad (30)$$

Ignoring the \mathfrak{g} function and the modified $\Sigma_{lk}^{[r]}$ matrices, we can see that MGCCA only takes into account the interactions between the same levels of factors, while TGCCA takes into account all the interactions.

D Complexity analysis

We propose in this section a time complexity analysis between RGCCA and the separable version of TGCCA. To simplify the computations and notations, we will say that all blocks have the same number of modes d , the same number of variables per mode q and therefore the same total number of variables $p = q^d$. We note n the number of observations and L the number of blocks. We will give for the two methods the complexity of the update and the complexity of the initialization. We will also consider that the estimates of the regularization matrices $\hat{\mathbf{M}}_l$ are regularized estimates of the block covariances Σ_{ll} .

D.1 RGCCA initialization

In the case of RGCCA, $\hat{\mathbf{M}}_l = \tau \mathbf{I}_p + (1 - \tau) \frac{\mathbf{X}_l^\top \mathbf{X}_l}{n}$. We can apply the same change of variable as in the separable version of TGCCA (see Section 4.1). In practice, we need to compute $\hat{\mathbf{M}}_l^{-\frac{1}{2}}$ and $\mathbf{X}_l \hat{\mathbf{M}}_l^{-\frac{1}{2}}$. Using the SVD of \mathbf{X}_l , we can write $\mathbf{X}_l = \mathbf{S} \mathbf{\Delta} \mathbf{T}^\top$, and we get $\hat{\mathbf{M}}_l^{-\frac{1}{2}} = \mathbf{T} (\tau + \frac{(1-\tau)}{n} \mathbf{\Delta}^2)^{-\frac{1}{2}} \mathbf{T}^\top$. The complexity of the SVD of \mathbf{X}_l is $\mathcal{O}(np \min(n, p))$ and the computation of $\hat{\mathbf{M}}_l$ is $\mathcal{O}(p^2 \min(n, p))$. The complexity of computing $\mathbf{X}_l \hat{\mathbf{M}}_l^{-\frac{1}{2}}$ is $\mathcal{O}(np^2)$.

We can show that this change of variable step is the bottleneck of RGCCA initialization and, as we need to do it for every block, the overall complexity is $\mathcal{O}(L(np(p + \min(n, p)))) = \mathcal{O}(Lnp^2)$.

D.2 Separable TGCCA initialization

In the case of separable TGCCA, $\hat{\mathbf{M}}_l = \hat{\mathbf{M}}_{l,d} \otimes \cdots \otimes \hat{\mathbf{M}}_{l,1} = \left(\hat{\Sigma}_{ll,d} + \sqrt[d]{\tau} \mathbf{I}_{p_d} \right) \otimes \cdots \otimes \left(\hat{\Sigma}_{ll,1} + \sqrt[d]{\tau} \mathbf{I}_{p_1} \right)$ and $\hat{\Sigma}_{ll,m}$ are obtained as in Section 4.2.1 of Min et al. (2019). Each of these estimates can be computed in $\mathcal{O}(npq)$. Then, we need to compute $\hat{\mathbf{M}}_{l,m}^{-\frac{1}{2}}$, which can be done in $\mathcal{O}(q^3)$. Finally, $\mathbf{X}_l \hat{\mathbf{M}}_l^{-\frac{1}{2}}$ must be computed, this can be done efficiently by folding \mathbf{X}_l back to $\mathcal{X}_l \in \mathbb{R}^{n \times q \times \cdots \times q}$ and computing $\mathcal{X}_l \times_2 \hat{\mathbf{M}}_{l,1}^{-\frac{1}{2}} \cdots \times_{d+1} \hat{\mathbf{M}}_{l,d}^{-\frac{1}{2}}$, where \times_m represents the mode-product between the m^{th} -mode of \mathcal{X}_l and $\hat{\mathbf{M}}_{l,m}^{-\frac{1}{2}}$. Each of these operations has a complexity of $\mathcal{O}(npq)$.

Since there are d operations per block and there are L blocks, the total cost of the change of variables is $\mathcal{O}(Ldq(np + q^2))$. As for RGCCA, this is also the bottleneck for the separable TGCCA initialization. Considering that there are at least 2 modes (i.e., $d \geq 2$) and that all modes have the same number of variables q , the complexity can be simplified to $\mathcal{O}(Lnpdq)$. We can see that we managed to trade a factor dq against a factor $p = q^d$ in RGCCA.

D.3 Updates

The bottlenecks of both RGCCA and separable TGCCA are the computations of $\mathbf{y}_l = \mathbf{X}_l \mathbf{w}_l$ and $\mathbf{z}_l = \sum_{k=1}^L c_{kl} \mathbf{g}'(\mathbf{y}_l^\top \mathbf{y}_k) \mathbf{y}_k$. The associated complexities are respectively $\mathcal{O}(np)$ and $\mathcal{O}(Ln)$. For both methods, these computations have to be repeated for each block but for separable TGCCA, these computations also have to be repeated for each mode. Therefore we get that the complexities of the updates of RGCCA and separable TGCCA are respectively $\mathcal{O}(Ln(p + L))$ and $\mathcal{O}(Ldn(p + L))$. We can see that, compared to RGCCA, we lose a factor d on the complexity of the update. This is due to the fact that we have added an extra layer of BCA compared to RGCCA.

If we note T^{RGCCA} and T^{TGCCA} the number of iterations needed for RGCCA and separable TGCCA to reach convergence, we have:

$$\begin{aligned} \text{complexity(RGCCA)} &= \mathcal{O}(Lnp^2 + T^{\text{RGCCA}} Ln(p + L)) \\ \text{complexity(TGCCA)} &= \mathcal{O}(Lnpdq + T^{\text{TGCCA}} Lnd(p + L)). \end{aligned}$$

E Retrieving the chemicals

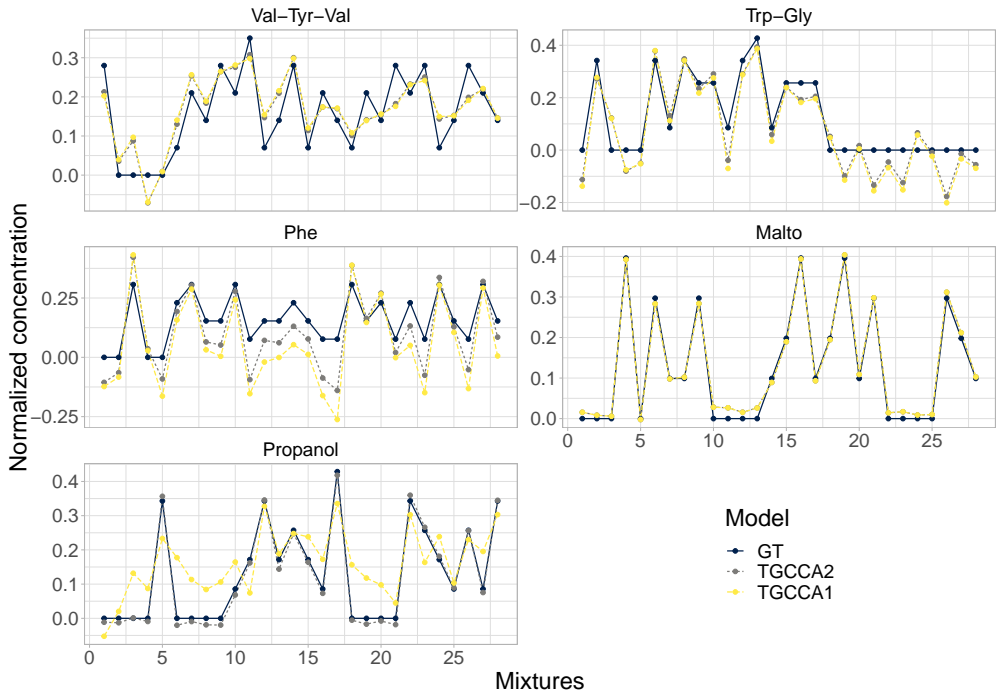


Figure 3: Normalized concentrations of the different chemicals for both rank-2 TGCCA and rank-1 TGCCA, we can see that rank-1 TGCCA does not capture Propanol as well as rank-2 TGCCA.

In the study of the dataset from Acar et al. (2014b), we are interested in finding the concentrations of the five chemicals in the 28 available mixtures. This information is contained in the matrix \mathbf{A} following the notation of (15). Nevertheless, we do not estimate this matrix using TGCCA. To avoid this problem, we suppose that, if \mathbf{B} and \mathbf{C} are well estimated, \mathbf{A} can be deduced through the following optimisation problem:

$$\operatorname{argmin}_{\mathbf{A}} \|\mathbf{X}_{(1)} - \mathbf{A}\mathbf{\Lambda}(\mathbf{B} \odot \mathbf{C})^\top\|_F^2, \quad (31)$$

where $\mathbf{\Lambda} = \operatorname{diag}(\boldsymbol{\lambda})$. Hence we get

$$\mathbf{A} = \mathbf{X}_{(1)}\mathbf{\Lambda}(\mathbf{B} \odot \mathbf{C}) (\mathbf{\Lambda}(\mathbf{B} \odot \mathbf{C})^\top(\mathbf{B} \odot \mathbf{C})\mathbf{\Lambda})^{-1}. \quad (32)$$

In the case of TGCCA of rank 2, we extract for the first block $\mathbf{W}_{1,1} \in \mathbb{R}^{13324 \times 2}$ and $\mathbf{W}_{1,2} \in \mathbb{R}^{8 \times 2}$. We use these two matrices respectively as our matrices \mathbf{C} and \mathbf{B} . As we imposed orthogonality constraints on columns of \mathbf{B} and \mathbf{C} , equation (32) gives $\mathbf{A} = \mathbf{X}_{(1)}(\mathbf{B} \odot \mathbf{C})\mathbf{\Lambda}^{-1}$. This gives us the first two columns of the matrix \mathbf{A} . For the next ones, we deflate the \mathcal{X} tensor and repeat the procedure. As the next extracted components are of rank 1, the next columns of \mathbf{A} are computed as $\mathbf{X}_{(1)}^{[k]} \mathbf{w}_1^{[k+1]}$ for $k \in [3]$ where $\mathbf{X}_{(1)}^{[k]}$ is the mode-1 matricization of the tensor after its k^{th} deflation, and $\mathbf{w}_1^{[k+1]}$ is the associated canonical vector returned by TGCCA.

E.1 Extracting Propanol

According to Acar et al. (2014b), the concentration of Propanol cannot be inferred from the matrix block. Therefore, we do not expect to properly find it as a component extracted by TGCCA. Instead, we use the fact that overestimating the rank of the canonical vector leads to estimating factors that explain some extra variance of the block. This is why we look for a first component of rank 2 and expect to find Propanol as the second extracted factor. This is indeed the case, and we can see that $\lambda_1^{(2)}$, the weight associated with the second factor of the first block, is really low (≈ 0.03). This means that TGCCA remains robust in estimating the correlated component, even when the rank is overestimated. Figure 3 shows that TGCCA with only rank-1 factors (i.e., MGCCA) cannot accurately estimate the true concentration of Propanol. Interestingly, Propanol is partially found as the fifth component extracted by rank-1 TGCCA. A better way to retrieve the Propanol concentration would be to have a specific way to identify unshared factors between blocks.

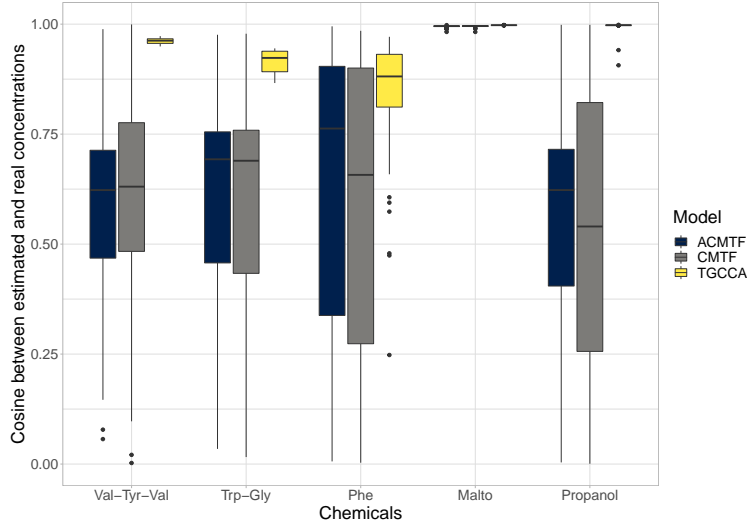


Figure 4: Boxplots of the cosines between the true concentrations and the estimated ones for TGCCA, CMTF and ACMTF.

E.2 Comparing best models

As TGCCA, CMTF and ACMTF are all unsupervised methods, we select the best model for each method by keeping the one with the best criterion. For CMTF and ACMTF, we choose the model that minimizes equation (15). For TGCCA, we sum the values obtained for criterion (3) for each component and keep the model with the highest sum. It is worth noting that, for both TGCCA and ACMTF, this best model does not correspond with the one that maximizes each of the cosines between the five estimated and real vectors of concentrations (see Figure 4). We plot in Figure 5 the vectors of concentrations reconstructed by the best models. We can witness that, for the columns of \mathbf{A} found after deflation (i.e., Val-Tyr-Val, Trp-Gly, and Phe), TGCCA seems less accurate than the other methods. This advocates elaborating a global algorithm to extract the different canonical vectors jointly.

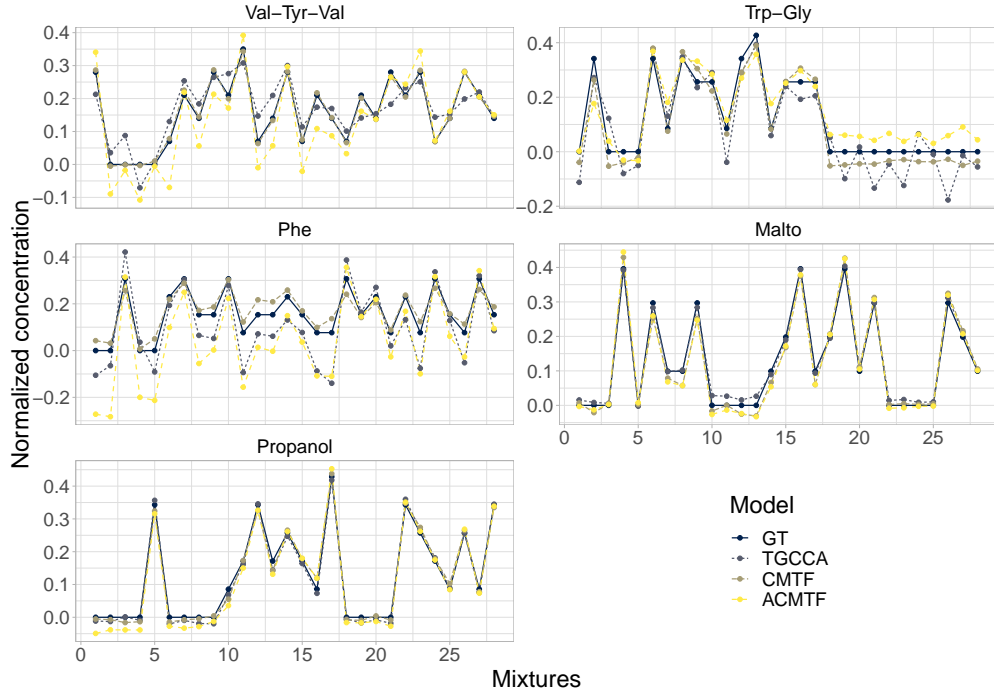


Figure 5: Normalized concentrations of the different chemicals for TGCCA, CMTF and ACMTF.

F Matching faces from the Multi-Pie Face dataset

F.1 Presentation of the dataset

The Multi-Pie Face dataset (Gross et al., 2008) consists of images of people’s faces. For each person, pictures are taken under 20 illumination conditions, 15 views, and different facial expressions. We take cropped images used in Tian et al. (2018), available on their github repository. This extraction consists of color images of size 128×128 from 250 subjects in two facial expressions (neutral and smile). We select the first 100 subjects to form our training set and the next 100 for the testing set. We use grayscale versions of the images and downsample them to size 64×64 using linear interpolation with the R package imager (Barthelmé and Tschumperlé, 2019). We select two views corresponding to cameras 05_1 and 05_0, which are positioned at angles 0° and -15° around the subject. We arbitrarily select 15 illumination conditions (2 to 6 and 10 to 19) and the neutral facial expression. The resulting images for the first subject are shown in Figure 6. For each pose, we stack the images to make a tensor of dimensions $100 \times 64 \times 64 \times 15$.



Figure 6: Images of the first subject in all illumination conditions. Each row corresponds to a different view.

F.2 Pairing subjects

Our goal is to use CCA methods to learn a common latent subspace between the two tensor blocks and use this learned representation in a classification task: given new subjects in the two views, pair the subjects across the two views. We compare RGCCA and spTGCCA with ranks 1 and 3. As the number of variables is much greater than the number of subjects, we use the identity matrix as the regularization matrix M_l in the RGCCA framework. The different canonical components are extracted using the deflation procedure for orthogonal components described in Section C.1.

Once this subspace has been learned, it can be used to project new images. The projection is obtained by applying the preprocessing (centering and uniform scaling) used on the training set to the testing set and multiplying the image with the corresponding canonical vector. However, this last step is impossible since the canonical vectors have been learned using the 15 illumination conditions. Leveraging the structure of canonical vectors in TGCCA, we propose a workaround. Let $\mathcal{X} \in \mathbb{R}^{64 \times 64 \times 15}$ and $\mathcal{W} = \mathbf{w}_1 \circ \mathbf{w}_2 \circ \mathbf{w}_3 \in \mathbb{R}^{64 \times 64 \times 15}$,

$$\mathbf{x}^\top \mathbf{w} = \mathcal{X} \times_1 \mathbf{w}_1 \times_2 \mathbf{w}_2 \times_3 \mathbf{w}_3 = \text{Vec}(\mathcal{X} \times_1 \mathbf{w}_1 \times_2 \mathbf{w}_2)^\top \mathbf{w}_3, \quad (33)$$

where \times_m denotes the mode- m product. If only slice j is available on the third mode of \mathcal{X} , only the product $\text{Vec}(\mathcal{X} \times_1 \mathbf{w}_1 \times_2 \mathbf{w}_2)_j w_{3,j}$ can be computed. This creates a partial projection equivalent to the full projection if the other tensor slices are filled with zeros. As training images have been centered, this zero-imputation reduces to imputing the missing slices to the means of the training subjects. If more slices are available (i.e., images of the same subjects are given in more than one illumination condition), (33) shows that they can just be added to the tensor while setting missing slices to zero. This reasoning works as-is for a rank- R tensor \mathcal{W} , so it can be applied even if the tensor rank is possibly high such as in the case of the folded version of a canonical vector obtained with RGCCA.

For both projecting and centering the testing images, it is necessary to know in which illumination conditions the images are. We assume these illumination conditions are unknown and must be inferred from the data using a Linear Discriminant Analysis (LDA) classifier. This classifier is trained on the $100 \times 15 \times 2 = 3000$ images of the training set that were downsampled to size 16×16 using linear interpolation. This downsampling allows having more images than variables while leaving enough information to predict the illumination condition from the image. Cross-validation on the training set showed that gathering images from the two views was more interesting than training two classifiers.

As projections are partial when images are not present in all illumination conditions, we investigate the impact of the number of available illumination conditions by varying this number from 1 to 15. Therefore, we create 15 classification tasks where we aim to pair subjects across views. Each subject in each view is represented by a tensor of dimensions $64 \times 64 \times i$ with $i \in [15]$. The first step is to predict the illumination condition of each image by downsampling it and applying the LDA classifier. Then, the missing slices of the tensor are zero-imputed. Finally, the completed tensors are projected using the learned canonical vectors.

The pairing is then done based on the distances between the projections of the subjects in each view. As in Lu (2013), we tried the ℓ_1 and ℓ_2 norms and the opposite of the cosine. Cross-validation on the training set showed that the cosine worked best for our task. Finding the best pairing is equivalent to finding the assignment that solves:

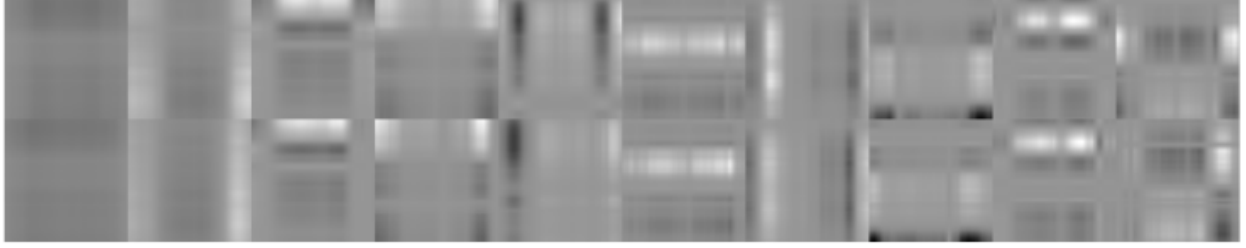
$$\underset{\mathbf{P} \in \{0,1\}^{n \times n}}{\text{maximize}} \sum_{i,j=1}^n p_{ij} d_{ij} \quad \text{s.t.} \quad \begin{cases} \forall i \in [n], \sum_{j=1}^n p_{ij} = 1, \\ \forall j \in [n], \sum_{i=1}^n p_{ij} = 1, \end{cases}$$

where $d_{ij} = -\frac{\mathbf{y}_{1i}^\top \mathbf{y}_{2j}}{\|\mathbf{y}_{1i}\|_2 \|\mathbf{y}_{2j}\|_2}$, and \mathbf{y}_{li} is the projection of subject i from view l . This problem can be efficiently solved using Integer Linear Programming. Finally, the accuracy of the matching can be measured and reported.

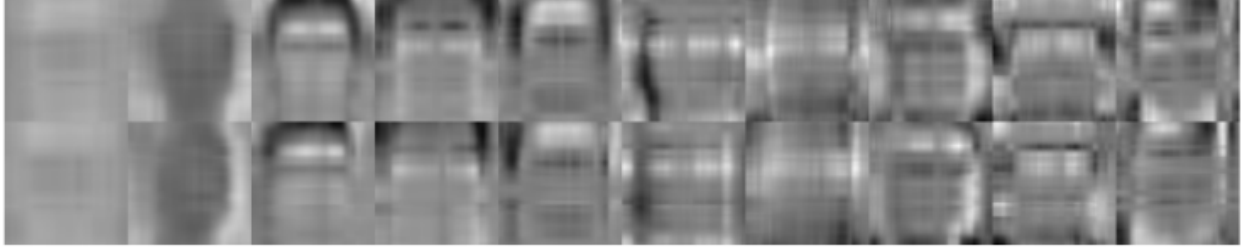
F.3 Results

Since the illumination conditions are randomly sampled, we repeat the experiments 100 times to get a better sense of the matching accuracy based on the latent subspaces learned by the different models. The results are shown in Figure 1. Rank-3 TGCCA seems to be the best-performing method, followed by rank-1 TGCCA and RGCCA. While RGCCA learns "eigenfaces", TGCCA models remain more abstract and focus on face locations with higher variations (see Figure 8).

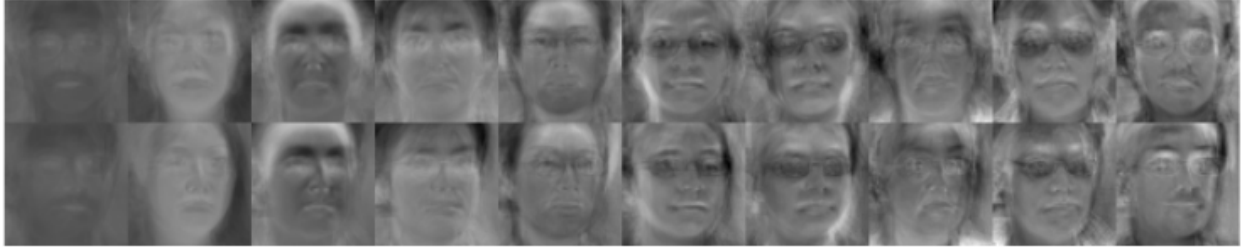
Figure 1 shows some dispersion even when the number of available illumination conditions is 15. This is explained by the fact that the classifier is applied to all test images at once without trying to predict 15 different illumination conditions for each subject. As a consequence, if an illumination condition is predicted twice, only one of the images will be used in the subject tensor, and the missing predictions will be set to zero. The variation is then due to the order in which the 15 illumination conditions are sampled.



(a) Rank-1 TGCCA



(b) Rank-3 TGCCA



(c) RGCCA

Figure 7: First 10 pairs of canonical vectors obtained with the three methods. Canonical vectors have been folded to shape $64 \times 64 \times 15$ and averaged over the last mode. Each row corresponds to a different view.

G Simulations

In this section, we present the data model used in the simulations presented in Section 5, we detail the parameters of the numerical experiments and give more results with different numbers of samples, different levels of signal-to-noise ratio (SNR), and different number of blocks.

G.1 Data model

To evaluate the quality of the estimates provided by TGCCA, we extend the probabilistic TCCA model described in Min et al. (2019). Let ρ_{lk} for $l, k \in [L]$ be the pairwise correlations between blocks and \mathbf{w}_l be given canonical vectors. We define:

- the block covariance matrix Σ_{ll}^η as:

$$\Sigma_{ll}^\eta = \mathbf{S}_l + \frac{\|\mathbf{S}_l\|_F}{\eta \|\mathbf{E}_l\|_F} \mathbf{E}_l, \quad \text{with} \quad \mathbf{S}_l = \frac{\mathbf{w}_l \mathbf{w}_l^\top}{\|\mathbf{w}_l\|_2^4} \quad \text{and} \quad \mathbf{E}_l = \mathbf{P}_l \mathbf{T}_l \mathbf{T}_l^\top \mathbf{P}_l, \quad (34)$$

where \mathbf{T}_l is a $p_l \times p_l$ arbitrary matrix, enabling noising \mathbf{x}_l ; and $\mathbf{P}_l = \mathbf{I}_{p_l} - \frac{\mathbf{w}_l \mathbf{w}_l^\top}{\|\mathbf{w}_l\|_2^2}$ is the projector onto the orthogonal of $\text{span}(\mathbf{w}_l)$, ensuring that $\mathbf{w}_l^\top \Sigma_{ll}^\eta \mathbf{w}_l = 1$. The SNR is controlled by the parameter η .

- a linear transformation $\mathbf{a}_l = \rho_l \Sigma_{ll}^\eta \mathbf{w}_l$, where $\rho_l \in [-1, 1]$ with $\rho_{lk} = \rho_l \rho_k$.

The simulated data is generated using the following latent factor model:

$$\mathbf{x}_l | z \sim \mathcal{N}(\mathbf{a}_l z, \Sigma_{ll}^\eta - \mathbf{a}_l \mathbf{a}_l^\top) \quad \text{with} \quad z \sim \mathcal{N}(0, 1).$$

This allows the joint distribution of $(\mathbf{x}_1, \dots, \mathbf{x}_L)$ to be $\mathcal{N}(0, \Sigma^\eta)$ where $\Sigma^\eta = [\Sigma_{lk}^\eta]_{\{l,k \in [L]\}}$ and $\Sigma_{lk}^\eta = \Sigma_{ll}^\eta \mathbf{w}_l \rho_{lk} \mathbf{w}_k^\top \Sigma_{kk}^\eta$. Thanks to this model, the blocks are correlated through the linear transformation of the latent variable z .

G.2 Data generation

In our numerical study, we generate data with $L = 5$ blocks. Information about the different blocks can be found in Table 4. The folded shapes of the first 4 canonical vectors can be seen in Figure 8. 10 folds of data are generated with $n = 1000$ samples per fold. $\rho_l = \sqrt{0.8}$ for $l \in [L]$ so every $\rho_{lk} = 0.8$.

Noise is added using the model described in (34). For block l , $\mathbf{E}_l = \mathbf{P}_l \mathbf{T}_l \mathbf{T}_l^\top \mathbf{P}_l$, with \mathbf{T}_l an arbitrary matrix in $\mathbb{R}^{p_l \times p_l}$. In order for Σ_{ll}^η to be positive-definite, $\mathbf{T}_l \mathbf{T}_l^\top$ has to be positive-definite. We choose \mathbf{T}_l such that $\mathbf{T}_l \mathbf{T}_l^\top = \mathbf{T}_l^u \mathbf{T}_l^{u\top} + \mathbf{t}_l^s \mathbf{t}_l^{s\top}$, where the first term defines unstructured noise and the second, structured one. These terms are defined as follows:

- Unstructured noise is generated by sampling independent random normal variables and organizing them in a lower triangular matrix \mathbf{T}_l^u of size $p_l \times p_l$. Therefore, using the Cholesky decomposition, the matrix $\mathbf{T}_l^u \mathbf{T}_l^{u\top}$ is a symmetric positive-definite matrix.
- Structured noise is added using 2D shapes shown in Figure 9 and described in Table 4. To create noise from these shapes, we just vectorize them in vectors \mathbf{t}_l^s .

Unstructured noise is added to every block, but no structured noise is added to the last block ("Vector"). Both types of noises are normalized by their Frobenius norms before being added together. Data has been generated for 4 levels of SNR: -20dB, -10.5dB, -6dB and 0dB (η equals respectively 0.1, 0.3, 0.5 and 1).

It is possible to split the folds from the 10 folds of $n = 1000$ samples each to generate different experiments. In this section, some results are given for

- 10 folds with $n = 1000$ samples per fold,
- 20 folds with $n = 500$ samples per fold,
- 33 folds with $n = 300$ samples per fold,
- 50 folds with $n = 200$ samples per fold,
- 100 folds with $n = 100$ samples per fold.

Results in the main text are presented for $n = 1000$, a SNR level of -20dB, and a selection of 2 blocks ("Gas" and "Cross (small)") among the 5 that were created, resulting in $L = 2$.

G.3 Methods

The models included in the comparison are, in the $L = 2$ settings, TGCCA, MGCCA (Gloaguen et al., 2020), TCCA (Min et al., 2019), 2DCCA (Chen et al., 2021), RGCCA (Tenenhaus et al., 2017) and the per block SVD. In the $L = 5$ settings, only TGCCA, MGCCA, RGCCA and the per block SVD are included. If relevant, the method's rank is added as a suffix and the separable assumption as a prefix with the letters "sp".

We apply small changes to the codes of Chen et al. (2021) and Min et al. (2019) to harmonize the experiments. We add the convergence criterion from the latter to the former to compare computation times, and we set the shrinkage parameter as a parameter of TCCA to have the same shrinkage parameter for all models. The shrinkage parameter τ is set to 0.001. As Chen et al. (2021) proposes a so-called "effective" initialization strategy, we use it to run 2DCCA1. TGCCA, MGCCA and TCCA are run with 5 different starts.



Figure 8: Folded canonical vectors used to generate the data.

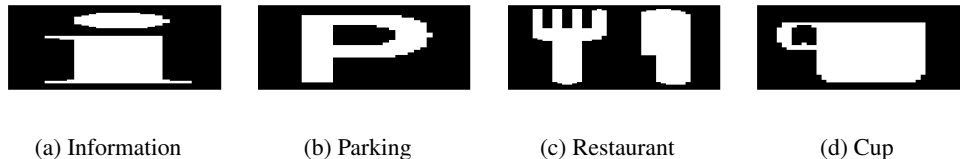


Figure 9: Folded shapes used to generate the structured noise.

We use TGCCA and MGCCA in a CCA settings, i.e.:

- The function g is the identity function,
- The elements of the design matrix \mathbf{C} are $c_{lk} = 1 - \delta_{lk}$ where δ is the Kronecker delta,
- For the constraint matrix \mathbf{M}_l , two cases are considered depending on the separable assumption made on these matrices (only the second case applies for MGCCA):
 - When \mathbf{M}_l is not assumed to be separable, $\hat{\mathbf{M}}_l = \hat{\Sigma}_{ll} + \tau_l \mathbf{I}_{p_l}$ which is a regularized version of the empirical covariance $\hat{\Sigma}_{ll}$. We choose $\tau_l = 0.001$ for $l \in [L]$.
 - When \mathbf{M}_l is assumed to be separable, a separable estimate of the covariance (Hoff, 2011; Min et al., 2019) is used. Without going into too much details, this estimator can be written as $\hat{\Sigma}_{ll} = \hat{\Sigma}_{ll,d_1} \otimes \cdots \otimes \hat{\Sigma}_{ll,1}$. We propose here a regularized version of it, where $\hat{\mathbf{M}}_l = \left(\hat{\Sigma}_{ll,d_1} + \sqrt[q]{\tau_l} \mathbf{I}_{p_l,d_1} \right) \otimes \cdots \otimes \left(\hat{\Sigma}_{ll,1} + \sqrt[q]{\tau_l} \mathbf{I}_{p_l,1} \right)$. Here, the regularization term is multiplied by $\sqrt[q]{\tau_l}$ instead of τ_l so that, when the Kronecker products are developed, the term in front of \mathbf{I}_{p_l} is τ_l , which is a way to have a similar level of regularization between the separable and non-separable cases. As before, for all blocks, τ_l is set to 0.001.

Concerning the normalization procedure, for all the methods, variables of each block were centered and scaled by $s_l = \sqrt{\frac{p_l}{n}} \|\mathbf{X}_l\|_F$, where $\|\cdot\|_F$ is the Frobenius norm.

G.4 Results

All experiments were run on a personal computer using the R language (R Core Team, 2020).

Results are given in tables 6 to 20. Cosines (with median and 2.5% and 97.5% quantiles over the different folds) between the canonical vectors used to generate the data and the estimated ones are reported. The computation time (with median and 2.5% and 97.5% quantiles over the different folds) is reported in seconds. For models run with multiple starts (TCCA, MGCCA and TGCCA), the computation time includes the 5 runs.

From tables 6 to 10, results are shown for the $L = 2$ settings and compare 2DCCA, TCCA, MGCCA, TGCCA, RGCCA and per-block SVD. From tables 11 to 15, results are shown for the $L = 5$ settings and compare MGCCA, TGCCA, RGCCA and per-block SVD. Finally, from tables 16 to 20 a comparison between the $L = 2$ and $L = 5$ settings is proposed. Each of the 15 tables is split into 4 smaller tables, one per SNR. Among one group of 5 tables (tables 6 to 10, tables 11 to 15 and tables 16 to 20), the number of folds is increasing and thus the number of samples per fold is decreasing.

Firstly, for all models but 2DCCA3, the accuracy increases with the SNR and the number of samples per fold. 2DCCA3 totally fails to retrieve the canonical vectors. We think that this is due to our experimental settings. Indeed, 2DCCA3 tries to find 3 canonical vectors of rank 1 such that the canonical components $y_l = \mathbf{w}_l^\top \mathbf{x}_l$ are uncorrelated while the

Table 4: Description of the generated blocks.

Block	Name	Structure	Folded shape	Rank	Noise name	Noise rank	Used in $L = 2$ setting?
1	Square	matrix	30×35	1	Information	8	×
2	Gas	matrix	45×38	12	Parking	11	✓
3	Cross	matrix	38×38	2	Restaurant	9	×
4	Cross (small)	matrix	19×19	2	Cup	6	✓
5	Vector	vector	100	NA	NA	NA	×

data is simulated from only one canonical component per block with the associated canonical vectors of ranks greater than 1. This illustrates the differences between rank and number of components discussed in Section C.

We can see that the accuracy is better with a much lower standard deviation when the SNR is greater than -20dB. When the SNR is low (-20dB), the different methods are more sensitive to the choice of the starting point. To highlight this last point, an additional experiment was held with a SNR of -20dB for MGCCA, TCCA and TGCCA. This time, instead of keeping the results associated with the best random initialization only, we display the median and 2.5% and 97.5% quantiles for each block ($L = 2$) through 100 random starts on a given fold (results are reported in Table 5). Even if the median coincides with the higher quantile, the lower quantile is extremely low. On the other hand, the "effective" strategy of 2DCCA1 does not always lead to a good initial point either (see, for example, the high standard deviation reported in Table 6 for 2DCCA1). We do not provide guidelines for choosing a good initial point. Still, if possible, we advise running MGCCA, TCCA and TGCCA multiple times with initial points chosen randomly and keeping the models with the highest correlation between blocks.

TGCCA3 and spTGCCA3 perform better than rank-1 models when the SNR is high. It is expected as the rank of the underlying canonical vectors is greater than 1 for every block except for the first block in the $L = 5$ settings. The opposite trend is observed for this block, even if TGCCA3 and spTGCCA3 remain very good. It can be explained by the fact that the weights of the different rank-1 factors are not null, but only one of them is far from zero (see Figure 10). On the other hand, when the SNR is low, TGCCA3 and spTGCCA3 tend to perform worse than the rank-1 methods. It is also expected as rank-3 models have more degrees of freedom and are more flexible. Therefore, when the SNR is too low, rank-3 models can describe both the relevant information and the noise (see factors 2 and 3 for "Square" and factor 3 for "Cross" and "Cross (small)" on Figure 10).

In the $L = 5$ settings, we see that the models take profit from the redundancy between blocks to estimate the canonical vectors more accurately. We can also point out that spTGCCA scales well with the number of blocks and remains fast when evaluated on the 5 blocks. To investigate the interest of analyzing more than 2 blocks jointly, we compared the same models both applied on 2 blocks and on 5 blocks (respectively denoted with suffixes "b2" and "b5"). It shows that having more correlated blocks acts like virtually increasing the SNR or the number of observations n . Hence the accuracy of the models applied on 5 blocks is much higher for SNR of -20dB and slightly better for higher SNR. See Tables 16-20.

Finally, spTGCCA appears to be the fastest method (considering that reported computation times correspond to 5 runs). spTGCCA is faster because it needs only to work with much smaller matrices ($\mathbf{M}_{l,m} \in \mathbb{R}^{p_{l,m} \times p_{l,m}}$), compute them once, make a change of variable and then work without regularization matrices. However, one must be cautious when comparing to TCCA because the Matlab code of TCCA was called from R, leading to some slight overestimation of the reported computation time.

G.5 Additional experiments with 3D canonical vectors

We repeat most of the previous experiments with 3D versions of the "Gas" and "Cross (small)" shapes shown in Figure 11. Shapes "Cross" and "Cross (small) 3D" are used in the $L = 2$ settings. Due to the size of the "Gas 3D" shape, the unstructured noise matrices \mathbf{T}_l^u have been replaced with homothety matrices. Results in the main text are presented for $n = 1000$, and a SNR level of -10dB in the $L = 2$ settings.

2DCCA is removed from these experiments since we did not find an available implementation for higher-order tensors. As "Gas 3D" is of high dimension, the regularization matrices \mathbf{M}_l are set to the identity matrices for RGCCA and

Table 5: Cosine between the true canonical vectors and the estimated ones for different models on block "Gas" and "Cross (little)" for SNR of -20dB for $n = 1000$, fold 1, with 100 random initial points. Median and quantiles (2.5% and 97.5%) are reported. The medians coincide with the higher quantile but the lower quantile is very low.

Model	Gas	Cross (small)
TCCA1	0.89 (0.00, 0.89)	0.86 (0.23, 0.86)
TGCCA1	0.89 (0.00, 0.89)	0.86 (0.23, 0.86)
spTCCA1	0.89 (0.00, 0.89)	0.86 (0.23, 0.86)
MGCCA	0.89 (0.00, 0.89)	0.86 (0.23, 0.86)
TCCA3	0.89 (0.00, 0.89)	0.86 (0.23, 0.86)
TGCCA3	0.95 (0.01, 0.95)	0.96 (0.08, 0.96)
spTCCA3	0.89 (0.00, 0.89)	0.86 (0.23, 0.87)
spTGCCA3	0.94 (0.01, 0.94)	0.95 (0.07, 0.95)

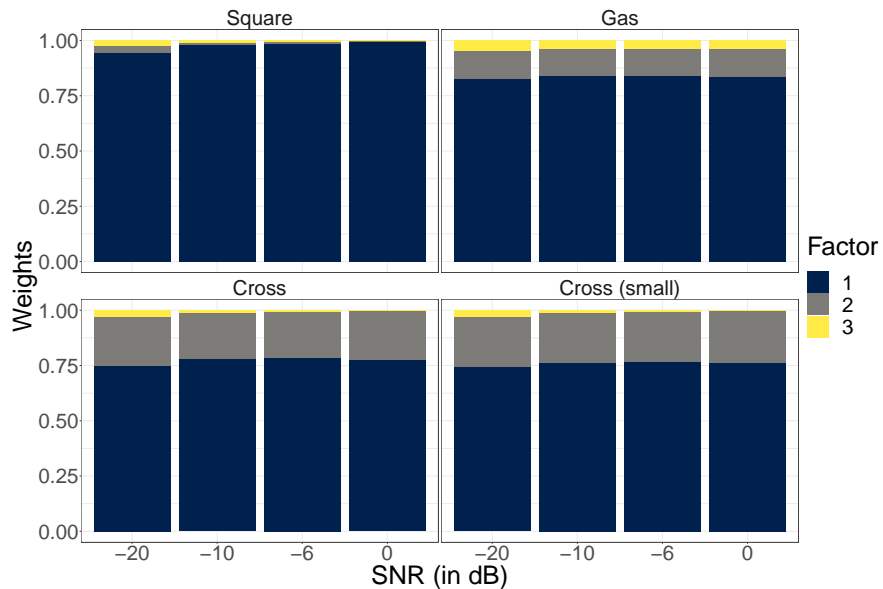


Figure 10: Contributions (λ_l) of the different rank-1 factors for spTGCC3 for $n = 1000$ and 10 folds. We can observe that the extra factors are cancelling out for the low rank canonical vectors when the SNR increases.

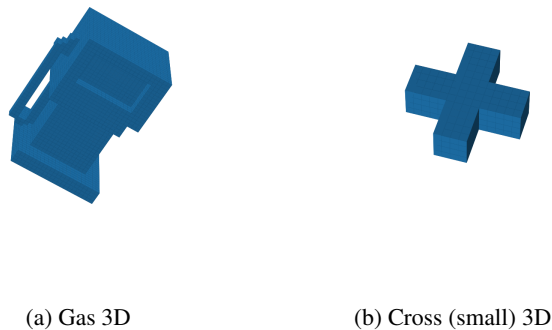


Figure 11: Folded shapes used in the 4D settings.

TGCCA in the $L = 5$ settings. Therefore, only spTGCCA is used and is reported as TGCCA. Orthogonality is imposed on the first mode for TGCCA models. All models are run with 10 different starting points. Tables 21 to 23 show the results for the $L = 2$ settings, and tables 24 to 26 show the results for the $L = 5$ settings.

Conclusions are similar to the previous experiments but RGCCA perform much better than before. This is probably due to the unstructured noise being simpler in these new experiments.

Table 6: Cosine between the true and the estimated canonical vectors for different models on blocks "Gas" and "Cross (small)", for levels of SNR -20dB, -10dB, -6dB and 0dB from top to bottom, and computation times, for n = 1000 and 10 folds. Median and quantiles (2.5% and 97.5%) are reported.

Model	Gas	Cross (small)	Computation time
2DCCA1	0.30 (0.01, 0.89)	0.43 (0.16, 0.85)	3.09 (2.76, 4.50)
TCCA1	0.89 (0.22, 0.90)	0.85 (0.32, 0.86)	7.72 (7.38, 9.17)
TGCCA1	0.89 (0.87, 0.90)	0.85 (0.83, 0.86)	8.60 (8.36, 9.12)
spTCCA1	0.89 (0.22, 0.90)	0.85 (0.32, 0.86)	7.43 (7.24, 8.04)
MGCCA	0.89 (0.87, 0.90)	0.86 (0.83, 0.86)	5.08 (4.85, 5.32)
2DCCA3	0.04 (0.01, 0.21)	0.13 (0.05, 0.31)	1.50 (1.41, 3.09)
TCCA3	0.89 (0.87, 0.90)	0.85 (0.83, 0.86)	7.93 (7.73, 8.92)
TGCCA3	0.91 (0.78, 0.94)	0.92 (0.79, 0.96)	11.32 (10.12, 15.94)
spTCCA3	0.89 (0.87, 0.90)	0.85 (0.83, 0.86)	7.32 (7.22, 7.51)
spTGCCA3	0.92 (0.82, 0.94)	0.93 (0.83, 0.96)	5.66 (5.52, 6.39)
RGCCA	0.17 (0.05, 0.26)	0.11 (0.06, 0.20)	13.12 (12.67, 14.07)
SVD	0.00 (0.00, 0.01)	0.01 (0.00, 0.03)	5.78 (5.44, 6.07)

Model	Gas	Cross (small)	Computation time
2DCCA1	0.90 (0.89, 0.91)	0.88 (0.87, 0.88)	2.89 (2.60, 4.57)
TCCA1	0.90 (0.89, 0.91)	0.88 (0.87, 0.88)	7.42 (7.38, 7.52)
TGCCA1	0.90 (0.89, 0.91)	0.88 (0.87, 0.88)	8.17 (8.02, 8.53)
spTCCA1	0.90 (0.89, 0.91)	0.88 (0.87, 0.88)	7.19 (7.11, 7.33)
MGCCA	0.90 (0.89, 0.91)	0.88 (0.87, 0.88)	4.84 (4.68, 5.35)
2DCCA3	0.13 (0.05, 0.23)	0.16 (0.03, 0.36)	1.51 (1.41, 3.07)
TCCA3	0.90 (0.89, 0.91)	0.88 (0.87, 0.88)	7.61 (7.58, 7.68)
TGCCA3	0.97 (0.96, 0.98)	0.99 (0.98, 0.99)	9.65 (9.23, 10.28)
spTCCA3	0.90 (0.89, 0.91)	0.88 (0.87, 0.88)	7.34 (7.13, 7.89)
spTGCCA3	0.97 (0.96, 0.98)	0.99 (0.98, 0.99)	5.10 (4.90, 5.48)
RGCCA	0.93 (0.91, 0.94)	0.97 (0.96, 0.98)	11.97 (11.38, 12.74)
SVD	0.02 (0.01, 0.06)	0.01 (0.00, 0.04)	5.45 (5.16, 5.94)

Model	Gas	Cross (small)	Computation time
2DCCA1	0.90 (0.90, 0.91)	0.88 (0.87, 0.88)	3.03 (2.81, 4.57)
TCCA1	0.90 (0.90, 0.91)	0.88 (0.87, 0.88)	7.40 (7.27, 7.49)
TGCCA1	0.90 (0.90, 0.91)	0.88 (0.87, 0.88)	8.07 (7.97, 8.25)
spTCCA1	0.90 (0.90, 0.91)	0.88 (0.87, 0.88)	7.19 (7.14, 7.35)
MGCCA	0.90 (0.90, 0.91)	0.88 (0.87, 0.88)	4.87 (4.56, 5.19)
2DCCA3	0.12 (0.03, 0.28)	0.06 (0.02, 0.34)	1.51 (1.40, 3.00)
TCCA3	0.90 (0.90, 0.91)	0.88 (0.87, 0.88)	7.67 (7.55, 7.84)
TGCCA3	0.98 (0.97, 0.98)	0.99 (0.98, 0.99)	9.51 (9.25, 10.76)
spTCCA3	0.90 (0.90, 0.91)	0.88 (0.87, 0.88)	7.42 (7.22, 7.69)
spTGCCA3	0.98 (0.97, 0.98)	0.99 (0.98, 0.99)	5.03 (4.89, 5.35)
RGCCA	0.95 (0.95, 0.96)	0.98 (0.97, 0.98)	11.78 (11.13, 12.13)
SVD	0.07 (0.01, 0.13)	0.05 (0.01, 0.21)	5.36 (5.18, 5.66)

Model	Gas	Cross (small)	Computation time
2DCCA1	0.91 (0.91, 0.91)	0.88 (0.88, 0.88)	3.24 (2.66, 4.78)
TCCA1	0.91 (0.91, 0.91)	0.88 (0.88, 0.88)	7.40 (7.32, 7.52)
TGCCA1	0.91 (0.91, 0.91)	0.88 (0.88, 0.88)	8.12 (7.88, 8.29)
spTCCA1	0.91 (0.91, 0.91)	0.88 (0.88, 0.88)	7.22 (7.12, 7.31)
MGCCA	0.91 (0.91, 0.91)	0.88 (0.88, 0.88)	4.79 (4.68, 5.11)
2DCCA3	0.09 (0.01, 0.21)	0.12 (0.07, 0.22)	1.54 (1.44, 3.24)
TCCA3	0.91 (0.91, 0.91)	0.88 (0.88, 0.88)	7.67 (7.54, 7.85)
TGCCA3	0.98 (0.98, 0.98)	1.00 (0.99, 1.00)	9.69 (9.35, 11.20)
spTCCA3	0.91 (0.91, 0.91)	0.88 (0.88, 0.88)	7.49 (7.28, 7.91)
spTGCCA3	0.98 (0.98, 0.98)	0.99 (0.99, 1.00)	4.97 (4.84, 5.33)
RGCCA	0.98 (0.97, 0.98)	0.99 (0.99, 0.99)	11.56 (11.04, 12.17)
SVD	0.99 (0.97, 0.99)	0.99 (0.96, 1.00)	5.32 (5.10, 5.59)

Table 7: Cosine between the true and the estimated canonical vectors for different models on blocks "Gas" and "Cross (small)", for levels of SNR -20dB, -10dB, -6dB and 0dB from top to bottom, and computation times, for n = 500 and 20 folds. Median and quantiles (2.5% and 97.5%) are reported.

Model	Gas	Cross (small)	Computation time
2DCCA1	0.03 (0.00, 0.85)	0.23 (0.05, 0.79)	2.32 (2.17, 5.39)
TCCA1	0.81 (0.00, 0.89)	0.77 (0.09, 0.86)	8.63 (7.56, 10.45)
TGCCA1	0.86 (0.68, 0.89)	0.82 (0.63, 0.86)	3.16 (3.02, 4.50)
spTCCA1	0.72 (0.00, 0.89)	0.62 (0.10, 0.86)	7.82 (7.25, 8.84)
MGCCA	0.86 (0.72, 0.89)	0.82 (0.69, 0.86)	2.81 (2.50, 3.18)
2DCCA3	0.03 (0.00, 0.12)	0.06 (0.01, 0.25)	0.95 (0.91, 2.14)
TCCA3	0.86 (0.36, 0.89)	0.82 (0.43, 0.86)	9.45 (7.81, 11.98)
TGCCA3	0.16 (0.01, 0.68)	0.19 (0.01, 0.64)	4.73 (3.49, 7.97)
spTCCA3	0.86 (0.14, 0.89)	0.83 (0.31, 0.86)	8.05 (7.19, 8.65)
spTGCCA3	0.20 (0.01, 0.70)	0.21 (0.02, 0.67)	2.79 (2.51, 3.53)
RGCCA	0.11 (0.00, 0.22)	0.07 (0.01, 0.15)	3.27 (3.06, 3.57)
SVD	0.01 (0.00, 0.03)	0.01 (0.00, 0.04)	1.19 (1.18, 1.28)

Model	Gas	Cross (small)	Computation time
2DCCA1	0.90 (0.87, 0.90)	0.87 (0.85, 0.88)	2.27 (2.11, 3.49)
TCCA1	0.90 (0.87, 0.90)	0.87 (0.85, 0.88)	7.32 (7.22, 7.47)
TGCCA1	0.90 (0.87, 0.90)	0.87 (0.85, 0.88)	2.80 (2.65, 3.04)
spTCCA1	0.90 (0.87, 0.90)	0.87 (0.85, 0.88)	7.08 (6.99, 7.31)
MGCCA	0.90 (0.87, 0.90)	0.87 (0.85, 0.88)	2.73 (2.49, 3.13)
2DCCA3	0.05 (0.01, 0.13)	0.06 (0.01, 0.23)	0.94 (0.91, 2.11)
TCCA3	0.90 (0.87, 0.90)	0.87 (0.85, 0.88)	7.58 (7.40, 7.87)
TGCCA3	0.96 (0.93, 0.96)	0.97 (0.94, 0.98)	3.68 (3.55, 3.95)
spTCCA3	0.90 (0.87, 0.90)	0.87 (0.85, 0.88)	7.09 (7.02, 7.31)
spTGCCA3	0.96 (0.92, 0.96)	0.97 (0.95, 0.98)	2.53 (2.45, 2.86)
RGCCA	0.86 (0.83, 0.89)	0.94 (0.88, 0.96)	3.00 (2.77, 3.46)
SVD	0.04 (0.00, 0.09)	0.02 (0.00, 0.08)	1.18 (1.17, 1.23)

Model	Gas	Cross (small)	Computation time
2DCCA1	0.90 (0.89, 0.91)	0.87 (0.86, 0.88)	2.26 (2.13, 3.34)
TCCA1	0.90 (0.89, 0.91)	0.87 (0.86, 0.88)	7.26 (7.16, 7.45)
TGCCA1	0.90 (0.89, 0.91)	0.87 (0.86, 0.88)	2.82 (2.67, 3.09)
spTCCA1	0.90 (0.89, 0.91)	0.87 (0.86, 0.88)	7.07 (6.98, 7.18)
MGCCA	0.90 (0.89, 0.91)	0.87 (0.86, 0.88)	2.51 (2.35, 2.91)
2DCCA3	0.05 (0.01, 0.16)	0.07 (0.00, 0.25)	0.92 (0.91, 2.06)
TCCA3	0.90 (0.89, 0.91)	0.87 (0.86, 0.88)	7.63 (7.48, 7.81)
TGCCA3	0.97 (0.96, 0.98)	0.98 (0.97, 0.99)	3.62 (3.39, 3.93)
spTCCA3	0.90 (0.89, 0.91)	0.87 (0.86, 0.88)	7.09 (7.03, 7.22)
spTGCCA3	0.97 (0.96, 0.97)	0.98 (0.97, 0.98)	2.60 (2.45, 2.93)
RGCCA	0.91 (0.89, 0.93)	0.96 (0.95, 0.97)	2.67 (2.54, 2.83)
SVD	0.09 (0.02, 0.18)	0.10 (0.01, 0.24)	1.27 (1.22, 1.37)

Model	Gas	Cross (small)	Computation time
2DCCA1	0.91 (0.90, 0.91)	0.88 (0.87, 0.88)	2.53 (2.31, 3.91)
TCCA1	0.91 (0.90, 0.91)	0.88 (0.87, 0.88)	7.33 (7.22, 8.20)
TGCCA1	0.91 (0.90, 0.91)	0.88 (0.87, 0.88)	2.69 (2.56, 2.97)
spTCCA1	0.91 (0.90, 0.91)	0.88 (0.87, 0.88)	7.13 (7.06, 7.25)
MGCCA	0.91 (0.90, 0.91)	0.88 (0.87, 0.88)	2.51 (2.34, 2.93)
2DCCA3	0.07 (0.01, 0.14)	0.07 (0.01, 0.21)	0.95 (0.90, 2.09)
TCCA3	0.91 (0.90, 0.91)	0.88 (0.87, 0.88)	7.63 (7.48, 7.80)
TGCCA3	0.98 (0.97, 0.98)	0.99 (0.98, 0.99)	3.58 (3.49, 3.96)
spTCCA3	0.91 (0.90, 0.91)	0.88 (0.87, 0.88)	7.11 (7.00, 7.43)
spTGCCA3	0.98 (0.97, 0.98)	0.99 (0.98, 0.99)	2.51 (2.36, 2.90)
RGCCA	0.94 (0.93, 0.95)	0.98 (0.97, 0.98)	2.48 (2.41, 2.58)
SVD	0.98 (0.95, 0.98)	0.99 (0.91, 0.99)	1.33 (1.28, 1.41)

Table 8: Cosine between the true and the estimated canonical vectors for different models on blocks "Gas" and "Cross (small)", for levels of SNR -20dB, -10dB, -6dB and 0dB from top to bottom, and computation times, for n = 300 and 33 folds. Median and quantiles (2.5% and 97.5%) are reported.

Model	Gas	Cross (small)	Computation time
2DCCA1	0.03 (0.00, 0.38)	0.22 (0.13, 0.49)	2.45 (2.01, 4.13)
TCCA1	0.04 (0.00, 0.80)	0.23 (0.15, 0.71)	9.21 (7.98, 10.50)
TGCCA1	0.25 (0.00, 0.85)	0.28 (0.05, 0.81)	1.78 (1.51, 2.65)
spTCCA1	0.04 (0.00, 0.75)	0.23 (0.15, 0.65)	8.10 (7.48, 8.65)
MGCCA	0.59 (0.00, 0.88)	0.44 (0.04, 0.84)	1.69 (1.59, 2.02)
2DCCA3	0.02 (0.00, 0.09)	0.04 (0.00, 0.22)	0.80 (0.72, 1.32)
TCCA3	0.19 (0.00, 0.88)	0.28 (0.15, 0.85)	10.45 (8.27, 13.22)
TGCCA3	0.07 (0.00, 0.35)	0.06 (0.00, 0.36)	2.27 (1.95, 3.44)
spTCCA3	0.07 (0.00, 0.85)	0.23 (0.16, 0.84)	8.05 (7.33, 9.52)
spTGCCA3	0.06 (0.00, 0.33)	0.05 (0.01, 0.33)	1.79 (1.60, 2.17)
RGCCA	0.07 (0.01, 0.17)	0.05 (0.00, 0.12)	1.03 (0.96, 1.11)
SVD	0.01 (0.00, 0.04)	0.02 (0.00, 0.05)	0.43 (0.43, 0.49)

Model	Gas	Cross (small)	Computation time
2DCCA1	0.89 (0.71, 0.90)	0.86 (0.68, 0.87)	2.38 (2.00, 3.50)
TCCA1	0.89 (0.86, 0.90)	0.86 (0.83, 0.87)	7.35 (7.25, 7.71)
TGCCA1	0.89 (0.85, 0.90)	0.86 (0.82, 0.87)	1.46 (1.37, 1.65)
spTCCA1	0.89 (0.85, 0.90)	0.86 (0.82, 0.87)	7.15 (7.06, 7.42)
MGCCA	0.89 (0.86, 0.90)	0.86 (0.83, 0.87)	1.59 (1.47, 1.72)
2DCCA3	0.03 (0.00, 0.13)	0.05 (0.00, 0.20)	0.74 (0.71, 1.24)
TCCA3	0.89 (0.86, 0.90)	0.86 (0.83, 0.87)	7.70 (7.53, 7.88)
TGCCA3	0.93 (0.88, 0.95)	0.95 (0.91, 0.97)	2.12 (1.94, 2.25)
spTCCA3	0.89 (0.85, 0.90)	0.86 (0.82, 0.87)	7.11 (7.01, 7.20)
spTGCCA3	0.93 (0.88, 0.95)	0.94 (0.91, 0.96)	1.64 (1.52, 1.82)
RGCCA	0.77 (0.35, 0.83)	0.88 (0.42, 0.93)	1.23 (1.06, 1.64)
SVD	0.05 (0.01, 0.13)	0.03 (0.00, 0.09)	0.46 (0.46, 0.50)

Model	Gas	Cross (small)	Computation time
2DCCA1	0.89 (0.88, 0.90)	0.87 (0.86, 0.88)	2.09 (1.95, 2.66)
TCCA1	0.90 (0.88, 0.90)	0.87 (0.86, 0.88)	7.32 (7.21, 7.48)
TGCCA1	0.90 (0.88, 0.90)	0.87 (0.85, 0.88)	1.47 (1.37, 1.68)
spTCCA1	0.90 (0.88, 0.90)	0.87 (0.85, 0.88)	7.15 (7.05, 7.28)
MGCCA	0.90 (0.88, 0.90)	0.87 (0.85, 0.87)	1.53 (1.45, 1.78)
2DCCA3	0.03 (0.01, 0.11)	0.08 (0.01, 0.21)	0.77 (0.70, 1.27)
TCCA3	0.90 (0.88, 0.90)	0.87 (0.86, 0.88)	7.70 (7.51, 7.88)
TGCCA3	0.96 (0.93, 0.97)	0.97 (0.95, 0.98)	2.11 (1.99, 2.30)
spTCCA3	0.90 (0.88, 0.90)	0.87 (0.85, 0.88)	7.07 (6.98, 7.22)
spTGCCA3	0.95 (0.93, 0.96)	0.97 (0.95, 0.98)	1.55 (1.45, 1.78)
RGCCA	0.83 (0.79, 0.86)	0.94 (0.91, 0.96)	0.99 (0.91, 1.09)
SVD	0.08 (0.00, 0.26)	0.11 (0.01, 0.51)	0.43 (0.42, 0.47)

Model	Gas	Cross (small)	Computation time
2DCCA1	0.90 (0.89, 0.90)	0.87 (0.86, 0.88)	2.76 (2.29, 3.92)
TCCA1	0.90 (0.89, 0.91)	0.88 (0.86, 0.88)	7.30 (7.17, 7.42)
TGCCA1	0.90 (0.89, 0.91)	0.88 (0.86, 0.88)	1.51 (1.35, 1.75)
spTCCA1	0.90 (0.89, 0.91)	0.88 (0.86, 0.88)	7.16 (7.07, 7.30)
MGCCA	0.90 (0.89, 0.91)	0.87 (0.86, 0.88)	1.52 (1.43, 1.70)
2DCCA3	0.05 (0.01, 0.13)	0.06 (0.00, 0.19)	0.74 (0.71, 1.21)
TCCA3	0.90 (0.89, 0.91)	0.88 (0.86, 0.88)	7.69 (7.48, 7.83)
TGCCA3	0.97 (0.96, 0.98)	0.99 (0.97, 0.99)	2.03 (1.93, 2.19)
spTCCA3	0.90 (0.89, 0.91)	0.88 (0.86, 0.88)	7.07 (6.94, 7.17)
spTGCCA3	0.96 (0.95, 0.97)	0.98 (0.96, 0.98)	1.55 (1.47, 1.75)
RGCCA	0.87 (0.84, 0.89)	0.96 (0.94, 0.97)	0.91 (0.86, 1.01)
SVD	0.97 (0.89, 0.97)	0.98 (0.87, 0.99)	0.42 (0.42, 0.47)

Table 9: Cosine between the true and the estimated canonical vectors for different models on blocks "Gas" and "Cross (small)", for levels of SNR -20dB, -10dB, -6dB and 0dB from top to bottom, and computation times, for n = 200 and 50 folds. Median and quantiles (2.5% and 97.5%) are reported.

Model	Gas	Cross (small)	Computation time
2DCCA1	0.02 (0.00, 0.28)	0.19 (0.11, 0.41)	1.93 (1.83, 2.99)
TCCA1	0.02 (0.00, 0.77)	0.21 (0.10, 0.71)	9.93 (8.33, 11.22)
TGCCA1	0.08 (0.00, 0.71)	0.24 (0.10, 0.62)	1.10 (0.94, 1.87)
spTCCA1	0.02 (0.00, 0.68)	0.21 (0.10, 0.61)	8.54 (7.77, 9.40)
MGCCA	0.18 (0.00, 0.79)	0.23 (0.04, 0.73)	1.15 (1.06, 1.61)
2DCCA3	0.01 (0.00, 0.06)	0.03 (0.00, 0.16)	0.63 (0.60, 0.73)
TCCA3	0.03 (0.00, 0.82)	0.22 (0.10, 0.76)	10.93 (8.80, 13.37)
TGCCA3	0.07 (0.00, 0.30)	0.08 (0.00, 0.26)	1.56 (1.34, 2.27)
spTCCA3	0.02 (0.00, 0.67)	0.22 (0.10, 0.59)	8.26 (7.46, 9.85)
spTGCCA3	0.05 (0.00, 0.32)	0.07 (0.01, 0.31)	1.19 (1.12, 1.44)
RGCCA	0.05 (0.01, 0.19)	0.06 (0.00, 0.13)	0.46 (0.41, 0.56)
SVD	0.02 (0.00, 0.06)	0.02 (0.00, 0.06)	0.19 (0.19, 0.23)

Model	Gas	Cross (small)	Computation time
2DCCA1	0.87 (0.03, 0.89)	0.85 (0.18, 0.87)	1.93 (1.83, 2.13)
TCCA1	0.88 (0.83, 0.89)	0.85 (0.81, 0.87)	7.59 (7.42, 8.49)
TGCCA1	0.88 (0.82, 0.89)	0.85 (0.80, 0.87)	0.99 (0.91, 1.14)
spTCCA1	0.88 (0.81, 0.89)	0.85 (0.79, 0.87)	7.70 (7.23, 8.14)
MGCCA	0.88 (0.83, 0.89)	0.85 (0.81, 0.86)	1.11 (1.02, 1.23)
2DCCA3	0.03 (0.00, 0.08)	0.06 (0.00, 0.23)	0.64 (0.61, 0.73)
TCCA3	0.88 (0.84, 0.89)	0.85 (0.81, 0.87)	7.76 (7.59, 8.16)
TGCCA3	0.90 (0.83, 0.93)	0.93 (0.85, 0.96)	1.52 (1.39, 1.81)
spTCCA3	0.88 (0.82, 0.89)	0.85 (0.80, 0.87)	7.13 (7.01, 7.40)
spTGCCA3	0.89 (0.83, 0.92)	0.92 (0.85, 0.94)	1.15 (1.08, 1.24)
RGCCA	0.59 (0.09, 0.75)	0.76 (0.17, 0.92)	0.66 (0.53, 1.80)
SVD	0.05 (0.00, 0.15)	0.05 (0.01, 0.15)	0.20 (0.20, 0.24)

Model	Gas	Cross (small)	Computation time
2DCCA1	0.88 (0.86, 0.89)	0.86 (0.83, 0.87)	1.93 (1.83, 2.96)
TCCA1	0.89 (0.87, 0.90)	0.86 (0.83, 0.87)	7.52 (7.30, 7.97)
TGCCA1	0.89 (0.87, 0.90)	0.86 (0.83, 0.87)	0.95 (0.86, 1.08)
spTCCA1	0.89 (0.85, 0.90)	0.86 (0.82, 0.87)	7.48 (7.18, 7.91)
MGCCA	0.89 (0.86, 0.90)	0.86 (0.83, 0.87)	1.09 (1.01, 1.21)
2DCCA3	0.02 (0.00, 0.10)	0.06 (0.00, 0.17)	0.66 (0.62, 0.78)
TCCA3	0.89 (0.87, 0.90)	0.86 (0.83, 0.87)	7.74 (7.55, 8.02)
TGCCA3	0.94 (0.90, 0.96)	0.96 (0.92, 0.97)	1.47 (1.36, 1.60)
spTCCA3	0.89 (0.87, 0.90)	0.86 (0.83, 0.87)	7.09 (6.99, 7.35)
spTGCCA3	0.93 (0.88, 0.94)	0.94 (0.91, 0.96)	1.12 (1.05, 1.22)
RGCCA	0.72 (0.62, 0.76)	0.91 (0.85, 0.94)	0.54 (0.45, 0.74)
SVD	0.14 (0.01, 0.45)	0.17 (0.01, 0.54)	0.18 (0.18, 0.22)

Model	Gas	Cross (small)	Computation time
2DCCA1	0.88 (0.86, 0.89)	0.87 (0.85, 0.87)	1.93 (1.85, 2.38)
TCCA1	0.90 (0.88, 0.90)	0.87 (0.86, 0.87)	7.39 (7.22, 8.03)
TGCCA1	0.90 (0.89, 0.91)	0.87 (0.86, 0.88)	0.87 (0.80, 1.01)
spTCCA1	0.90 (0.88, 0.91)	0.87 (0.86, 0.88)	7.66 (7.27, 8.03)
MGCCA	0.90 (0.87, 0.90)	0.87 (0.85, 0.87)	1.07 (0.99, 1.25)
2DCCA3	0.03 (0.01, 0.09)	0.06 (0.01, 0.15)	0.66 (0.62, 0.80)
TCCA3	0.90 (0.88, 0.90)	0.87 (0.86, 0.87)	7.69 (7.54, 7.93)
TGCCA3	0.97 (0.94, 0.98)	0.98 (0.96, 0.99)	1.40 (1.35, 1.56)
spTCCA3	0.90 (0.89, 0.91)	0.87 (0.86, 0.88)	7.09 (6.97, 7.21)
spTGCCA3	0.94 (0.91, 0.95)	0.96 (0.94, 0.97)	1.08 (1.00, 1.28)
RGCCA	0.73 (0.67, 0.79)	0.94 (0.92, 0.96)	0.49 (0.43, 0.56)
SVD	0.95 (0.81, 0.96)	0.96 (0.66, 0.98)	0.19 (0.18, 0.22)

Table 10: Cosine between the true and the estimated canonical vectors for different models on blocks "Gas" and "Cross (small)", for levels of SNR -20dB, -10dB, -6dB and 0dB from top to bottom, and computation times, for n = 100 and 100 folds. Median and quantiles (2.5% and 97.5%) are reported.

Model	Gas	Cross (small)	Computation time
2DCCA1	0.02 (0.00, 0.14)	0.17 (0.04, 0.35)	2.28 (1.93, 3.22)
TCCA1	0.02 (0.00, 0.21)	0.19 (0.09, 0.39)	10.69 (9.35, 11.81)
TGCCA1	0.04 (0.00, 0.52)	0.20 (0.01, 0.45)	0.62 (0.51, 0.91)
spTCCA1	0.02 (0.00, 0.40)	0.20 (0.05, 0.38)	9.32 (8.48, 10.05)
MGCCA	0.07 (0.00, 0.56)	0.18 (0.01, 0.50)	0.72 (0.64, 0.87)
2DCCA3	0.01 (0.00, 0.05)	0.03 (0.00, 0.13)	0.53 (0.51, 0.61)
TCCA3	0.02 (0.00, 0.57)	0.19 (0.09, 0.48)	13.11 (10.14, 13.55)
TGCCA3	0.06 (0.00, 0.35)	0.07 (0.01, 0.24)	1.01 (0.90, 1.72)
spTCCA3	0.02 (0.00, 0.52)	0.20 (0.05, 0.42)	9.63 (7.77, 11.28)
spTGCCA3	0.05 (0.00, 0.30)	0.06 (0.00, 0.27)	0.73 (0.63, 0.90)
RGCCA	0.05 (0.00, 0.17)	0.04 (0.00, 0.14)	0.22 (0.16, 0.29)
SVD	0.03 (0.00, 0.08)	0.03 (0.00, 0.08)	0.04 (0.04, 0.08)

Model	Gas	Cross (small)	Computation time
2DCCA1	0.27 (0.01, 0.80)	0.56 (0.03, 0.84)	1.90 (1.81, 2.65)
TCCA1	0.80 (0.00, 0.86)	0.81 (0.10, 0.85)	8.74 (8.08, 11.07)
TGCCA1	0.84 (0.62, 0.88)	0.81 (0.36, 0.86)	0.58 (0.49, 0.86)
spTCCA1	0.83 (0.00, 0.88)	0.79 (0.15, 0.86)	8.27 (7.84, 9.34)
MGCCA	0.83 (0.66, 0.87)	0.80 (0.64, 0.85)	0.68 (0.61, 0.82)
2DCCA3	0.01 (0.00, 0.05)	0.04 (0.00, 0.12)	0.53 (0.51, 0.68)
TCCA3	0.80 (0.01, 0.86)	0.81 (0.12, 0.85)	8.22 (7.81, 11.55)
TGCCA3	0.78 (0.19, 0.88)	0.81 (0.07, 0.93)	1.04 (0.89, 2.11)
spTCCA3	0.83 (0.01, 0.88)	0.80 (0.16, 0.86)	7.42 (7.10, 9.28)
spTGCCA3	0.76 (0.12, 0.83)	0.80 (0.15, 0.89)	0.76 (0.65, 1.01)
RGCCA	0.17 (0.01, 0.53)	0.31 (0.04, 0.79)	0.28 (0.19, 0.75)
SVD	0.06 (0.00, 0.19)	0.07 (0.01, 0.24)	0.05 (0.04, 0.07)

Model	Gas	Cross (small)	Computation time
2DCCA1	0.70 (0.10, 0.78)	0.82 (0.31, 0.84)	1.91 (1.82, 2.12)
TCCA1	0.82 (0.02, 0.85)	0.83 (0.35, 0.85)	8.32 (7.94, 9.10)
TGCCA1	0.88 (0.81, 0.89)	0.85 (0.75, 0.87)	0.53 (0.45, 0.66)
spTCCA1	0.87 (0.01, 0.89)	0.84 (0.18, 0.86)	7.27 (7.11, 8.26)
MGCCA	0.86 (0.81, 0.88)	0.83 (0.77, 0.86)	0.67 (0.60, 0.75)
2DCCA3	0.02 (0.00, 0.05)	0.04 (0.00, 0.11)	0.54 (0.51, 0.62)
TCCA3	0.82 (0.33, 0.85)	0.83 (0.48, 0.85)	8.02 (7.77, 8.79)
TGCCA3	0.89 (0.78, 0.93)	0.92 (0.82, 0.95)	0.93 (0.85, 1.06)
spTCCA3	0.88 (0.39, 0.89)	0.85 (0.47, 0.87)	7.81 (7.66, 8.12)
spTGCCA3	0.84 (0.72, 0.88)	0.87 (0.80, 0.91)	0.69 (0.62, 0.80)
RGCCA	0.47 (0.14, 0.57)	0.84 (0.34, 0.90)	0.34 (0.22, 0.93)
SVD	0.17 (0.01, 0.67)	0.19 (0.01, 0.87)	0.05 (0.04, 0.08)

Model	Gas	Cross (small)	Computation time
2DCCA1	0.63 (0.50, 0.75)	0.81 (0.77, 0.85)	1.92 (1.83, 2.14)
TCCA1	0.81 (0.73, 0.86)	0.84 (0.80, 0.86)	8.38 (8.03, 8.88)
TGCCA1	0.89 (0.86, 0.90)	0.86 (0.84, 0.88)	0.48 (0.42, 0.55)
spTCCA1	0.89 (0.86, 0.90)	0.86 (0.84, 0.87)	7.25 (7.13, 7.55)
MGCCA	0.88 (0.84, 0.89)	0.85 (0.82, 0.87)	0.64 (0.59, 0.72)
2DCCA3	0.02 (0.00, 0.05)	0.04 (0.00, 0.14)	0.53 (0.51, 0.60)
TCCA3	0.81 (0.73, 0.86)	0.84 (0.80, 0.86)	8.13 (7.91, 9.43)
TGCCA3	0.94 (0.88, 0.97)	0.96 (0.93, 0.98)	0.92 (0.84, 1.02)
spTCCA3	0.89 (0.86, 0.90)	0.86 (0.84, 0.88)	7.13 (7.00, 7.33)
spTGCCA3	0.86 (0.79, 0.90)	0.90 (0.87, 0.92)	0.67 (0.60, 0.76)
RGCCA	0.46 (0.38, 0.57)	0.90 (0.87, 0.93)	0.22 (0.15, 0.33)
SVD	0.90 (0.39, 0.93)	0.94 (0.53, 0.97)	0.05 (0.04, 0.08)

Table 11: Cosine between the true and the estimated canonical vectors for different models on blocks "Square", "Gas", "Cross", "Cross (small)" and "Vector", for levels of SNR -20dB, -10dB, -6dB, and 0dB from top to bottom, and computation times, for n = 1000 and 10 folds. Median and quantiles (2.5% and 97.5%) are reported.

Model	Square	Gas	Cross	Cross (small)	Vector	Computation time
TGCCA1	0.99 (0.97, 0.99)	0.90 (0.89, 0.90)	0.88 (0.87, 0.88)	0.86 (0.85, 0.87)	0.94 (0.92, 0.96)	20.35 (19.73, 21.34)
MGCCA	0.99 (0.97, 0.99)	0.90 (0.89, 0.90)	0.88 (0.87, 0.88)	0.87 (0.85, 0.87)	0.94 (0.92, 0.96)	9.88 (9.61, 10.20)
TGCCA3	0.96 (0.94, 0.97)	0.96 (0.94, 0.97)	0.97 (0.94, 0.97)	0.96 (0.95, 0.97)	0.94 (0.93, 0.96)	23.55 (22.51, 27.70)
spTGCCA3	0.96 (0.94, 0.97)	0.96 (0.94, 0.97)	0.97 (0.94, 0.97)	0.96 (0.95, 0.97)	0.94 (0.93, 0.96)	10.15 (9.91, 10.61)
RGCCA	0.88 (0.84, 0.89)	0.86 (0.79, 0.88)	0.87 (0.82, 0.88)	0.91 (0.87, 0.93)	0.93 (0.92, 0.96)	32.44 (28.48, 36.78)
SVD	0.01 (0.00, 0.02)	0.00 (0.00, 0.01)	0.01 (0.00, 0.02)	0.01 (0.00, 0.03)	0.07 (0.01, 0.13)	12.85 (12.65, 13.01)

Model	Square	Gas	Cross	Cross (small)	Vector	Computation time
TGCCA1	1.00 (0.99, 1.00)	0.91 (0.90, 0.91)	0.89 (0.89, 0.89)	0.88 (0.87, 0.88)	0.98 (0.98, 0.99)	19.02 (18.88, 19.45)
MGCCA	1.00 (0.99, 1.00)	0.91 (0.90, 0.91)	0.89 (0.89, 0.89)	0.88 (0.87, 0.88)	0.98 (0.98, 0.99)	9.63 (9.46, 10.26)
TGCCA3	0.99 (0.98, 0.99)	0.98 (0.97, 0.98)	0.99 (0.99, 0.99)	0.99 (0.99, 0.99)	0.98 (0.98, 0.99)	24.19 (22.21, 25.08)
spTGCCA3	0.99 (0.98, 0.99)	0.98 (0.97, 0.98)	0.99 (0.99, 0.99)	0.99 (0.99, 0.99)	0.98 (0.98, 0.99)	9.77 (9.62, 10.19)
RGCCA	0.96 (0.95, 0.96)	0.95 (0.94, 0.95)	0.95 (0.95, 0.96)	0.98 (0.97, 0.98)	0.98 (0.98, 0.99)	29.80 (28.21, 31.24)
SVD	0.02 (0.00, 0.11)	0.02 (0.01, 0.06)	0.01 (0.00, 0.06)	0.01 (0.00, 0.04)	0.98 (0.97, 0.99)	12.93 (12.86, 13.74)

Model	Square	Gas	Cross	Cross (small)	Vector	Computation time
TGCCA1	1.00 (1.00, 1.00)	0.91 (0.91, 0.91)	0.89 (0.89, 0.89)	0.88 (0.88, 0.88)	0.99 (0.98, 0.99)	18.97 (18.66, 19.40)
MGCCA	1.00 (1.00, 1.00)	0.91 (0.91, 0.91)	0.89 (0.89, 0.89)	0.88 (0.88, 0.88)	0.99 (0.98, 0.99)	9.83 (9.61, 10.37)
TGCCA3	0.99 (0.99, 0.99)	0.98 (0.98, 0.98)	0.99 (0.99, 0.99)	0.99 (0.99, 1.00)	0.99 (0.98, 0.99)	22.76 (22.00, 24.48)
spTGCCA3	0.99 (0.99, 0.99)	0.98 (0.98, 0.98)	0.99 (0.99, 0.99)	0.99 (0.99, 0.99)	0.99 (0.98, 0.99)	9.91 (9.72, 10.28)
RGCCA	0.97 (0.97, 0.98)	0.97 (0.96, 0.97)	0.97 (0.96, 0.97)	0.98 (0.98, 0.99)	0.99 (0.98, 0.99)	28.99 (27.72, 30.75)
SVD	0.06 (0.02, 0.19)	0.07 (0.01, 0.13)	0.03 (0.00, 0.15)	0.05 (0.01, 0.21)	0.99 (0.99, 0.99)	11.88 (11.75, 11.92)

Model	Square	Gas	Cross	Cross (small)	Vector	Computation time
TGCCA1	1.00 (1.00, 1.00)	0.91 (0.91, 0.91)	0.89 (0.89, 0.89)	0.88 (0.88, 0.88)	0.99 (0.99, 1.00)	18.24 (18.08, 18.48)
MGCCA	1.00 (1.00, 1.00)	0.91 (0.91, 0.91)	0.89 (0.89, 0.89)	0.88 (0.88, 0.88)	0.99 (0.99, 1.00)	9.66 (9.47, 10.26)
TGCCA3	1.00 (1.00, 1.00)	0.98 (0.98, 0.98)	1.00 (0.99, 1.00)	1.00 (0.99, 1.00)	0.99 (0.99, 1.00)	22.02 (21.74, 22.83)
spTGCCA3	1.00 (0.99, 1.00)	0.98 (0.98, 0.98)	1.00 (0.99, 1.00)	1.00 (0.99, 1.00)	0.99 (0.99, 1.00)	9.72 (9.48, 10.25)
RGCCA	0.99 (0.98, 0.99)	0.98 (0.98, 0.99)	0.98 (0.98, 0.99)	0.99 (0.99, 0.99)	0.99 (0.99, 1.00)	30.16 (29.33, 31.02)
SVD	0.99 (0.99, 0.99)	0.99 (0.97, 0.99)	0.99 (0.98, 0.99)	0.99 (0.96, 1.00)	1.00 (1.00, 1.00)	12.80 (12.68, 13.13)

Table 12: Cosine between the true and the estimated canonical vectors for different models on blocks "Square", "Gas", "Cross", "Cross (small)" and "Vector", for levels of SNR -20dB, -10dB, -6dB, and 0dB from top to bottom, and computation times, for n = 500 and 20 folds. Median and quantiles (2.5% and 97.5%) are reported.

Model	Square	Gas	Cross	Cross (small)	Vector	Computation time
TGCCA1	0.98 (0.91, 0.99)	0.89 (0.82, 0.89)	0.87 (0.73, 0.88)	0.86 (0.83, 0.87)	0.90 (0.85, 0.93)	6.91 (6.33, 8.42)
MGCCA	0.98 (0.94, 0.99)	0.89 (0.84, 0.89)	0.87 (0.78, 0.88)	0.86 (0.82, 0.87)	0.90 (0.86, 0.93)	5.34 (4.95, 5.77)
TGCCA3	0.92 (0.78, 0.94)	0.91 (0.68, 0.94)	0.93 (0.76, 0.95)	0.93 (0.83, 0.95)	0.89 (0.81, 0.92)	9.56 (8.90, 10.66)
spTGCCA3	0.92 (0.79, 0.93)	0.91 (0.69, 0.94)	0.93 (0.79, 0.95)	0.93 (0.84, 0.94)	0.89 (0.81, 0.93)	5.60 (5.38, 6.32)
RGCCA	0.78 (0.41, 0.82)	0.74 (0.41, 0.80)	0.76 (0.47, 0.80)	0.81 (0.50, 0.87)	0.87 (0.66, 0.92)	9.16 (7.81, 11.87)
SVD	0.01 (0.00, 0.04)	0.01 (0.00, 0.03)	0.02 (0.00, 0.03)	0.01 (0.00, 0.04)	0.03 (0.00, 0.17)	3.31 (2.90, 3.53)
Model	Square	Gas	Cross	Cross (small)	Vector	Computation time
TGCCA1	0.99 (0.98, 1.00)	0.90 (0.89, 0.90)	0.88 (0.87, 0.89)	0.87 (0.86, 0.88)	0.97 (0.95, 0.97)	6.01 (5.77, 6.60)
MGCCA	0.99 (0.98, 1.00)	0.90 (0.88, 0.90)	0.88 (0.87, 0.89)	0.87 (0.86, 0.88)	0.97 (0.95, 0.97)	5.10 (4.96, 5.52)
TGCCA3	0.97 (0.96, 0.98)	0.97 (0.95, 0.97)	0.98 (0.96, 0.98)	0.98 (0.96, 0.98)	0.97 (0.95, 0.98)	8.79 (8.46, 9.60)
spTGCCA3	0.97 (0.96, 0.97)	0.96 (0.95, 0.97)	0.98 (0.96, 0.98)	0.98 (0.96, 0.98)	0.97 (0.95, 0.98)	5.30 (5.10, 5.74)
RGCCA	0.92 (0.90, 0.93)	0.90 (0.88, 0.91)	0.91 (0.89, 0.92)	0.95 (0.93, 0.96)	0.97 (0.95, 0.98)	6.43 (6.22, 7.21)
SVD	0.03 (0.00, 0.13)	0.04 (0.00, 0.09)	0.03 (0.01, 0.07)	0.02 (0.00, 0.08)	0.95 (0.92, 0.97)	3.50 (3.29, 3.57)
Model	Square	Gas	Cross	Cross (small)	Vector	Computation time
TGCCA1	1.00 (0.99, 1.00)	0.91 (0.90, 0.91)	0.89 (0.88, 0.89)	0.88 (0.87, 0.88)	0.98 (0.97, 0.98)	6.00 (5.80, 6.24)
MGCCA	1.00 (0.99, 1.00)	0.90 (0.90, 0.91)	0.89 (0.88, 0.89)	0.88 (0.86, 0.88)	0.98 (0.97, 0.98)	5.21 (5.05, 5.59)
TGCCA3	0.98 (0.98, 0.99)	0.98 (0.97, 0.98)	0.99 (0.98, 0.99)	0.99 (0.98, 0.99)	0.98 (0.97, 0.98)	8.87 (8.60, 9.45)
spTGCCA3	0.98 (0.97, 0.98)	0.97 (0.97, 0.98)	0.98 (0.98, 0.99)	0.99 (0.97, 0.99)	0.98 (0.97, 0.98)	5.36 (5.09, 5.73)
RGCCA	0.95 (0.94, 0.96)	0.93 (0.92, 0.94)	0.94 (0.93, 0.95)	0.97 (0.96, 0.97)	0.98 (0.97, 0.98)	6.79 (6.60, 7.09)
SVD	0.08 (0.01, 0.25)	0.09 (0.02, 0.18)	0.06 (0.01, 0.24)	0.10 (0.01, 0.24)	0.98 (0.97, 0.99)	3.50 (2.87, 3.56)
Model	Square	Gas	Cross	Cross (small)	Vector	Computation time
TGCCA1	1.00 (1.00, 1.00)	0.91 (0.90, 0.91)	0.89 (0.88, 0.89)	0.88 (0.87, 0.88)	0.99 (0.99, 0.99)	5.87 (5.65, 6.12)
MGCCA	1.00 (0.99, 1.00)	0.91 (0.90, 0.91)	0.89 (0.88, 0.89)	0.88 (0.87, 0.88)	0.99 (0.99, 0.99)	5.10 (4.91, 5.49)
TGCCA3	0.99 (0.99, 0.99)	0.98 (0.98, 0.98)	0.99 (0.99, 0.99)	0.99 (0.99, 1.00)	0.99 (0.99, 0.99)	8.90 (8.34, 9.83)
spTGCCA3	0.99 (0.99, 0.99)	0.98 (0.97, 0.98)	0.99 (0.98, 0.99)	0.99 (0.99, 0.99)	0.99 (0.99, 0.99)	5.34 (5.00, 5.77)
RGCCA	0.97 (0.96, 0.98)	0.96 (0.95, 0.97)	0.96 (0.95, 0.97)	0.98 (0.98, 0.99)	0.99 (0.99, 0.99)	6.46 (6.33, 6.91)
SVD	0.98 (0.96, 0.99)	0.98 (0.95, 0.98)	0.98 (0.94, 0.98)	0.99 (0.91, 0.99)	0.99 (0.99, 0.99)	3.16 (2.92, 3.33)

Table 13: Cosine between the true and the estimated canonical vectors for different models on blocks "Square", "Gas", "Cross", "Cross (small)" and "Vector", for levels of SNR -20dB, -10dB, -6dB, and 0dB from top to bottom, and computation times, for n = 300 and 33 folds. Median and quantiles (2.5% and 97.5%) are reported.

Model	Square	Gas	Cross	Cross (small)	Vector	Computation time
TGCCA1	0.95 (0.44, 0.98)	0.87 (0.50, 0.89)	0.85 (0.33, 0.87)	0.82 (0.52, 0.86)	0.83 (0.51, 0.89)	4.09 (3.55, 5.89)
MGCCA	0.95 (0.83, 0.97)	0.87 (0.75, 0.89)	0.85 (0.69, 0.87)	0.83 (0.76, 0.86)	0.84 (0.73, 0.89)	3.55 (3.27, 4.01)
TGCCA3	0.86 (0.31, 0.90)	0.82 (0.39, 0.89)	0.87 (0.39, 0.91)	0.86 (0.47, 0.91)	0.82 (0.51, 0.89)	6.44 (5.64, 10.08)
spTGCCA3	0.85 (0.35, 0.89)	0.82 (0.41, 0.88)	0.87 (0.46, 0.91)	0.87 (0.53, 0.91)	0.82 (0.56, 0.89)	3.77 (3.37, 4.40)
RGCCA	0.67 (0.21, 0.72)	0.62 (0.27, 0.69)	0.64 (0.31, 0.70)	0.69 (0.33, 0.78)	0.79 (0.42, 0.84)	3.10 (2.64, 4.01)
SVD	0.02 (0.00, 0.06)	0.01 (0.00, 0.04)	0.02 (0.00, 0.06)	0.02 (0.00, 0.05)	0.04 (0.01, 0.15)	1.12 (1.08, 1.16)

Model	Square	Gas	Cross	Cross (small)	Vector	Computation time
TGCCA1	0.99 (0.97, 0.99)	0.90 (0.88, 0.90)	0.88 (0.85, 0.88)	0.87 (0.85, 0.87)	0.94 (0.92, 0.96)	3.18 (3.03, 3.38)
MGCCA	0.99 (0.98, 0.99)	0.90 (0.87, 0.90)	0.88 (0.85, 0.89)	0.86 (0.84, 0.87)	0.94 (0.92, 0.96)	3.27 (3.04, 3.49)
TGCCA3	0.96 (0.94, 0.97)	0.95 (0.92, 0.96)	0.96 (0.93, 0.97)	0.96 (0.94, 0.98)	0.94 (0.92, 0.96)	5.21 (5.00, 5.43)
spTGCCA3	0.95 (0.93, 0.96)	0.95 (0.92, 0.96)	0.96 (0.93, 0.97)	0.96 (0.94, 0.97)	0.95 (0.92, 0.96)	3.34 (3.07, 3.57)
RGCCA	0.87 (0.85, 0.89)	0.83 (0.80, 0.87)	0.85 (0.82, 0.88)	0.91 (0.89, 0.94)	0.94 (0.92, 0.96)	2.22 (2.05, 2.43)
SVD	0.04 (0.00, 0.13)	0.05 (0.01, 0.13)	0.03 (0.00, 0.12)	0.03 (0.00, 0.09)	0.90 (0.69, 0.95)	0.96 (0.93, 1.00)

Model	Square	Gas	Cross	Cross (small)	Vector	Computation time
TGCCA1	0.99 (0.97, 1.00)	0.90 (0.89, 0.91)	0.88 (0.88, 0.89)	0.87 (0.86, 0.88)	0.96 (0.95, 0.98)	3.14 (2.94, 3.33)
MGCCA	0.99 (0.98, 1.00)	0.90 (0.89, 0.90)	0.88 (0.87, 0.89)	0.87 (0.86, 0.88)	0.96 (0.95, 0.98)	3.26 (3.06, 3.42)
TGCCA3	0.97 (0.95, 0.98)	0.97 (0.96, 0.97)	0.98 (0.97, 0.98)	0.98 (0.97, 0.98)	0.96 (0.95, 0.98)	5.04 (4.86, 5.34)
spTGCCA3	0.96 (0.95, 0.97)	0.96 (0.95, 0.97)	0.97 (0.96, 0.97)	0.97 (0.96, 0.98)	0.96 (0.95, 0.98)	3.39 (3.09, 3.66)
RGCCA	0.90 (0.88, 0.93)	0.88 (0.85, 0.89)	0.89 (0.86, 0.90)	0.95 (0.93, 0.96)	0.97 (0.95, 0.98)	2.18 (2.09, 2.36)
SVD	0.11 (0.00, 0.29)	0.08 (0.00, 0.26)	0.05 (0.01, 0.21)	0.11 (0.01, 0.51)	0.97 (0.95, 0.98)	1.02 (0.93, 1.09)

Model	Square	Gas	Cross	Cross (small)	Vector	Computation time
TGCCA1	1.00 (0.99, 1.00)	0.91 (0.90, 0.91)	0.89 (0.88, 0.89)	0.88 (0.87, 0.88)	0.98 (0.97, 0.99)	3.08 (2.95, 3.33)
MGCCA	1.00 (0.99, 1.00)	0.90 (0.90, 0.91)	0.89 (0.88, 0.89)	0.88 (0.87, 0.88)	0.98 (0.97, 0.99)	3.34 (3.03, 3.49)
TGCCA3	0.99 (0.98, 0.99)	0.98 (0.97, 0.98)	0.99 (0.98, 0.99)	0.99 (0.98, 0.99)	0.98 (0.97, 0.99)	5.03 (4.86, 5.31)
spTGCCA3	0.98 (0.97, 0.98)	0.97 (0.96, 0.97)	0.98 (0.97, 0.98)	0.98 (0.97, 0.99)	0.98 (0.97, 0.99)	3.38 (3.15, 3.81)
RGCCA	0.94 (0.91, 0.95)	0.91 (0.89, 0.92)	0.92 (0.89, 0.93)	0.97 (0.96, 0.98)	0.98 (0.97, 0.99)	2.03 (1.96, 2.18)
SVD	0.96 (0.88, 0.98)	0.97 (0.89, 0.97)	0.97 (0.92, 0.98)	0.98 (0.87, 0.99)	0.99 (0.98, 0.99)	1.07 (1.06, 1.20)

Table 14: Cosine between the true and the estimated canonical vectors for different models on blocks "Square", "Gas", "Cross", "Cross (small)" and "Vector", for levels of SNR -20dB, -10dB, -6dB, and 0dB from top to bottom, and computation times, for n = 200 and 50 folds. Median and quantiles (2.5% and 97.5%) are reported.

Model	Square	Gas	Cross	Cross (small)	Vector	Computation time
TGCCA1	0.91 (0.57, 0.96)	0.84 (0.49, 0.87)	0.83 (0.23, 0.86)	0.79 (0.61, 0.85)	0.77 (0.50, 0.85)	3.23 (2.59, 5.80)
MGCCA	0.92 (0.62, 0.96)	0.85 (0.50, 0.87)	0.83 (0.32, 0.86)	0.80 (0.70, 0.84)	0.79 (0.52, 0.85)	2.59 (2.39, 3.13)
TGCCA3	0.70 (0.18, 0.85)	0.68 (0.07, 0.83)	0.68 (0.09, 0.88)	0.74 (0.10, 0.88)	0.69 (0.14, 0.84)	5.38 (4.37, 9.74)
spTGCCA3	0.72 (0.06, 0.82)	0.70 (0.05, 0.82)	0.75 (0.05, 0.87)	0.76 (0.07, 0.88)	0.72 (0.07, 0.84)	2.97 (2.62, 3.96)
RGCCA	0.57 (0.24, 0.67)	0.52 (0.20, 0.63)	0.55 (0.22, 0.67)	0.63 (0.29, 0.78)	0.67 (0.36, 0.81)	2.07 (1.52, 3.81)
SVD	0.02 (0.00, 0.06)	0.02 (0.00, 0.06)	0.02 (0.00, 0.06)	0.02 (0.00, 0.06)	0.05 (0.01, 0.20)	0.49 (0.42, 0.53)

Model	Square	Gas	Cross	Cross (small)	Vector	Computation time
TGCCA1	0.98 (0.96, 0.99)	0.89 (0.86, 0.90)	0.87 (0.84, 0.88)	0.86 (0.84, 0.87)	0.92 (0.87, 0.94)	2.20 (2.10, 2.39)
MGCCA	0.98 (0.96, 0.99)	0.89 (0.86, 0.90)	0.87 (0.85, 0.88)	0.86 (0.83, 0.87)	0.92 (0.87, 0.94)	2.36 (2.22, 2.60)
TGCCA3	0.94 (0.90, 0.96)	0.93 (0.89, 0.95)	0.94 (0.91, 0.96)	0.95 (0.92, 0.96)	0.92 (0.87, 0.94)	3.87 (3.65, 4.21)
spTGCCA3	0.91 (0.88, 0.94)	0.92 (0.88, 0.94)	0.93 (0.90, 0.95)	0.94 (0.90, 0.95)	0.92 (0.87, 0.95)	2.42 (2.29, 2.67)
RGCCA	0.80 (0.74, 0.85)	0.76 (0.70, 0.80)	0.77 (0.72, 0.81)	0.88 (0.85, 0.91)	0.92 (0.87, 0.95)	1.18 (1.05, 1.37)
SVD	0.05 (0.00, 0.20)	0.05 (0.00, 0.15)	0.07 (0.02, 0.13)	0.05 (0.01, 0.15)	0.78 (0.10, 0.93)	0.46 (0.44, 0.48)

Model	Square	Gas	Cross	Cross (small)	Vector	Computation time
TGCCA1	0.99 (0.97, 1.00)	0.90 (0.88, 0.90)	0.88 (0.87, 0.88)	0.87 (0.86, 0.87)	0.95 (0.89, 0.96)	2.12 (2.00, 2.33)
MGCCA	0.99 (0.97, 0.99)	0.89 (0.89, 0.90)	0.88 (0.87, 0.88)	0.86 (0.85, 0.87)	0.95 (0.90, 0.96)	2.39 (2.22, 2.67)
TGCCA3	0.96 (0.94, 0.97)	0.95 (0.93, 0.96)	0.97 (0.95, 0.97)	0.97 (0.95, 0.98)	0.95 (0.90, 0.96)	3.99 (3.81, 4.25)
spTGCCA3	0.94 (0.91, 0.95)	0.94 (0.92, 0.95)	0.95 (0.94, 0.96)	0.95 (0.93, 0.97)	0.95 (0.90, 0.96)	2.40 (2.26, 2.56)
RGCCA	0.84 (0.80, 0.88)	0.79 (0.74, 0.81)	0.80 (0.76, 0.84)	0.92 (0.88, 0.93)	0.95 (0.90, 0.97)	1.10 (1.04, 1.32)
SVD	0.10 (0.01, 0.50)	0.14 (0.01, 0.45)	0.08 (0.01, 0.38)	0.17 (0.01, 0.54)	0.95 (0.89, 0.97)	0.45 (0.43, 0.49)

Model	Square	Gas	Cross	Cross (small)	Vector	Computation time
TGCCA1	1.00 (0.99, 1.00)	0.90 (0.89, 0.91)	0.89 (0.87, 0.89)	0.88 (0.86, 0.88)	0.97 (0.95, 0.98)	1.99 (1.89, 2.23)
MGCCA	0.99 (0.99, 1.00)	0.90 (0.89, 0.90)	0.88 (0.87, 0.89)	0.87 (0.86, 0.88)	0.97 (0.95, 0.98)	2.30 (2.17, 2.46)
TGCCA3	0.98 (0.97, 0.99)	0.97 (0.96, 0.98)	0.98 (0.97, 0.99)	0.98 (0.97, 0.99)	0.97 (0.95, 0.98)	3.88 (3.74, 4.07)
spTGCCA3	0.95 (0.94, 0.96)	0.95 (0.94, 0.96)	0.96 (0.95, 0.97)	0.97 (0.95, 0.97)	0.97 (0.95, 0.98)	2.37 (2.23, 2.61)
RGCCA	0.86 (0.82, 0.89)	0.80 (0.76, 0.84)	0.82 (0.76, 0.85)	0.94 (0.92, 0.95)	0.97 (0.96, 0.98)	1.13 (1.01, 1.22)
SVD	0.95 (0.86, 0.97)	0.95 (0.81, 0.96)	0.95 (0.73, 0.97)	0.96 (0.66, 0.98)	0.98 (0.97, 0.99)	0.45 (0.44, 0.49)

Table 15: Cosine between the true and the estimated canonical vectors for different models on blocks "Square", "Gas", "Cross", "Cross (small)" and "Vector", for levels of SNR -20dB, -10dB, -6dB, and 0dB from top to bottom, and computation times, for n = 100 and 100 folds. Median and quantiles (2.5% and 97.5%) are reported.

Model	Square	Gas	Cross	Cross (small)	Vector	Computation time
TGCCA1	0.51 (0.00, 0.92)	0.53 (0.00, 0.84)	0.34 (0.01, 0.81)	0.40 (0.02, 0.81)	0.44 (0.01, 0.80)	2.38 (1.78, 4.78)
MGCCA	0.78 (0.00, 0.92)	0.66 (0.00, 0.83)	0.70 (0.01, 0.81)	0.65 (0.00, 0.81)	0.63 (0.01, 0.80)	1.72 (1.58, 2.05)
TGCCA3	0.27 (0.01, 0.73)	0.27 (0.01, 0.72)	0.24 (0.00, 0.74)	0.24 (0.01, 0.77)	0.29 (0.04, 0.74)	4.58 (3.18, 7.75)
spTGCCA3	0.24 (0.00, 0.71)	0.20 (0.00, 0.69)	0.25 (0.00, 0.70)	0.22 (0.00, 0.74)	0.30 (0.03, 0.74)	2.01 (1.70, 3.17)
RGCCA	0.25 (0.03, 0.51)	0.24 (0.02, 0.44)	0.25 (0.01, 0.49)	0.33 (0.02, 0.62)	0.32 (0.03, 0.62)	1.38 (0.74, 3.78)
SVD	0.03 (0.00, 0.09)	0.03 (0.00, 0.08)	0.03 (0.00, 0.09)	0.03 (0.00, 0.08)	0.06 (0.00, 0.18)	0.10 (0.09, 0.14)

Model	Square	Gas	Cross	Cross (small)	Vector	Computation time
TGCCA1	0.97 (0.89, 0.98)	0.87 (0.81, 0.89)	0.85 (0.75, 0.87)	0.84 (0.76, 0.86)	0.85 (0.75, 0.91)	1.39 (1.25, 1.66)
MGCCA	0.95 (0.92, 0.97)	0.86 (0.80, 0.88)	0.84 (0.79, 0.87)	0.83 (0.76, 0.85)	0.85 (0.75, 0.92)	1.48 (1.38, 1.64)
TGCCA3	0.88 (0.79, 0.92)	0.86 (0.76, 0.91)	0.89 (0.78, 0.93)	0.89 (0.78, 0.94)	0.85 (0.74, 0.91)	2.79 (2.62, 3.13)
spTGCCA3	0.82 (0.74, 0.86)	0.82 (0.73, 0.87)	0.85 (0.79, 0.89)	0.86 (0.78, 0.91)	0.85 (0.74, 0.91)	1.57 (1.48, 1.71)
RGCCA	0.61 (0.49, 0.70)	0.56 (0.45, 0.63)	0.56 (0.46, 0.65)	0.76 (0.64, 0.83)	0.85 (0.72, 0.90)	0.58 (0.46, 0.89)
SVD	0.07 (0.00, 0.22)	0.06 (0.00, 0.19)	0.07 (0.00, 0.26)	0.07 (0.01, 0.24)	0.23 (0.01, 0.79)	0.10 (0.09, 0.15)

Model	Square	Gas	Cross	Cross (small)	Vector	Computation time
TGCCA1	0.98 (0.93, 0.99)	0.89 (0.85, 0.90)	0.87 (0.83, 0.88)	0.86 (0.83, 0.87)	0.88 (0.81, 0.93)	1.29 (1.19, 1.43)
MGCCA	0.97 (0.93, 0.98)	0.87 (0.84, 0.89)	0.85 (0.83, 0.87)	0.85 (0.81, 0.86)	0.88 (0.81, 0.93)	1.48 (1.38, 1.61)
TGCCA3	0.93 (0.87, 0.95)	0.91 (0.86, 0.94)	0.93 (0.88, 0.96)	0.94 (0.89, 0.96)	0.89 (0.81, 0.93)	2.85 (2.71, 3.04)
spTGCCA3	0.84 (0.80, 0.89)	0.87 (0.80, 0.90)	0.88 (0.84, 0.91)	0.89 (0.85, 0.92)	0.88 (0.81, 0.93)	1.52 (1.43, 1.63)
RGCCA	0.63 (0.53, 0.71)	0.57 (0.47, 0.62)	0.57 (0.49, 0.67)	0.80 (0.73, 0.87)	0.89 (0.82, 0.94)	0.50 (0.41, 0.63)
SVD	0.18 (0.01, 0.74)	0.17 (0.01, 0.67)	0.14 (0.01, 0.71)	0.19 (0.01, 0.87)	0.86 (0.46, 0.94)	0.11 (0.10, 0.15)

Model	Square	Gas	Cross	Cross (small)	Vector	Computation time
TGCCA1	0.99 (0.97, 0.99)	0.90 (0.87, 0.90)	0.88 (0.86, 0.89)	0.87 (0.84, 0.88)	0.90 (0.83, 0.94)	1.22 (1.15, 1.33)
MGCCA	0.98 (0.96, 0.99)	0.89 (0.86, 0.90)	0.87 (0.84, 0.88)	0.86 (0.83, 0.87)	0.90 (0.83, 0.94)	1.46 (1.37, 1.65)
TGCCA3	0.96 (0.93, 0.98)	0.95 (0.92, 0.97)	0.97 (0.94, 0.98)	0.97 (0.94, 0.98)	0.91 (0.83, 0.94)	2.77 (2.61, 2.94)
spTGCCA3	0.86 (0.81, 0.88)	0.88 (0.85, 0.90)	0.90 (0.88, 0.92)	0.91 (0.88, 0.93)	0.91 (0.83, 0.94)	1.44 (1.37, 1.59)
RGCCA	0.60 (0.52, 0.69)	0.52 (0.46, 0.62)	0.56 (0.47, 0.62)	0.80 (0.73, 0.86)	0.93 (0.87, 0.95)	0.42 (0.36, 0.54)
SVD	0.92 (0.47, 0.94)	0.90 (0.39, 0.93)	0.90 (0.46, 0.94)	0.94 (0.53, 0.97)	0.96 (0.93, 0.98)	0.11 (0.10, 0.14)

Table 16: Cosine between the true and the estimated canonical vectors for different models on blocks "Gas" and "Cross (small)", for levels of SNR -20dB, -10dB, -6dB and 0dB from top to bottom, and computation times, for n = 1000 and 10 folds. Median and quantiles (2.5% and 97.5%) are reported. Models that saw only 2 blocks (suffixed with "b2") are compare with models that saw the 5 blocks (suffixed with "b5").

Model	Gas	Cross (small)	Computation time
TGCCA1b2	0.89 (0.87, 0.90)	0.85 (0.83, 0.86)	8.60 (8.36, 9.12)
TGCCA1b5	0.90 (0.89, 0.90)	0.86 (0.85, 0.87)	20.35 (19.73, 21.34)
MGCCAb2	0.89 (0.87, 0.90)	0.86 (0.83, 0.86)	5.08 (4.85, 5.32)
MGCCAb5	0.90 (0.89, 0.90)	0.87 (0.85, 0.87)	9.88 (9.61, 10.20)
TGCCA3b2	0.91 (0.78, 0.94)	0.92 (0.79, 0.96)	11.32 (10.12, 15.94)
TGCCA3b5	0.96 (0.94, 0.97)	0.96 (0.95, 0.97)	23.55 (22.51, 27.70)
spTGCCA3b2	0.92 (0.82, 0.94)	0.93 (0.83, 0.96)	5.66 (5.52, 6.39)
spTGCCA3b5	0.96 (0.94, 0.97)	0.96 (0.95, 0.97)	10.15 (9.91, 10.61)
RGCCAb2	0.17 (0.05, 0.26)	0.11 (0.06, 0.20)	13.12 (12.67, 14.07)
RGCCAb5	0.86 (0.79, 0.88)	0.91 (0.87, 0.93)	32.44 (28.48, 36.78)

Model	Gas	Cross (small)	Computation time
TGCCA1b2	0.90 (0.89, 0.91)	0.88 (0.87, 0.88)	8.17 (8.02, 8.53)
TGCCA1b5	0.91 (0.90, 0.91)	0.88 (0.87, 0.88)	19.02 (18.88, 19.45)
MGCCAb2	0.90 (0.89, 0.91)	0.88 (0.87, 0.88)	4.84 (4.68, 5.35)
MGCCAb5	0.91 (0.90, 0.91)	0.88 (0.87, 0.88)	9.63 (9.46, 10.26)
TGCCA3b2	0.97 (0.96, 0.98)	0.99 (0.98, 0.99)	9.65 (9.23, 10.28)
TGCCA3b5	0.98 (0.97, 0.98)	0.99 (0.99, 0.99)	24.19 (22.21, 25.08)
spTGCCA3b2	0.97 (0.96, 0.98)	0.99 (0.98, 0.99)	5.10 (4.90, 5.48)
spTGCCA3b5	0.98 (0.97, 0.98)	0.99 (0.99, 0.99)	9.77 (9.62, 10.19)
RGCCAb2	0.93 (0.91, 0.94)	0.97 (0.96, 0.98)	11.97 (11.38, 12.74)
RGCCAb5	0.95 (0.94, 0.95)	0.98 (0.97, 0.98)	29.80 (28.21, 31.24)

Model	Gas	Cross (small)	Computation time
TGCCA1b2	0.90 (0.90, 0.91)	0.88 (0.87, 0.88)	8.07 (7.97, 8.25)
TGCCA1b5	0.91 (0.91, 0.91)	0.88 (0.88, 0.88)	18.97 (18.66, 19.40)
MGCCAb2	0.90 (0.90, 0.91)	0.88 (0.87, 0.88)	4.87 (4.56, 5.19)
MGCCAb5	0.91 (0.91, 0.91)	0.88 (0.88, 0.88)	9.83 (9.61, 10.37)
TGCCA3b2	0.98 (0.97, 0.98)	0.99 (0.98, 0.99)	9.51 (9.25, 10.76)
TGCCA3b5	0.98 (0.98, 0.98)	0.99 (0.99, 1.00)	22.76 (22.00, 24.48)
spTGCCA3b2	0.98 (0.97, 0.98)	0.99 (0.98, 0.99)	5.03 (4.89, 5.35)
spTGCCA3b5	0.98 (0.98, 0.98)	0.99 (0.99, 0.99)	9.91 (9.72, 10.28)
RGCCAb2	0.95 (0.95, 0.96)	0.98 (0.97, 0.98)	11.78 (11.13, 12.13)
RGCCAb5	0.97 (0.96, 0.97)	0.98 (0.98, 0.99)	28.99 (27.72, 30.75)

Model	Gas	Cross (small)	Computation time
TGCCA1b2	0.91 (0.91, 0.91)	0.88 (0.88, 0.88)	8.12 (7.88, 8.29)
TGCCA1b5	0.91 (0.91, 0.91)	0.88 (0.88, 0.88)	18.24 (18.08, 18.48)
MGCCAb2	0.91 (0.91, 0.91)	0.88 (0.88, 0.88)	4.79 (4.68, 5.11)
MGCCAb5	0.91 (0.91, 0.91)	0.88 (0.88, 0.88)	9.66 (9.47, 10.26)
TGCCA3b2	0.98 (0.98, 0.98)	1.00 (0.99, 1.00)	9.69 (9.35, 11.20)
TGCCA3b5	0.98 (0.98, 0.98)	1.00 (0.99, 1.00)	22.02 (21.74, 22.83)
spTGCCA3b2	0.98 (0.98, 0.98)	0.99 (0.99, 1.00)	4.97 (4.84, 5.33)
spTGCCA3b5	0.98 (0.98, 0.98)	1.00 (0.99, 1.00)	9.72 (9.48, 10.25)
RGCCAb2	0.98 (0.97, 0.98)	0.99 (0.99, 0.99)	11.56 (11.04, 12.17)
RGCCAb5	0.98 (0.98, 0.99)	0.99 (0.99, 0.99)	30.16 (29.33, 31.02)

Table 17: Cosine between the true and the estimated canonical vectors for different models on blocks "Gas" and "Cross (small)", for levels of SNR -20dB, -10dB, -6dB and 0dB from top to bottom, and computation times, for n = 500 and 20 folds. Median and quantiles (2.5% and 97.5%) are reported. Models that saw only 2 blocks (suffixed with "b2") are compare with models that saw the 5 blocks (suffixed with "b5").

Model	Gas	Cross (small)	Computation time
TGCCA1b2	0.86 (0.68, 0.89)	0.82 (0.63, 0.86)	3.16 (3.02, 4.50)
TGCCA1b5	0.89 (0.82, 0.89)	0.86 (0.83, 0.87)	6.91 (6.33, 8.42)
MGCCAb2	0.86 (0.72, 0.89)	0.82 (0.69, 0.86)	2.81 (2.50, 3.18)
MGCCAb5	0.89 (0.84, 0.89)	0.86 (0.82, 0.87)	5.34 (4.95, 5.77)
TGCCA3b2	0.16 (0.01, 0.68)	0.19 (0.01, 0.64)	4.73 (3.49, 7.97)
TGCCA3b5	0.91 (0.68, 0.94)	0.93 (0.83, 0.95)	9.56 (8.90, 10.66)
spTGCCA3b2	0.20 (0.01, 0.70)	0.21 (0.02, 0.67)	2.79 (2.51, 3.53)
spTGCCA3b5	0.91 (0.69, 0.94)	0.93 (0.84, 0.94)	5.60 (5.38, 6.32)
RGCCAb2	0.11 (0.00, 0.22)	0.07 (0.01, 0.15)	3.27 (3.06, 3.57)
RGCCAb5	0.74 (0.41, 0.80)	0.81 (0.50, 0.87)	9.16 (7.81, 11.87)

Model	Gas	Cross (small)	Computation time
TGCCA1b2	0.90 (0.87, 0.90)	0.87 (0.85, 0.88)	2.80 (2.65, 3.04)
TGCCA1b5	0.90 (0.89, 0.90)	0.87 (0.86, 0.88)	6.01 (5.77, 6.60)
MGCCAb2	0.90 (0.87, 0.90)	0.87 (0.85, 0.88)	2.73 (2.49, 3.13)
MGCCAb5	0.90 (0.88, 0.90)	0.87 (0.86, 0.88)	5.10 (4.96, 5.52)
TGCCA3b2	0.96 (0.93, 0.96)	0.97 (0.94, 0.98)	3.68 (3.55, 3.95)
TGCCA3b5	0.97 (0.95, 0.97)	0.98 (0.96, 0.98)	8.79 (8.46, 9.60)
spTGCCA3b2	0.96 (0.92, 0.96)	0.97 (0.95, 0.98)	2.53 (2.45, 2.86)
spTGCCA3b5	0.96 (0.95, 0.97)	0.98 (0.96, 0.98)	5.30 (5.10, 5.74)
RGCCAb2	0.86 (0.83, 0.89)	0.94 (0.88, 0.96)	3.00 (2.77, 3.46)
RGCCAb5	0.90 (0.88, 0.91)	0.95 (0.93, 0.96)	6.43 (6.22, 7.21)

Model	Gas	Cross (small)	Computation time
TGCCA1b2	0.90 (0.89, 0.91)	0.87 (0.86, 0.88)	2.82 (2.67, 3.09)
TGCCA1b5	0.91 (0.90, 0.91)	0.88 (0.87, 0.88)	6.00 (5.80, 6.24)
MGCCAb2	0.90 (0.89, 0.91)	0.87 (0.86, 0.88)	2.51 (2.35, 2.91)
MGCCAb5	0.90 (0.90, 0.91)	0.88 (0.86, 0.88)	5.21 (5.05, 5.59)
TGCCA3b2	0.97 (0.96, 0.98)	0.98 (0.97, 0.99)	3.62 (3.39, 3.93)
TGCCA3b5	0.98 (0.97, 0.98)	0.99 (0.98, 0.99)	8.87 (8.60, 9.45)
spTGCCA3b2	0.97 (0.96, 0.97)	0.98 (0.97, 0.98)	2.60 (2.45, 2.93)
spTGCCA3b5	0.97 (0.97, 0.98)	0.99 (0.97, 0.99)	5.36 (5.09, 5.73)
RGCCAb2	0.91 (0.89, 0.93)	0.96 (0.95, 0.97)	2.67 (2.54, 2.83)
RGCCAb5	0.93 (0.92, 0.94)	0.97 (0.96, 0.97)	6.79 (6.60, 7.09)

Model	Gas	Cross (small)	Computation time
TGCCA1b2	0.91 (0.90, 0.91)	0.88 (0.87, 0.88)	2.69 (2.56, 2.97)
TGCCA1b5	0.91 (0.90, 0.91)	0.88 (0.87, 0.88)	5.87 (5.65, 6.12)
MGCCAb2	0.91 (0.90, 0.91)	0.88 (0.87, 0.88)	2.51 (2.34, 2.93)
MGCCAb5	0.91 (0.90, 0.91)	0.88 (0.87, 0.88)	5.10 (4.91, 5.49)
TGCCA3b2	0.98 (0.97, 0.98)	0.99 (0.98, 0.99)	3.58 (3.49, 3.96)
TGCCA3b5	0.98 (0.98, 0.98)	0.99 (0.99, 1.00)	8.90 (8.34, 9.83)
spTGCCA3b2	0.98 (0.97, 0.98)	0.99 (0.98, 0.99)	2.51 (2.36, 2.90)
spTGCCA3b5	0.98 (0.97, 0.98)	0.99 (0.99, 0.99)	5.34 (5.00, 5.77)
RGCCAb2	0.94 (0.93, 0.95)	0.98 (0.97, 0.98)	2.48 (2.41, 2.58)
RGCCAb5	0.96 (0.95, 0.97)	0.98 (0.98, 0.99)	6.46 (6.33, 6.91)

Table 18: Cosine between the true and the estimated canonical vectors for different models on blocks "Gas" and "Cross (small)", for levels of SNR -20dB, -10dB, -6dB and 0dB from top to bottom, and computation times, for n = 300 and 33 folds. Median and quantiles (2.5% and 97.5%) are reported. Models that saw only 2 blocks (suffixed with "b2") are compare with models that saw the 5 blocks (suffixed with "b5").

Model	Gas	Cross (small)	Computation time
TGCCA1b2	0.25 (0.00, 0.85)	0.28 (0.05, 0.81)	1.78 (1.51, 2.65)
TGCCA1b5	0.87 (0.50, 0.89)	0.82 (0.52, 0.86)	4.09 (3.55, 5.89)
MGCCAb2	0.59 (0.00, 0.88)	0.44 (0.04, 0.84)	1.69 (1.59, 2.02)
MGCCAb5	0.87 (0.75, 0.89)	0.83 (0.76, 0.86)	3.55 (3.27, 4.01)
TGCCA3b2	0.07 (0.00, 0.35)	0.06 (0.00, 0.36)	2.27 (1.95, 3.44)
TGCCA3b5	0.82 (0.39, 0.89)	0.86 (0.47, 0.91)	6.44 (5.64, 10.08)
spTGCCA3b2	0.06 (0.00, 0.33)	0.05 (0.01, 0.33)	1.79 (1.60, 2.17)
spTGCCA3b5	0.82 (0.41, 0.88)	0.87 (0.53, 0.91)	3.77 (3.37, 4.40)
RGCCAb2	0.07 (0.01, 0.17)	0.05 (0.00, 0.12)	1.03 (0.96, 1.11)
RGCCAb5	0.62 (0.27, 0.69)	0.69 (0.33, 0.78)	3.10 (2.64, 4.01)

Model	Gas	Cross (small)	Computation time
TGCCA1b2	0.89 (0.85, 0.90)	0.86 (0.82, 0.87)	1.46 (1.37, 1.65)
TGCCA1b5	0.90 (0.88, 0.90)	0.87 (0.85, 0.87)	3.18 (3.03, 3.38)
MGCCAb2	0.89 (0.86, 0.90)	0.86 (0.83, 0.87)	1.59 (1.47, 1.72)
MGCCAb5	0.90 (0.87, 0.90)	0.86 (0.84, 0.87)	3.27 (3.04, 3.49)
TGCCA3b2	0.93 (0.88, 0.95)	0.95 (0.91, 0.97)	2.12 (1.94, 2.25)
TGCCA3b5	0.95 (0.92, 0.96)	0.96 (0.94, 0.98)	5.21 (5.00, 5.43)
spTGCCA3b2	0.93 (0.88, 0.95)	0.94 (0.91, 0.96)	1.64 (1.52, 1.82)
spTGCCA3b5	0.95 (0.92, 0.96)	0.96 (0.94, 0.97)	3.34 (3.07, 3.57)
RGCCAb2	0.77 (0.35, 0.83)	0.88 (0.42, 0.93)	1.23 (1.06, 1.64)
RGCCAb5	0.83 (0.80, 0.87)	0.91 (0.89, 0.94)	2.22 (2.05, 2.43)

Model	Gas	Cross (small)	Computation time
TGCCA1b2	0.90 (0.88, 0.90)	0.87 (0.85, 0.88)	1.47 (1.37, 1.68)
TGCCA1b5	0.90 (0.89, 0.91)	0.87 (0.86, 0.88)	3.14 (2.94, 3.33)
MGCCAb2	0.90 (0.88, 0.90)	0.87 (0.85, 0.87)	1.53 (1.45, 1.78)
MGCCAb5	0.90 (0.89, 0.90)	0.87 (0.86, 0.88)	3.26 (3.06, 3.42)
TGCCA3b2	0.96 (0.93, 0.97)	0.97 (0.95, 0.98)	2.11 (1.99, 2.30)
TGCCA3b5	0.97 (0.96, 0.97)	0.98 (0.97, 0.98)	5.04 (4.86, 5.34)
spTGCCA3b2	0.95 (0.93, 0.96)	0.97 (0.95, 0.98)	1.55 (1.45, 1.78)
spTGCCA3b5	0.96 (0.95, 0.97)	0.97 (0.96, 0.98)	3.39 (3.09, 3.66)
RGCCAb2	0.83 (0.79, 0.86)	0.94 (0.91, 0.96)	0.99 (0.91, 1.09)
RGCCAb5	0.88 (0.85, 0.89)	0.95 (0.93, 0.96)	2.18 (2.09, 2.36)

Model	Gas	Cross (small)	Computation time
TGCCA1b2	0.90 (0.89, 0.91)	0.88 (0.86, 0.88)	1.51 (1.35, 1.75)
TGCCA1b5	0.91 (0.90, 0.91)	0.88 (0.87, 0.88)	3.08 (2.95, 3.33)
MGCCAb2	0.90 (0.89, 0.91)	0.87 (0.86, 0.88)	1.52 (1.43, 1.70)
MGCCAb5	0.90 (0.90, 0.91)	0.88 (0.87, 0.88)	3.34 (3.03, 3.49)
TGCCA3b2	0.97 (0.96, 0.98)	0.99 (0.97, 0.99)	2.03 (1.93, 2.19)
TGCCA3b5	0.98 (0.97, 0.98)	0.99 (0.98, 0.99)	5.03 (4.86, 5.31)
spTGCCA3b2	0.96 (0.95, 0.97)	0.98 (0.96, 0.98)	1.55 (1.47, 1.75)
spTGCCA3b5	0.97 (0.96, 0.97)	0.98 (0.97, 0.99)	3.38 (3.15, 3.81)
RGCCAb2	0.87 (0.84, 0.89)	0.96 (0.94, 0.97)	0.91 (0.86, 1.01)
RGCCAb5	0.91 (0.89, 0.92)	0.97 (0.96, 0.98)	2.03 (1.96, 2.18)

Table 19: Cosine between the true and the estimated canonical vectors for different models on blocks "Gas" and "Cross (small)", for levels of SNR -20dB, -10dB, -6dB and 0dB from top to bottom, and computation times, for n = 200 and 50 folds. Median and quantiles (2.5% and 97.5%) are reported. Models that saw only 2 blocks (suffixed with "b2") are compare with models that saw the 5 blocks (suffixed with "b5").

Model	Gas	Cross (small)	Computation time
TGCCA1b2	0.08 (0.00, 0.71)	0.24 (0.10, 0.62)	1.10 (0.94, 1.87)
TGCCA1b5	0.84 (0.49, 0.87)	0.79 (0.61, 0.85)	3.23 (2.59, 5.80)
MGCCAb2	0.18 (0.00, 0.79)	0.23 (0.04, 0.73)	1.15 (1.06, 1.61)
MGCCAb5	0.85 (0.50, 0.87)	0.80 (0.70, 0.84)	2.59 (2.39, 3.13)
TGCCA3b2	0.07 (0.00, 0.30)	0.08 (0.00, 0.26)	1.56 (1.34, 2.27)
TGCCA3b5	0.68 (0.07, 0.83)	0.74 (0.10, 0.88)	5.38 (4.37, 9.74)
spTGCCA3b2	0.05 (0.00, 0.32)	0.07 (0.01, 0.31)	1.19 (1.12, 1.44)
spTGCCA3b5	0.70 (0.05, 0.82)	0.76 (0.07, 0.88)	2.97 (2.62, 3.96)
RGCCAb2	0.05 (0.01, 0.19)	0.06 (0.00, 0.13)	0.46 (0.41, 0.56)
RGCCAb5	0.52 (0.20, 0.63)	0.63 (0.29, 0.78)	2.07 (1.52, 3.81)
Model	Gas	Cross (small)	Computation time
TGCCA1b2	0.88 (0.82, 0.89)	0.85 (0.80, 0.87)	0.99 (0.91, 1.14)
TGCCA1b5	0.89 (0.86, 0.90)	0.86 (0.84, 0.87)	2.20 (2.10, 2.39)
MGCCAb2	0.88 (0.83, 0.89)	0.85 (0.81, 0.86)	1.11 (1.02, 1.23)
MGCCAb5	0.89 (0.86, 0.90)	0.86 (0.83, 0.87)	2.36 (2.22, 2.60)
TGCCA3b2	0.90 (0.83, 0.93)	0.93 (0.85, 0.96)	1.52 (1.39, 1.81)
TGCCA3b5	0.93 (0.89, 0.95)	0.95 (0.92, 0.96)	3.87 (3.65, 4.21)
spTGCCA3b2	0.89 (0.83, 0.92)	0.92 (0.85, 0.94)	1.15 (1.08, 1.24)
spTGCCA3b5	0.92 (0.88, 0.94)	0.94 (0.90, 0.95)	2.42 (2.29, 2.67)
RGCCAb2	0.59 (0.09, 0.75)	0.76 (0.17, 0.92)	0.66 (0.53, 1.80)
RGCCAb5	0.76 (0.70, 0.80)	0.88 (0.85, 0.91)	1.18 (1.05, 1.37)
Model	Gas	Cross (small)	Computation time
TGCCA1b2	0.89 (0.87, 0.90)	0.86 (0.83, 0.87)	0.95 (0.86, 1.08)
TGCCA1b5	0.90 (0.88, 0.90)	0.87 (0.86, 0.87)	2.12 (2.00, 2.33)
MGCCAb2	0.89 (0.86, 0.90)	0.86 (0.83, 0.87)	1.09 (1.01, 1.21)
MGCCAb5	0.89 (0.89, 0.90)	0.86 (0.85, 0.87)	2.39 (2.22, 2.67)
TGCCA3b2	0.94 (0.90, 0.96)	0.96 (0.92, 0.97)	1.47 (1.36, 1.60)
TGCCA3b5	0.95 (0.93, 0.96)	0.97 (0.95, 0.98)	3.99 (3.81, 4.25)
spTGCCA3b2	0.93 (0.88, 0.94)	0.94 (0.91, 0.96)	1.12 (1.05, 1.22)
spTGCCA3b5	0.94 (0.92, 0.95)	0.95 (0.93, 0.97)	2.40 (2.26, 2.56)
RGCCAb2	0.72 (0.62, 0.76)	0.91 (0.85, 0.94)	0.54 (0.45, 0.74)
RGCCAb5	0.79 (0.74, 0.81)	0.92 (0.88, 0.93)	1.10 (1.04, 1.32)
Model	Gas	Cross (small)	Computation time
TGCCA1b2	0.90 (0.89, 0.91)	0.87 (0.86, 0.88)	0.87 (0.80, 1.01)
TGCCA1b5	0.90 (0.89, 0.91)	0.88 (0.86, 0.88)	1.99 (1.89, 2.23)
MGCCAb2	0.90 (0.87, 0.90)	0.87 (0.85, 0.87)	1.07 (0.99, 1.25)
MGCCAb5	0.90 (0.89, 0.90)	0.87 (0.86, 0.88)	2.30 (2.17, 2.46)
TGCCA3b2	0.97 (0.94, 0.98)	0.98 (0.96, 0.99)	1.40 (1.35, 1.56)
TGCCA3b5	0.97 (0.96, 0.98)	0.98 (0.97, 0.99)	3.88 (3.74, 4.07)
spTGCCA3b2	0.94 (0.91, 0.95)	0.96 (0.94, 0.97)	1.08 (1.00, 1.28)
spTGCCA3b5	0.95 (0.94, 0.96)	0.97 (0.95, 0.97)	2.37 (2.23, 2.61)
RGCCAb2	0.73 (0.67, 0.79)	0.94 (0.92, 0.96)	0.49 (0.43, 0.56)
RGCCAb5	0.80 (0.76, 0.84)	0.94 (0.92, 0.95)	1.13 (1.01, 1.22)

Table 20: Cosine between the true and the estimated canonical vectors for different models on blocks "Gas" and "Cross (small)", for levels of SNR -20dB, -10dB, -6dB and 0dB from top to bottom, and computation times, for n = 100 and 100 folds. Median and quantiles (2.5% and 97.5%) are reported. Models that saw only 2 blocks (suffixed with "b2") are compare with models that saw the 5 blocks (suffixed with "b5").

Model	Gas	Cross (small)	Computation time
TGCCA1b2	0.04 (0.00, 0.52)	0.20 (0.01, 0.45)	0.62 (0.51, 0.91)
TGCCA1b5	0.53 (0.00, 0.84)	0.40 (0.02, 0.81)	2.38 (1.78, 4.78)
MGCCAb2	0.07 (0.00, 0.56)	0.18 (0.01, 0.50)	0.72 (0.64, 0.87)
MGCCAb5	0.66 (0.00, 0.83)	0.65 (0.00, 0.81)	1.72 (1.58, 2.05)
TGCCA3b2	0.06 (0.00, 0.35)	0.07 (0.01, 0.24)	1.01 (0.90, 1.72)
TGCCA3b5	0.27 (0.01, 0.72)	0.24 (0.01, 0.77)	4.58 (3.18, 7.75)
spTGCCA3b2	0.05 (0.00, 0.30)	0.06 (0.00, 0.27)	0.73 (0.63, 0.90)
spTGCCA3b5	0.20 (0.00, 0.69)	0.22 (0.00, 0.74)	2.01 (1.70, 3.17)
RGCCAb2	0.05 (0.00, 0.17)	0.04 (0.00, 0.14)	0.22 (0.16, 0.29)
RGCCAb5	0.24 (0.02, 0.44)	0.33 (0.02, 0.62)	1.38 (0.74, 3.78)

Model	Gas	Cross (small)	Computation time
TGCCA1b2	0.84 (0.62, 0.88)	0.81 (0.36, 0.86)	0.58 (0.49, 0.86)
TGCCA1b5	0.87 (0.81, 0.89)	0.84 (0.76, 0.86)	1.39 (1.25, 1.66)
MGCCAb2	0.83 (0.66, 0.87)	0.80 (0.64, 0.85)	0.68 (0.61, 0.82)
MGCCAb5	0.86 (0.80, 0.88)	0.83 (0.76, 0.85)	1.48 (1.38, 1.64)
TGCCA3b2	0.78 (0.19, 0.88)	0.81 (0.07, 0.93)	1.04 (0.89, 2.11)
TGCCA3b5	0.86 (0.76, 0.91)	0.89 (0.78, 0.94)	2.79 (2.62, 3.13)
spTGCCA3b2	0.76 (0.12, 0.83)	0.80 (0.15, 0.89)	0.76 (0.65, 1.01)
spTGCCA3b5	0.82 (0.73, 0.87)	0.86 (0.78, 0.91)	1.57 (1.48, 1.71)
RGCCAb2	0.17 (0.01, 0.53)	0.31 (0.04, 0.79)	0.28 (0.19, 0.75)
RGCCAb5	0.56 (0.45, 0.63)	0.76 (0.64, 0.83)	0.58 (0.46, 0.89)

Model	Gas	Cross (small)	Computation time
TGCCA1b2	0.88 (0.81, 0.89)	0.85 (0.75, 0.87)	0.53 (0.45, 0.66)
TGCCA1b5	0.89 (0.85, 0.90)	0.86 (0.83, 0.87)	1.29 (1.19, 1.43)
MGCCAb2	0.86 (0.81, 0.88)	0.83 (0.77, 0.86)	0.67 (0.60, 0.75)
MGCCAb5	0.87 (0.84, 0.89)	0.85 (0.81, 0.86)	1.48 (1.38, 1.61)
TGCCA3b2	0.89 (0.78, 0.93)	0.92 (0.82, 0.95)	0.93 (0.85, 1.06)
TGCCA3b5	0.91 (0.86, 0.94)	0.94 (0.89, 0.96)	2.85 (2.71, 3.04)
spTGCCA3b2	0.84 (0.72, 0.88)	0.87 (0.80, 0.91)	0.69 (0.62, 0.80)
spTGCCA3b5	0.87 (0.80, 0.90)	0.89 (0.85, 0.92)	1.52 (1.43, 1.63)
RGCCAb2	0.47 (0.14, 0.57)	0.84 (0.34, 0.90)	0.34 (0.22, 0.93)
RGCCAb5	0.57 (0.47, 0.62)	0.80 (0.73, 0.87)	0.50 (0.41, 0.63)

Model	Gas	Cross (small)	Computation time
TGCCA1b2	0.89 (0.86, 0.90)	0.86 (0.84, 0.88)	0.48 (0.42, 0.55)
TGCCA1b5	0.90 (0.87, 0.90)	0.87 (0.84, 0.88)	1.22 (1.15, 1.33)
MGCCAb2	0.88 (0.84, 0.89)	0.85 (0.82, 0.87)	0.64 (0.59, 0.72)
MGCCAb5	0.89 (0.86, 0.90)	0.86 (0.83, 0.87)	1.46 (1.37, 1.65)
TGCCA3b2	0.94 (0.88, 0.97)	0.96 (0.93, 0.98)	0.92 (0.84, 1.02)
TGCCA3b5	0.95 (0.92, 0.97)	0.97 (0.94, 0.98)	2.77 (2.61, 2.94)
spTGCCA3b2	0.86 (0.79, 0.90)	0.90 (0.87, 0.92)	0.67 (0.60, 0.76)
spTGCCA3b5	0.88 (0.85, 0.90)	0.91 (0.88, 0.93)	1.44 (1.37, 1.59)
RGCCAb2	0.46 (0.38, 0.57)	0.90 (0.87, 0.93)	0.22 (0.15, 0.33)
RGCCAb5	0.52 (0.46, 0.62)	0.80 (0.73, 0.86)	0.42 (0.36, 0.54)

Table 21: Cosine between the true and the estimated canonical vectors for different models on blocks "Cross" and "Cross (small) 3D", for levels of SNR -20dB, -10dB, -6dB and 0dB from top to bottom, and computation times, for n = 1000 and 10 folds. Median and quantiles (2.5% and 97.5%) are reported (3D settings).

Model	Cross	Cross (small) 3D	Computation time
TCCA1	0.24 (0.01, 0.58)	0.06 (0.01, 0.19)	19.61 (17.14, 23.42)
TGCCA1	0.22 (0.01, 0.56)	0.06 (0.01, 0.18)	15.13 (11.93, 19.30)
spTCCA1	0.23 (0.01, 0.57)	0.06 (0.01, 0.19)	18.73 (15.60, 23.77)
spTGCCA1	0.30 (0.05, 0.79)	0.08 (0.01, 0.72)	22.23 (15.21, 24.41)
TCCA3	0.23 (0.01, 0.58)	0.06 (0.01, 0.19)	29.14 (20.87, 36.34)
TGCCA3	0.15 (0.00, 0.36)	0.07 (0.03, 0.15)	32.84 (20.78, 48.05)
spTCCA3	0.24 (0.01, 0.57)	0.06 (0.02, 0.18)	17.92 (16.03, 24.10)
spTGCCA3	0.15 (0.00, 0.33)	0.03 (0.00, 0.09)	172.59 (28.87, 237.88)
RGCCA	0.07 (0.04, 0.20)	0.08 (0.00, 0.13)	114.81 (113.06, 116.57)
SVD	0.00 (0.00, 0.01)	0.00 (0.00, 0.01)	1.55 (1.30, 1.67)

Model	Cross	Cross (small) 3D	Computation time
TCCA1	0.88 (0.87, 0.89)	0.88 (0.85, 0.88)	17.31 (16.74, 18.94)
TGCCA1	0.88 (0.87, 0.89)	0.88 (0.85, 0.88)	14.29 (13.24, 21.84)
spTCCA1	0.88 (0.87, 0.89)	0.88 (0.85, 0.88)	15.70 (15.32, 23.05)
spTGCCA1	0.88 (0.87, 0.89)	0.87 (0.87, 0.88)	15.90 (15.10, 24.15)
TCCA3	0.88 (0.87, 0.89)	0.88 (0.85, 0.88)	23.89 (19.64, 26.21)
TGCCA3	0.98 (0.96, 1.00)	0.88 (0.82, 0.88)	21.58 (20.46, 25.45)
spTCCA3	0.88 (0.87, 0.89)	0.88 (0.85, 0.88)	17.96 (15.65, 20.41)
spTGCCA3	0.98 (0.96, 0.99)	0.99 (0.95, 0.99)	49.52 (27.35, 113.45)
RGCCA	0.97 (0.92, 0.98)	0.98 (0.84, 0.98)	115.32 (113.21, 116.23)
SVD	0.01 (0.00, 0.03)	0.01 (0.00, 0.03)	1.62 (1.54, 1.73)

Model	Cross	Cross (small) 3D	Computation time
TCCA1	0.89 (0.88, 0.89)	0.88 (0.87, 0.88)	17.94 (17.03, 26.41)
TGCCA1	0.89 (0.88, 0.89)	0.88 (0.87, 0.88)	14.49 (13.84, 21.02)
spTCCA1	0.89 (0.88, 0.89)	0.88 (0.87, 0.88)	15.71 (14.92, 21.62)
spTGCCA1	0.89 (0.88, 0.89)	0.87 (0.87, 0.88)	16.05 (15.50, 23.93)
TCCA3	0.89 (0.88, 0.89)	0.88 (0.87, 0.88)	23.86 (19.44, 25.04)
TGCCA3	0.99 (0.98, 1.00)	0.88 (0.86, 0.88)	21.14 (17.63, 25.03)
spTCCA3	0.89 (0.88, 0.89)	0.88 (0.87, 0.88)	18.64 (15.72, 20.52)
spTGCCA3	0.99 (0.98, 0.99)	0.99 (0.98, 0.99)	47.89 (24.79, 167.48)
RGCCA	0.99 (0.98, 0.99)	0.99 (0.96, 0.99)	113.52 (111.30, 116.14)
SVD	0.04 (0.01, 0.09)	0.03 (0.00, 0.08)	1.63 (1.54, 1.72)

Model	Cross	Cross (small) 3D	Computation time
TCCA1	0.89 (0.89, 0.89)	0.88 (0.88, 0.88)	18.27 (16.99, 23.82)
TGCCA1	0.89 (0.89, 0.89)	0.88 (0.88, 0.88)	13.91 (13.27, 20.08)
spTCCA1	0.89 (0.89, 0.89)	0.88 (0.88, 0.88)	15.91 (15.35, 22.04)
spTGCCA1	0.89 (0.89, 0.89)	0.88 (0.88, 0.88)	16.06 (15.53, 21.57)
TCCA3	0.89 (0.89, 0.89)	0.88 (0.88, 0.88)	22.42 (19.75, 25.23)
TGCCA3	1.00 (1.00, 1.00)	0.88 (0.88, 0.88)	20.80 (17.94, 22.61)
spTCCA3	0.89 (0.89, 0.89)	0.88 (0.88, 0.88)	19.52 (15.88, 21.04)
spTGCCA3	0.98 (0.98, 0.99)	0.99 (0.99, 0.99)	27.30 (17.14, 90.72)
RGCCA	1.00 (0.99, 1.00)	1.00 (0.99, 1.00)	113.00 (111.78, 115.33)
SVD	1.00 (0.99, 1.00)	1.00 (0.99, 1.00)	1.63 (1.59, 1.73)

Table 22: Cosine between the true and the estimated canonical vectors for different models on blocks "Cross" and "Cross (small) 3D", for levels of SNR -20dB, -10dB, -6dB and 0dB from top to bottom, and computation times, for n = 500 and 20 folds. Median and quantiles (2.5% and 97.5%) are reported (3D settings).

Model	Cross	Cross (small) 3D	Computation time
TCCA1	0.06 (0.01, 0.42)	0.06 (0.02, 0.07)	21.45 (16.77, 31.91)
TGCCA1	0.08 (0.00, 0.41)	0.06 (0.02, 0.07)	9.01 (7.68, 22.16)
spTCCA1	0.06 (0.00, 0.42)	0.06 (0.02, 0.07)	17.69 (14.87, 24.50)
spTGCCA1	0.07 (0.00, 0.57)	0.06 (0.02, 0.48)	12.85 (8.34, 32.45)
TCCA3	0.05 (0.01, 0.42)	0.06 (0.02, 0.07)	26.90 (19.81, 47.01)
TGCCA3	0.09 (0.02, 0.32)	0.06 (0.01, 0.07)	26.20 (13.77, 39.07)
spTCCA3	0.07 (0.00, 0.43)	0.06 (0.02, 0.07)	16.76 (15.78, 17.82)
spTGCCA3	0.07 (0.00, 0.26)	0.02 (0.00, 0.07)	59.22 (17.32, 136.30)
RGCCA	0.07 (0.01, 0.16)	0.03 (0.00, 0.11)	43.93 (41.26, 50.34)
SVD	0.01 (0.00, 0.01)	0.01 (0.00, 0.01)	0.59 (0.51, 0.62)

Model	Cross	Cross (small) 3D	Computation time
TCCA1	0.88 (0.62, 0.89)	0.88 (0.45, 0.88)	17.17 (16.40, 21.12)
TGCCA1	0.88 (0.61, 0.89)	0.88 (0.43, 0.88)	9.41 (8.69, 13.23)
spTCCA1	0.88 (0.61, 0.89)	0.88 (0.44, 0.88)	15.16 (14.56, 18.62)
spTGCCA1	0.88 (0.63, 0.89)	0.87 (0.51, 0.88)	10.05 (9.60, 11.24)
TCCA3	0.88 (0.62, 0.89)	0.88 (0.45, 0.88)	19.23 (18.46, 21.65)
TGCCA3	0.98 (0.71, 0.99)	0.88 (0.51, 0.88)	19.15 (15.27, 25.04)
spTCCA3	0.88 (0.61, 0.89)	0.88 (0.42, 0.88)	15.90 (15.45, 17.63)
spTGCCA3	0.98 (0.78, 0.99)	0.99 (0.69, 0.99)	38.84 (19.85, 81.09)
RGCCA	0.94 (0.70, 0.97)	0.95 (0.56, 0.98)	44.26 (43.34, 48.29)
SVD	0.02 (0.00, 0.04)	0.02 (0.00, 0.05)	0.55 (0.48, 0.60)

Model	Cross	Cross (small) 3D	Computation time
TCCA1	0.89 (0.87, 0.89)	0.88 (0.87, 0.88)	16.66 (16.14, 17.07)
TGCCA1	0.89 (0.87, 0.89)	0.88 (0.87, 0.88)	9.35 (8.86, 9.82)
spTCCA1	0.89 (0.87, 0.89)	0.88 (0.87, 0.88)	14.85 (14.38, 15.29)
spTGCCA1	0.88 (0.87, 0.89)	0.87 (0.87, 0.88)	9.94 (9.60, 10.61)
TCCA3	0.89 (0.87, 0.89)	0.88 (0.87, 0.88)	19.15 (18.67, 19.75)
TGCCA3	0.99 (0.96, 1.00)	0.88 (0.86, 0.88)	17.95 (14.35, 23.21)
spTCCA3	0.89 (0.87, 0.89)	0.88 (0.87, 0.88)	15.79 (15.58, 16.21)
spTGCCA3	0.98 (0.97, 0.99)	0.99 (0.97, 0.99)	25.63 (12.37, 55.75)
RGCCA	0.98 (0.96, 0.99)	0.98 (0.94, 0.99)	42.46 (41.55, 44.22)
SVD	0.05 (0.00, 0.11)	0.05 (0.01, 0.12)	0.54 (0.48, 0.60)

Model	Cross	Cross (small) 3D	Computation time
TCCA1	0.89 (0.89, 0.89)	0.88 (0.88, 0.88)	16.86 (16.36, 17.19)
TGCCA1	0.89 (0.89, 0.89)	0.88 (0.88, 0.88)	9.28 (8.75, 9.62)
spTCCA1	0.89 (0.89, 0.89)	0.88 (0.88, 0.88)	15.07 (14.73, 15.55)
spTGCCA1	0.89 (0.88, 0.89)	0.88 (0.88, 0.88)	10.30 (9.84, 10.90)
TCCA3	0.89 (0.89, 0.89)	0.88 (0.88, 0.88)	19.49 (19.05, 19.92)
TGCCA3	1.00 (0.99, 1.00)	0.88 (0.88, 0.88)	16.19 (13.70, 21.50)
spTCCA3	0.89 (0.89, 0.89)	0.88 (0.88, 0.88)	15.90 (15.53, 16.08)
spTGCCA3	0.98 (0.97, 0.99)	0.99 (0.98, 0.99)	15.36 (10.07, 29.10)
RGCCA	0.99 (0.98, 1.00)	1.00 (0.99, 1.00)	42.02 (40.34, 43.26)
SVD	1.00 (0.99, 1.00)	1.00 (0.99, 1.00)	0.56 (0.50, 0.60)

Table 23: Cosine between the true and the estimated canonical vectors for different models on blocks "Cross" and "Cross (small) 3D", for levels of SNR -20dB, -10dB, -6dB and 0dB from top to bottom, and computation times, for n = 100 and 100 folds. Median and quantiles (2.5% and 97.5%) are reported (3D settings).

Model	Cross	Cross (small) 3D	Computation time
TCCA1	0.17 (0.01, 0.55)	0.06 (0.03, 0.12)	17.21 (15.96, 30.30)
TGCCA1	0.17 (0.01, 0.55)	0.06 (0.03, 0.13)	5.62 (5.23, 14.25)
spTCCA1	0.17 (0.01, 0.55)	0.06 (0.03, 0.12)	14.95 (14.03, 23.36)
spTGCCA1	0.18 (0.01, 0.51)	0.06 (0.02, 0.12)	5.95 (5.29, 18.29)
TCCA3	0.17 (0.01, 0.55)	0.06 (0.03, 0.12)	20.94 (19.06, 47.97)
TGCCA3	0.11 (0.01, 0.38)	0.06 (0.01, 0.15)	21.61 (13.30, 32.11)
spTCCA3	0.18 (0.01, 0.55)	0.06 (0.03, 0.12)	15.67 (15.13, 19.94)
spTGCCA3	0.10 (0.00, 0.36)	0.02 (0.00, 0.12)	56.55 (11.67, 111.47)
RGCCA	0.07 (0.00, 0.23)	0.05 (0.00, 0.16)	4.48 (3.91, 6.17)
SVD	0.01 (0.00, 0.04)	0.01 (0.00, 0.03)	0.07 (0.06, 0.08)

Model	Cross	Cross (small) 3D	Computation time
TCCA1	0.63 (0.03, 0.88)	0.22 (0.01, 0.88)	17.07 (15.80, 23.87)
TGCCA1	0.63 (0.05, 0.88)	0.29 (0.01, 0.88)	6.80 (5.42, 11.47)
spTCCA1	0.62 (0.03, 0.88)	0.21 (0.01, 0.88)	14.89 (14.03, 19.35)
spTGCCA1	0.76 (0.08, 0.88)	0.84 (0.01, 0.88)	7.35 (5.48, 19.28)
TCCA3	0.64 (0.03, 0.88)	0.22 (0.01, 0.88)	20.49 (18.56, 31.50)
TGCCA3	0.65 (0.02, 0.97)	0.30 (0.02, 0.87)	16.94 (12.28, 26.38)
spTCCA3	0.59 (0.03, 0.88)	0.18 (0.01, 0.88)	15.51 (14.93, 19.97)
spTGCCA3	0.75 (0.03, 0.96)	0.78 (0.02, 0.98)	50.95 (21.01, 90.79)
RGCCA	0.40 (0.05, 0.81)	0.36 (0.03, 0.80)	4.69 (4.12, 8.02)
SVD	0.03 (0.00, 0.13)	0.03 (0.00, 0.11)	0.07 (0.06, 0.08)

Model	Cross	Cross (small) 3D	Computation time
TCCA1	0.87 (0.38, 0.89)	0.87 (0.14, 0.88)	16.73 (15.54, 24.19)
TGCCA1	0.87 (0.48, 0.89)	0.87 (0.11, 0.88)	6.82 (6.08, 13.48)
spTCCA1	0.87 (0.48, 0.89)	0.87 (0.11, 0.88)	14.90 (13.84, 21.18)
spTGCCA1	0.87 (0.57, 0.89)	0.87 (0.16, 0.88)	6.94 (6.20, 9.30)
TCCA3	0.87 (0.49, 0.89)	0.87 (0.11, 0.88)	19.14 (18.15, 29.49)
TGCCA3	0.96 (0.34, 0.99)	0.86 (0.19, 0.88)	15.35 (11.38, 24.68)
spTCCA3	0.87 (0.48, 0.89)	0.87 (0.11, 0.88)	15.46 (15.01, 18.89)
spTGCCA3	0.95 (0.56, 0.98)	0.98 (0.38, 0.99)	30.15 (12.53, 63.18)
RGCCA	0.90 (0.31, 0.96)	0.89 (0.32, 0.97)	4.56 (4.18, 5.82)
SVD	0.08 (0.00, 0.32)	0.09 (0.00, 0.29)	0.07 (0.06, 0.09)

Model	Cross	Cross (small) 3D	Computation time
TCCA1	0.88 (0.84, 0.89)	0.88 (0.86, 0.88)	16.28 (15.47, 17.49)
TGCCA1	0.89 (0.85, 0.89)	0.88 (0.86, 0.88)	6.65 (6.11, 7.20)
spTCCA1	0.89 (0.84, 0.89)	0.88 (0.86, 0.88)	14.64 (14.02, 15.35)
spTGCCA1	0.88 (0.84, 0.89)	0.88 (0.86, 0.88)	6.94 (6.34, 7.69)
TCCA3	0.88 (0.84, 0.89)	0.88 (0.86, 0.88)	19.04 (18.41, 20.70)
TGCCA3	0.99 (0.93, 1.00)	0.88 (0.84, 0.88)	13.91 (10.93, 21.65)
spTCCA3	0.89 (0.85, 0.89)	0.88 (0.86, 0.88)	15.27 (14.91, 15.71)
spTGCCA3	0.97 (0.91, 0.98)	0.98 (0.93, 0.99)	15.74 (8.26, 51.21)
RGCCA	0.97 (0.90, 0.99)	0.98 (0.90, 0.99)	4.04 (3.85, 4.38)
SVD	0.99 (0.92, 1.00)	0.99 (0.93, 1.00)	0.06 (0.06, 0.07)

Table 24: Cosine between the true and the estimated canonical vectors for different models on blocks "Square", "Gas 3D", "Cross", "Cross (small) 3D" and "Vector", for levels of SNR -20dB, -10dB, -6dB, and 0dB from top to bottom, and computation times, for n = 1000 and 10 folds. Median and quantiles (2.5% and 97.5%) are reported (3D settings).

Model	Square	Gas 3D	Cross	Cross (small) 3D	Vector	Computation time
TGCCA1	0.24 (0.14, 0.37)	0.26 (0.12, 0.48)	0.18 (0.02, 0.40)	0.07 (0.01, 0.70)	0.16 (0.01, 0.37)	102.51 (92.84, 130.29)
TGCCA3	0.07 (0.04, 0.25)	0.13 (0.02, 0.54)	0.08 (0.03, 0.25)	0.05 (0.01, 0.77)	0.10 (0.02, 0.33)	894.58 (600.22, 1137.62)
RGCCA	0.09 (0.05, 0.20)	0.11 (0.02, 0.43)	0.09 (0.02, 0.23)	0.20 (0.04, 0.38)	0.19 (0.04, 0.32)	56.37 (52.75, 81.20)
SVD	0.00 (0.00, 0.00)	0.00 (0.00, 0.01)	0.00 (0.00, 0.01)	0.00 (0.00, 0.01)	0.86 (0.79, 0.86)	7.27 (7.16, 7.73)

Model	Square	Gas 3D	Cross	Cross (small) 3D	Vector	Computation time
TGCCA1	0.99 (0.98, 1.00)	0.90 (0.86, 0.91)	0.88 (0.86, 0.89)	0.88 (0.87, 0.88)	0.99 (0.99, 0.99)	87.24 (82.68, 93.08)
TGCCA3	0.99 (0.98, 1.00)	0.97 (0.91, 0.98)	0.98 (0.95, 1.00)	1.00 (0.98, 1.00)	0.99 (0.99, 0.99)	468.38 (355.33, 972.80)
RGCCA	0.98 (0.96, 0.99)	0.98 (0.92, 0.99)	0.97 (0.93, 0.99)	0.98 (0.95, 0.99)	0.99 (0.99, 0.99)	54.54 (52.96, 56.11)
SVD	0.01 (0.00, 0.02)	0.01 (0.00, 0.04)	0.01 (0.00, 0.03)	0.01 (0.00, 0.03)	1.00 (1.00, 1.00)	7.02 (6.78, 7.54)

Model	Square	Gas 3D	Cross	Cross (small) 3D	Vector	Computation time
TGCCA1	1.00 (0.99, 1.00)	0.90 (0.89, 0.91)	0.89 (0.88, 0.89)	0.88 (0.88, 0.88)	1.00 (1.00, 1.00)	96.43 (89.20, 100.14)
TGCCA3	1.00 (0.99, 1.00)	0.97 (0.95, 0.98)	0.99 (0.98, 1.00)	1.00 (0.99, 1.00)	1.00 (1.00, 1.00)	433.26 (258.66, 1038.78)
RGCCA	0.99 (0.99, 1.00)	0.99 (0.97, 1.00)	0.99 (0.98, 1.00)	0.99 (0.98, 1.00)	1.00 (1.00, 1.00)	51.94 (51.62, 53.71)
SVD	0.02 (0.00, 0.04)	0.02 (0.01, 0.09)	0.04 (0.01, 0.09)	0.03 (0.00, 0.08)	1.00 (1.00, 1.00)	7.22 (6.97, 7.66)

Model	Square	Gas 3D	Cross	Cross (small) 3D	Vector	Computation time
TGCCA1	1.00 (1.00, 1.00)	0.91 (0.90, 0.91)	0.89 (0.89, 0.89)	0.88 (0.88, 0.88)	1.00 (1.00, 1.00)	90.34 (81.72, 96.86)
TGCCA3	1.00 (1.00, 1.00)	0.98 (0.97, 0.98)	1.00 (1.00, 1.00)	1.00 (1.00, 1.00)	1.00 (1.00, 1.00)	318.09 (278.49, 488.14)
RGCCA	1.00 (1.00, 1.00)	1.00 (0.99, 1.00)	1.00 (0.99, 1.00)	1.00 (0.99, 1.00)	1.00 (1.00, 1.00)	50.88 (49.51, 51.21)
SVD	1.00 (1.00, 1.00)	1.00 (0.99, 1.00)	1.00 (0.99, 1.00)	1.00 (0.99, 1.00)	1.00 (1.00, 1.00)	7.32 (6.64, 7.51)

Table 25: Cosine between the true and the estimated canonical vectors for different models on blocks "Square", "Gas 3D", "Cross", "Cross (small) 3D" and "Vector", for levels of SNR -20dB, -10dB, -6dB, and 0dB from top to bottom, and computation times, for n = 500 and 20 folds. Median and quantiles (2.5% and 97.5%) are reported (3D settings).

Model	Square	Gas 3D	Cross	Cross (small) 3D	Vector	Computation time
TGCCA1	0.21 (0.13, 0.28)	0.26 (0.02, 0.50)	0.17 (0.01, 0.33)	0.06 (0.01, 0.12)	0.13 (0.03, 0.30)	47.79 (44.19, 105.24)
TGCCA3	0.05 (0.01, 0.13)	0.15 (0.01, 0.45)	0.11 (0.01, 0.16)	0.04 (0.01, 0.15)	0.11 (0.03, 0.25)	479.49 (322.46, 659.61)
RGCCA	0.04 (0.00, 0.13)	0.10 (0.01, 0.34)	0.05 (0.00, 0.19)	0.07 (0.01, 0.26)	0.11 (0.04, 0.22)	33.73 (29.62, 46.39)
SVD	0.00 (0.00, 0.01)	0.00 (0.00, 0.01)	0.01 (0.00, 0.01)	0.01 (0.00, 0.01)	0.68 (0.23, 0.79)	3.25 (3.16, 3.34)

Model	Square	Gas 3D	Cross	Cross (small) 3D	Vector	Computation time
TGCCA1	0.99 (0.95, 1.00)	0.90 (0.84, 0.91)	0.88 (0.81, 0.89)	0.88 (0.86, 0.88)	0.98 (0.97, 0.98)	47.90 (45.36, 52.12)
TGCCA3	0.99 (0.94, 0.99)	0.96 (0.89, 0.98)	0.98 (0.92, 1.00)	0.99 (0.96, 1.00)	0.98 (0.97, 0.98)	406.33 (195.60, 849.59)
RGCCA	0.97 (0.92, 0.98)	0.96 (0.89, 0.98)	0.96 (0.89, 0.98)	0.96 (0.91, 0.98)	0.98 (0.97, 0.98)	30.73 (29.50, 32.24)
SVD	0.01 (0.00, 0.03)	0.02 (0.00, 0.05)	0.02 (0.00, 0.04)	0.02 (0.00, 0.05)	0.99 (0.99, 0.99)	3.24 (3.19, 3.32)

Model	Square	Gas 3D	Cross	Cross (small) 3D	Vector	Computation time
TGCCA1	1.00 (0.98, 1.00)	0.90 (0.88, 0.91)	0.89 (0.87, 0.89)	0.88 (0.88, 0.88)	0.99 (0.99, 0.99)	48.20 (45.88, 51.06)
TGCCA3	1.00 (0.98, 1.00)	0.97 (0.94, 0.98)	0.99 (0.97, 1.00)	1.00 (0.99, 1.00)	0.99 (0.99, 0.99)	312.56 (179.07, 665.36)
RGCCA	0.99 (0.97, 0.99)	0.99 (0.96, 0.99)	0.99 (0.96, 0.99)	0.99 (0.97, 0.99)	0.99 (0.99, 0.99)	29.12 (28.51, 29.76)
SVD	0.02 (0.00, 0.08)	0.04 (0.00, 0.13)	0.05 (0.00, 0.11)	0.05 (0.01, 0.12)	1.00 (1.00, 1.00)	3.24 (3.17, 3.41)

Model	Square	Gas 3D	Cross	Cross (small) 3D	Vector	Computation time
TGCCA1	1.00 (1.00, 1.00)	0.91 (0.90, 0.91)	0.89 (0.89, 0.89)	0.88 (0.88, 0.88)	1.00 (1.00, 1.00)	47.05 (44.25, 48.98)
TGCCA3	1.00 (1.00, 1.00)	0.97 (0.97, 0.98)	1.00 (0.99, 1.00)	1.00 (1.00, 1.00)	1.00 (1.00, 1.00)	225.44 (160.94, 370.20)
RGCCA	1.00 (0.99, 1.00)	1.00 (0.99, 1.00)	1.00 (0.99, 1.00)	1.00 (0.99, 1.00)	1.00 (1.00, 1.00)	28.28 (27.72, 29.33)
SVD	1.00 (0.99, 1.00)	1.00 (0.98, 1.00)	1.00 (0.99, 1.00)	1.00 (0.99, 1.00)	1.00 (1.00, 1.00)	3.24 (3.19, 3.39)

Table 26: Cosine between the true and the estimated canonical vectors for different models on blocks "Square", "Gas 3D", "Cross", "Cross (small) 3D" and "Vector", for levels of SNR -20dB, -10dB, -6dB, and 0dB from top to bottom, and computation times, for n = 100 and 100 folds. Median and quantiles (2.5% and 97.5%) are reported (3D settings).

Model	Square	Gas 3D	Cross	Cross (small) 3D	Vector	Computation time
TGCCA1	0.21 (0.13, 0.26)	0.24 (0.04, 0.65)	0.12 (0.00, 0.31)	0.06 (0.04, 0.10)	0.09 (0.00, 0.30)	17.42 (15.67, 56.83)
TGCCA3	0.04 (0.00, 0.13)	0.13 (0.00, 0.67)	0.08 (0.00, 0.19)	0.03 (0.00, 0.10)	0.09 (0.00, 0.29)	187.55 (93.68, 362.93)
RGCCA	0.03 (0.00, 0.14)	0.08 (0.00, 0.24)	0.03 (0.00, 0.16)	0.06 (0.00, 0.22)	0.10 (0.00, 0.29)	11.69 (10.68, 14.37)
SVD	0.01 (0.00, 0.03)	0.01 (0.00, 0.03)	0.01 (0.00, 0.04)	0.01 (0.00, 0.03)	0.24 (0.01, 0.51)	0.85 (0.80, 0.90)
Model	Square	Gas 3D	Cross	Cross (small) 3D	Vector	Computation time
TGCCA1	0.90 (0.36, 0.99)	0.86 (0.39, 0.91)	0.80 (0.42, 0.89)	0.86 (0.04, 0.88)	0.88 (0.53, 0.94)	22.36 (17.51, 46.05)
TGCCA3	0.87 (0.32, 0.98)	0.90 (0.48, 0.97)	0.84 (0.29, 0.98)	0.93 (0.29, 1.00)	0.88 (0.54, 0.94)	169.14 (98.52, 277.69)
RGCCA	0.80 (0.30, 0.92)	0.82 (0.49, 0.93)	0.77 (0.27, 0.92)	0.81 (0.42, 0.91)	0.88 (0.60, 0.95)	11.96 (10.83, 15.24)
SVD	0.03 (0.00, 0.09)	0.03 (0.00, 0.09)	0.03 (0.00, 0.13)	0.03 (0.00, 0.11)	0.97 (0.95, 0.98)	0.85 (0.80, 0.91)
Model	Square	Gas 3D	Cross	Cross (small) 3D	Vector	Computation time
TGCCA1	0.99 (0.85, 1.00)	0.89 (0.81, 0.91)	0.88 (0.70, 0.89)	0.88 (0.77, 0.88)	0.96 (0.93, 0.98)	18.04 (16.77, 21.64)
spTGCCA3	0.98 (0.84, 0.99)	0.96 (0.86, 0.98)	0.97 (0.82, 0.99)	0.99 (0.84, 1.00)	0.97 (0.93, 0.98)	161.40 (82.43, 257.82)
RGCCA	0.94 (0.81, 0.97)	0.94 (0.84, 0.98)	0.93 (0.77, 0.97)	0.94 (0.78, 0.97)	0.97 (0.94, 0.98)	10.89 (10.50, 11.46)
SVD	0.08 (0.01, 0.24)	0.08 (0.00, 0.25)	0.08 (0.00, 0.32)	0.09 (0.00, 0.29)	0.99 (0.98, 0.99)	0.85 (0.79, 0.91)
Model	Square	Gas 3D	Cross	Cross (small) 3D	Vector	Computation time
TGCCA1	1.00 (0.96, 1.00)	0.90 (0.88, 0.91)	0.89 (0.84, 0.89)	0.88 (0.87, 0.88)	0.99 (0.98, 0.99)	17.57 (16.66, 18.65)
TGCCA3	0.99 (0.96, 1.00)	0.97 (0.95, 0.98)	0.99 (0.94, 1.00)	1.00 (0.97, 1.00)	0.99 (0.98, 0.99)	98.43 (63.25, 199.98)
RGCCA	0.98 (0.95, 0.99)	0.98 (0.96, 0.99)	0.98 (0.93, 0.99)	0.99 (0.93, 0.99)	0.99 (0.98, 0.99)	10.33 (10.04, 10.68)
SVD	0.99 (0.91, 1.00)	0.99 (0.91, 1.00)	0.99 (0.92, 1.00)	0.99 (0.93, 1.00)	1.00 (1.00, 1.00)	0.84 (0.80, 0.91)